Studies on indolyl- and pyrrolylsilanes as potential precursors for Si-centred ligands

Tim Evers BSc

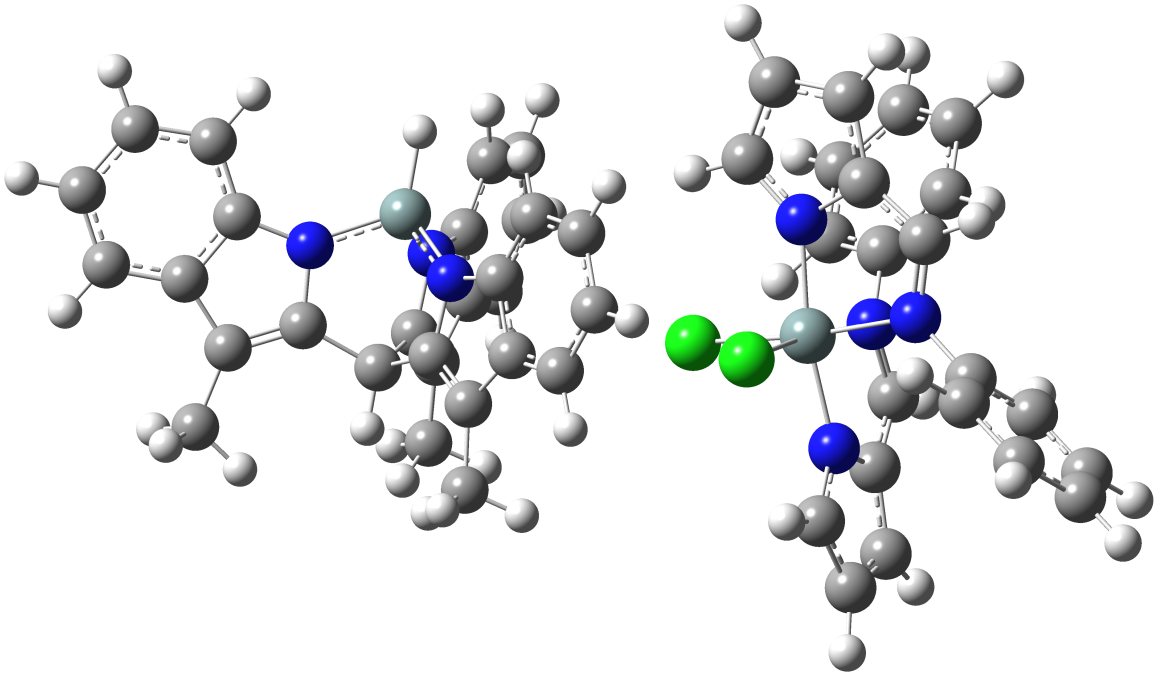

Master thesis

Supervisor:
Dr. Marc-Etienne Moret

Universiteit Utrecht

Organic Chemistry and Catalysis

December 2013

Abstract

Reaction of tris(3-methylindol-2-yl)methane (tris(skatyl)methane, $tsmH_3$) with $HSiCl_3$ and $SiCl_4$ was attempted, in order to eventually synthesise tris(3-methylindol-2-yl)methane silanide ($tsmSi^-$). This is projected to be a very strong-field ligand. Unfortunately, synthesis of both precursors tsmSiH and tsmSiCl has failed, and it was suggested this is due to large strain energy and consequent preference for polymerisation instead of intermolecular reaction.

In addition to these synthesis attempts, DFT calculations were done. These indicate similar strain energies between $tsmSi^-$ and tsmP, while both tsmSiH and tsmSiCl are approximately 15 kcal/mol higher, showing a higher preference for a more open structure, for example polymers. 1,1,2-tris(3-methylindol-2-yl)ethane is instead proposed as a scaffold for eventual silanide synthesis.

Focus then switched to penta- and hexacoordinate silicon compounds with two related ligands: N-phenyl-2-formiminopyrrolyl (pfp) and N-(2,6-diisopropylphenyl)-2-formiminopyrrolyl (dipfp). The reaction of two equivalents of pfp with tetrachlorosilane afforded a hexacoordinate compound $Si(pfp)_2Cl_2$. Using dipfp instead of pfp also showed a reaction but it could not be ascertained whether one or two equivalents of dipfp were involved. The reaction of one equivalent of dipfp with trichlorosilane afforded first the pentacoordinate $SiH(dipfp)Cl_2$, which undergoes hydrosilylation to form the tetracoordinate $SiLCl_2$, where L is (2,6-diisopropylphenyl)(2-pyrrolylmethyl)amide. Reduction of $Si(pfp)_2Cl_2$ has been unsuccessfully attempted.

Here also DFT has been employed to gain insight into both synthesis properties and reduction properties. These show that instead of reducing to a silylene, instead a biradical with electrons in the ligands may be formed.

Contents

Part I.
Introduction

1. Introduction

1.1. Ligands in catalysis: silylenes and silanides

One of the most common ligands used in catalysis are phosphines [1, 2, 3]. They have the advantage of being relatively labile, thereby having the possibility of creating a free site on the metal for catalysis), and their bulk and electronic properties are tunable depending on the substitutents on the phosphorus. They can range from the very small, electron-rich trimethylphosphine to the big tris(cyclohexyl)phosphine and electron-poor trimethoxyphosphine. They bind metals not just by donation of the lone pair on phosphorus, but also by back-bonding into P−C σ^*-orbitals, which are shown in figure 1a.

A class of ligand related to the phosphines is the N-heterocyclic carbene, or NHC. These singlet carbene ligands bind more strongly than phosphines [4], which brings them more into the class of non-labile ligands. While they can still accept electrons from the metal in a back-bonding interaction, it is less favourable than with phosphines. The electrons from the metal are placed into the N−C−N antibonding orbital (shown in figure 1b), which has strong C−N π^*-character and is therefore high in energy. The contribution from back-bonding into the overall bond is therefore small [5]. This can also be explained by drawing a resonance structure which has the NHC as an ylide, filling the p-obital and making it unavailable for further bonding.NHC's are very well known [6], with the first stable NHC was reported in 1991 [7]. Later even air-stable carbenes were reported [8], and they are now used in a variety of catalysts (for example [9]).

Related to the NHC's, moving one element down in the periodic table, are the N-heterocyclic silylenes or NHSi's. These are less well known, in fact the first stable NHSi was not synthesised until 1994 [10], and the second not until 1996 [11]). Both structures are shown in figure 2. These formally silicon(II) compounds have some different properties when compared to the NHC's. Due to size mismatch between the silicon and nitrogen p-orbitals (see figure 1d), the ylide contribution is smaller and the empty p-orbital on silicon is more available for bonding, so back-bonding is increased [5].

An additional feature of silylenes is that they can be stabilised by a lone pair, also when metal-bound (for example [14]). This is also related to the size mismatch in the orbitals of silicon and nitrogen, which makes the empty orbital on silicon more available for binding an additional ligand.

A final related class of ligands are the silyl anions or the silanides, one example of which is trispyrrolylsilanide [15]. Its electron-accepting orbitals are shown in figure 1c. These are very similar to those of the isoelectronic phosphine (figure 1a). Instead of stabilising the lone pair with a Lewis-base, a negatively charged ligand forms a full covalent bond with the silicon centre.

The nature of the N-substituent on silicon is important. As explained above, the lone pair on nitrogen can be donated to form an ylide. A nitrogen atom which is part of an aromatic ring cannot donate this lone pair because that would break the aromaticity. This makes the p-orbital on silicon more available for bonding, increasing π-acidity.

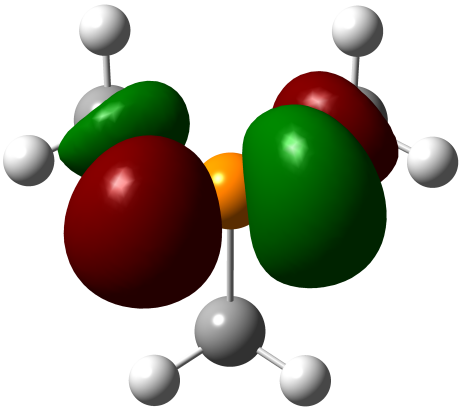

(a) *Trimethylphosphine (LUMO+1)*

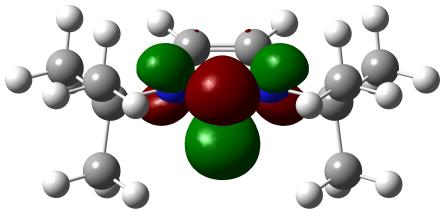

(b) *NHC (LUMO+1)*

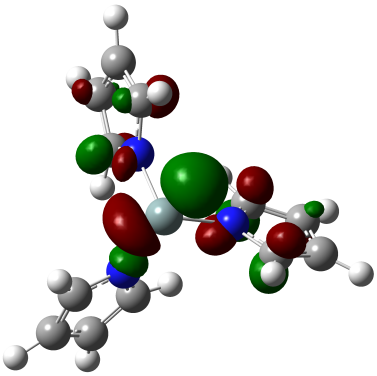

(c) *Tris(pyrrolyl)silanide (LUMO)*

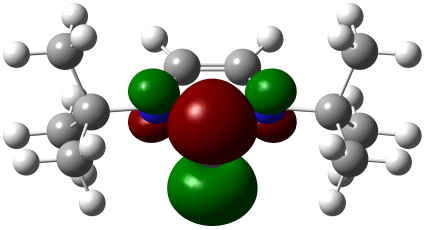

(d) *NHSi (LUMO)*

Figure 1: *One of the electron-accepting orbitals of trimethylphosphine, a typical NHC, a typical NHSi and tris(pyrrolyl)silanide.*

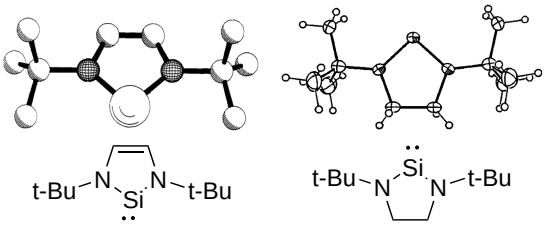

Figure 2: *Electron diffraction image and structure of the first stable silylene [10], and x-ray diffraction image and structure of the second stable silylene [11]. ED and XRD images edited from their respective sources.*

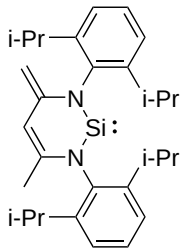

(a) *Non-stabilised NHSi [12]*

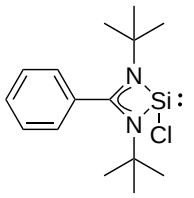

(b) *Stabilised NHSi [13]*

Figure 3: *The two different types of NHSi's.*

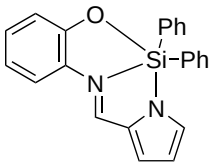

(a) *Pentacoordinate silicon [16].*

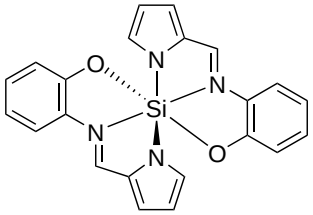

(b) *Hexacoordinate silicon [16].*

Figure 4: *Examples of penta- and hexacoordinate silicon.*

1.2. Hypervalency in silicon

Hypervalency is when a main-group atom seemingly breaks the octet rule and forms more bonds than predicted by it. For example, according to the octet rule phosphorus can only form three bonds like in triphenylphosphine PPh_3, but well-known are triphenylphosphine oxide $Ph_3P{=}O$ and the phosphate ion PO_4^{3-}, where phosphorus forms five, and also hexafluorophosphate PF_6^- with six bonds is known. Likewise, sulphur usually forms two (H_2S), but can form four (DMSO, $H_3CS(=O)CH_3$) or six (SF_6), and chlorine can form any odd number of bonds from 1 through 7.

Silicon is also known to form both penta- and hexacoordinate species, with one example of each shown in figure 4. Both types of compounds are quite well-known, though not as common as the tetracoordinate non-hypervalent variety. While compounds which are formally heptacoordinated or higher are known [17], these seem to fall in the bis(η^n-(hetero)aryl)family.

Figure 5 shows an MO-diagram which is typical for an octahedral AH_6-type compound [18], here filled in for SiH_6^{2-}. This diagram shows the interaction of the s- and p-orbitals on A with the three sets of orbitals formed by introducing a H_6-cluster without centre atom. The lowest lying orbital is simply the additive mix of all s-orbitals. The three orbitals above that are three-centre orbitals formed by the in-phase overlap of two *trans*-hydrogens with the centre p-orbitals. These three three-centre-two-electron-bonds are the main feature of the structure. Then two non-bonding orbitals are derived directly from the H_6-cluster. The lowest-lying antibonding orbital is formed from the out-of-phase overlap of the s-orbital on the centre atom with the s-orbitals of the hydrogens, and the highest set of three antibonding orbitals is from the out-of-phase overlap of a p-orbital on A with two *trans*-s-orbitals.

This clearly shows that hypervalency can be achieved without invoking d-orbitals. These are commonly accepted to be too high in energy to be significantly involved in bonding, and even adding them does not significantly change the diagram above, they will only lower the non-bonding orbitals slightly [18].

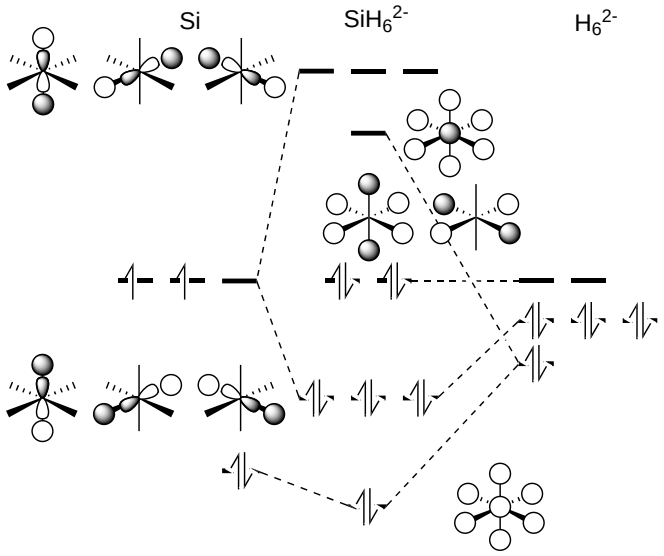

Figure 5: *Part of molecular orbital diagram of an octahedral SiH_6^{2-} molecule from the s and p orbitals of Si and the orbitals H_6, without including d orbitals on Si. In general true for any octahedral AH_6-system. Adapted from [18]*

Filling non-bonding orbitals will result in a transfer of electron density to the ligands, as these are only ligand centred. As in silicon (figure 5) these are filled, using ligands capable of accepting these electrons will result in stabilisation of this hexacoordinate center.

A similar discussion can be held for five-coordinate silicon, with the main observation that the bonding in the equatorial ligands can be described by a more common sp^2-s-overlap, and that therefore electron-accepting ligands will prefer the axial positions.

1.3. The metal

The silylenes and silanides described are intended as ligands for iron. This metal is cheap and abundant, and is known to catalyse for example C−H-bond oxidation [19] and the Kumada cross-coupling [20, 21]. An important downside of this metal is its propensity for one-electron processes. Iron has a lot of accessible oxidation states (0 to +5). Palladium for example, which is also known to catalyse cross coupling [1, 22], only has the 0, +2 and +4 states, which only allows two-electron processes. This avoids paramagnetic compounds and in general makes for more well-behaved reactions. A way of making iron do two-electron processes may be to use the aforementioned silylenes. As mentioned these bind strongly which may force iron low-spin.

1.4. Density Functional Theory

A major part of this thesis involves the use of density functional theory or DFT for the calculation of molecule energies. The main idea behind this computational method is to reduce the amount of variables involved in the calculation. It still involves approximately solving the Schrödinger equation $E\Psi = (\frac{1}{2}\nabla^2 + V_e)\Psi$ under the Born-Oppenheimer approximation, which is to assume the nuclei are stationary and therefore have no kinetic energy and a constant nucleus-nucleus repulsion. Instead of using each electron on its own which introduces four variables per electron (three spatial, one spin), it instead uses the total electron density which is only depend-

ant on the three spacial coordinates. It can be shown that knowing the exact electron density is equivalent to knowing the exact ground-state wave function and will result in the ground-state energy of the system.

This leaves the problem of how to determine this electron density. For this, the so-called Kohn-Sham orbitals are introduced. These are orbitals for hypothetical non-interacting particles, in this case non-interacting electrons, which in total give the same electron density as the interacting system. This simplifies calculations by a huge amount, because there are no electron-electron repulsions which have to be taken into account. Unfortunately, the energy extracted from these Kohn-Sham orbitals is not quite physically meaningful. Making the particles non-interacting introduces a difference between their kinetic energy and the true kinetic energy of the system. This difference (among some other problems) is unknown, and means the full functional where DFT gets its name from is unknown. It can however be approximated.

In a calculation, two things must be chosen: the basis set, with values for the Kohn-Sham orbitals used, and the functional, which is an approach for approximating the non-analytic part of the calculation. Both can have profound effects on the results acquired from the calculation.

(This entire section is summarized from [23].)

1.5. Experimental and DFT silicon-NMR

An important tool for characterising silicon compounds is ^{29}Si-NMR and its decoupled version ^{29}Si$\{^{1}$H$\}$-NMR. It is very sensitive to the coordination around silicon, with values in the -150 to -200 ppm typical for hexacoordinate silanes (see experimental and for example [16]), while for pentacoordinate silanes values around -60 to -100 ppm are more common (for example [16, 24]). They show some overlap with tetracoordinate silanes, but these are generally found at higher ppm-values.

Common for these types of compounds is a long relaxation time. When a hydrogen is present, this tends not to be a problem, but for the compounds mentioned in this thesis with a Cl_2N_4-coordination around silicon, getting any signal in ^{29}Si$\{^{1}$H$\}$-NMR is difficult. In this case, a relaxation agent can be added. This paramagnetic compound reduces relaxation times, making it possible to measure chemical shifts, but has the downside of making the NMR-sample unusable in subsequent reaction unless purification is done [25]. Due to other requirements such as solubility and inertness, the chromium(III) compound $Cr(acac)_3$ is suitable for this project. This compound is soluble in apolar solvents and does not react with the type of compound used here.

Approximating NMR-shifts and coupling constants by DFT has different requirements from a normal optimisation. For optimisations, correct simulation of the valence electrons is most important. These are involved in bonding and are most responsible for bond lengths and angles. For NMR, simulation of core electrons becomes important. These electrons have a big effect on chemical shifts as they are closest to the nucleus. Special basis sets have been developed for the simulation of the core electrons, and are used on structures which have been optimised in a more usual basis set. The shifts obtained from these calculations must be referenced to a known compound, which in the case of both ^{1}H-NMR and ^{29}Si$\{^{1}$H$\}$-NMR can simply be tetramethylsilane.

1.6. Aim

The aim of the project is the synthesis of pyrrole-based silanes as potential precursors for Si-centred ligands. First, the pyrrole-containing organic moieties will be synthesised. These will

then be reacted with a suitable silicon precursor.

Part II.
Tris(2-methylindol-2-yl)methane

2. Introduction

Following the ideas outlined in the general introduction, a silanide was designed which may be the desired high-field ligand. It uses a cage-like structure for stabilisation and bulk.

2.1. Target compound

Tris(3-methylindol-2-yl)methane was chosen as a scaffold. Indoles have similar properties to pyrroles, while adding bulk to prevent further reactions at silicon. It is also straightforward to synthesise [26] using an electrophilic aromatic substitution. From there the planned synthesis route is shown in scheme 1, reaction with trichlorosilane may afford the desired pre-ligand. If this fails, reaction with tetrachlorosilane could be attempted. This pre-ligand could then be deprotonated (in the case of an Si−H bond) or reduced (Si−Cl) into the desired silanide.

2.2. Known compounds

Three known compounds are combined here to form the final target compund. First of all, there is a cage-like silanide known [27], and shown in figure 6a. This compound indicates that the bicyclo[2.2.2]octane-like structure can be achieved. It uses a pyrazole framework with a lithium atom as bottom bridging group.

Second is the phosphorus analogue of the target compound [28] shown in figure 6b. Synthesis of this compound is quite straightforward, using tris(3-methylindol-2-yl)methane, phosphorus trichloride and triethylamine as a base. It shows the ligand which is planned to be used here can bind phosphorus in the same way silicon is planned to be bound.

Third is tris(pyrroyl)silane [15]. This compound is known to bind ruthenium and osmium as silanide [29]. Synthesis is again utilises tris(3-methylindol-2-yl)methane and triethylamine with trichlorosilane as silicon source, indicating synthesis of the pre-ligand **2a** may be achieved in a similar way.

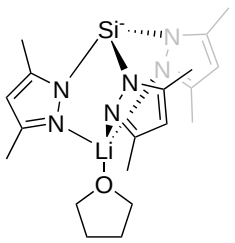

(a) *A known cage-like silanide [27].*

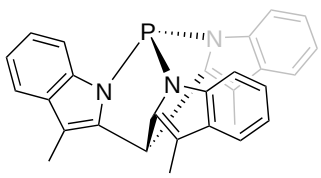

(b) *A known cage-like phosphine [28].*

Figure 6: *Known and related cage-like compounds.*

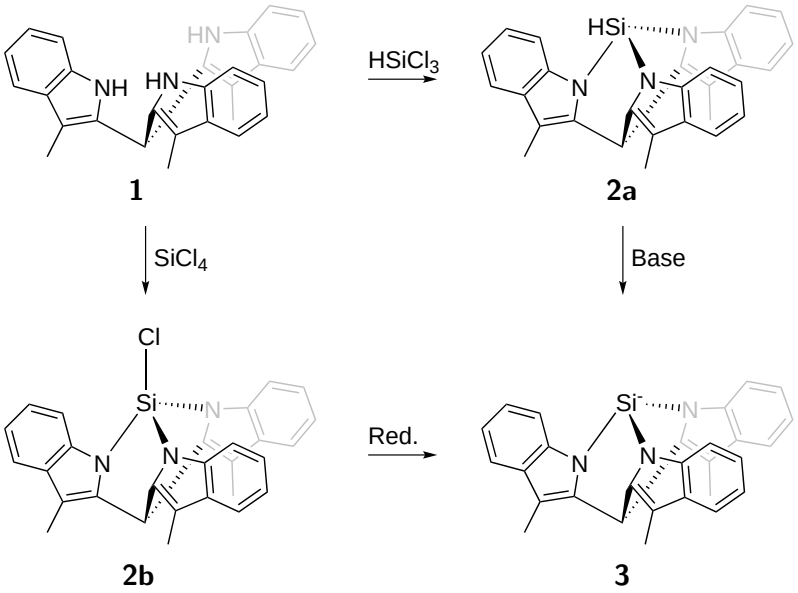

Scheme 1: *The general synthesis scheme for **3**.*

3. Results and discussion

3.1. Synthesis of tris(3-methylindol-2-y)l methane and trispyrrolylsilane

Tris(3-methylindol-2-yl)methane **1** was synthesised from 3-methylindole and triethylorthoformate (scheme 2) [26] in good yield (82 %). This reaction involves a carbocation formation by attack of the acid on triethylorthoformate and splitting off of ethanol. This carbocation can then attack the indole in a typical electrophilic aromatic substitution reaction [30]. This process repeats three times (scheme 3).

Trispyrrolylsilane **4** was synthesised from pyrrole, trichlorosilane and triethylamine (scheme 4) [15] in moderate yield (36 %). This reaction most likely involves transient deprotonation of the pyrrole, which can then attack the silicon in a pseudo-S_N2 reaction with release of chloride.

3.2. Attempted syntheses of silanes

At this point, several attempts were made to synthesise **2a,b** in order to then synthesise **3**, and an overview is shown in scheme 5. As none of them worked, they will be described in some detail below.

First of all, a synthesis procedure analogous to the one used for **4** was attempted, using trichlorosilane, **1** and excess triethylamine. No reaction was observed in ^{1}H-NMR, although

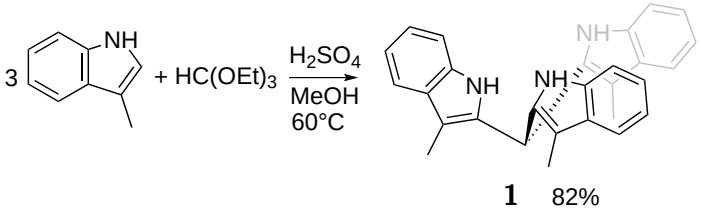

Scheme 2: *Synthesis of **1**.*

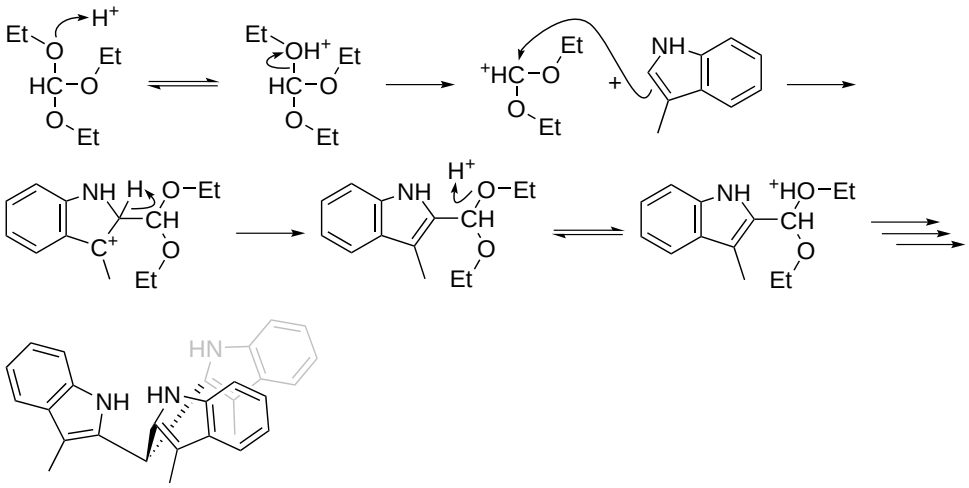

1

Scheme 3: *Mechanism of the formation of* ***1*** *[30].*

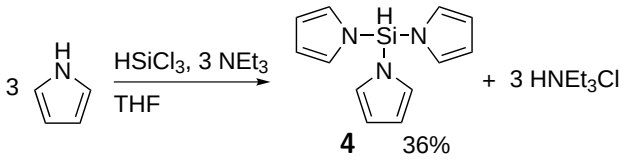

4 36%

Scheme 4: *Synthesis of* ***4****.*

1 + NaH + $HSiCl_3$ ⟶ No aromatic protons

1 + NEt_3 + $HSiCl_3$ ⟶ No reaction

1 + *n*BuLi + $HSiCl_3$ ⟶ No silane formed

1 + $HSi(NMe_2)_3$ ⟶ No reaction

1 + $HSi(NMe_2)_3$ $\xrightarrow{\text{LiHDMS}}$ No reaction

1 + $SiCl_4$ ⟶ Complex mixture

1 + *n*BuLi + $SiCl_4$ ⟶ Complex mixture including starting material

Scheme 5: *Attempted syntheses of* ***2a,b***

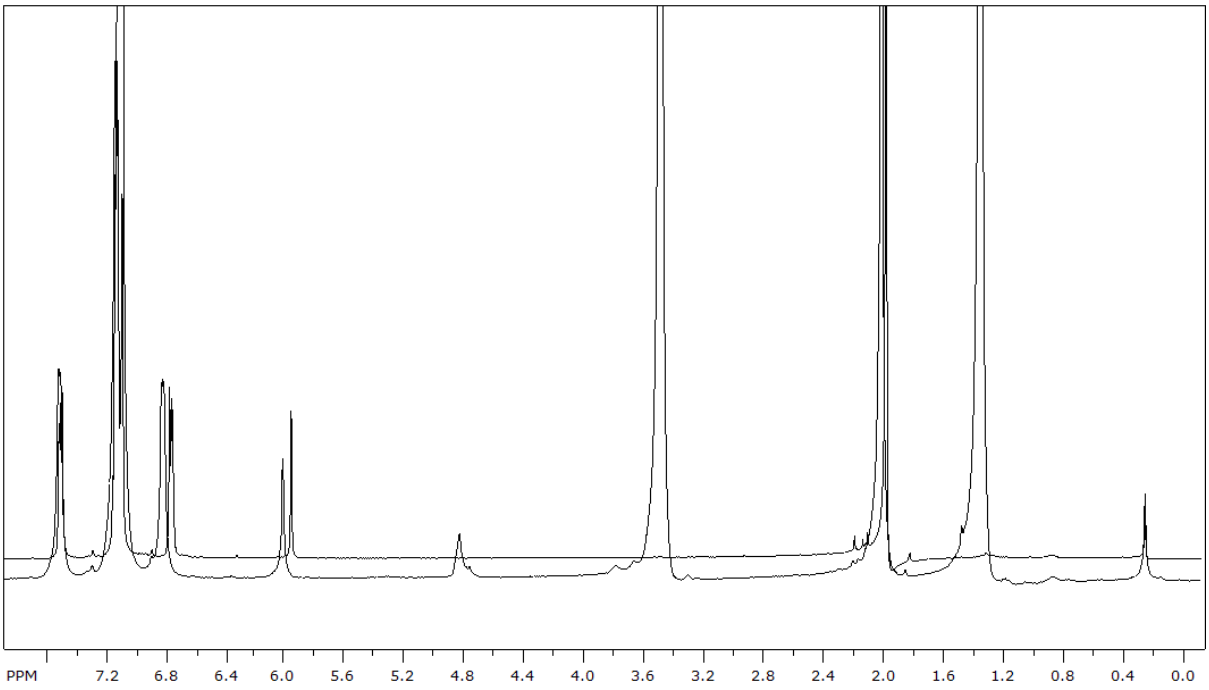

Figure 7: *Comparison of the ^{1}H-NMRs of **1** (top) and **5** after reaction with D_2O. Peaks at 1.5 and 3.6* ppm *are residual THF.*

a white precipitate was visible. After this, the mixture was heated to reflux for two hours, after which still no product and only remaining starting material was observed in ^{1}H-NMR. More triethylamine and trichlorosilane were added and the mixture refluxed overnight, which caused a large amount of peaks to appear in the aliphatic region (between 0.5 and 2.5 ppm) in ^{1}H-NMR, indicating a failed reaction. It was hypothesised that the base-catalysed transient deprotonation of the indoles was not enough, and therefore another base was used.

Sodium hydride has been used to deprotonate **1** before reacting the resulting trianion with three equivalents of chlorodiphenylphosphine to form a tridentate ligand [31]. Unfortunately, after formation of the trianion and subsequent reaction with $HSiCl_3$ in THF, only starting material was present in ^{1}H-NMR, although again a precipitate was formed. Here the counterion was changed by again changing base.

This third base was *n*-butyllithium, still using THF as a solvent, and again deprotonating first and reaction with trichlorosilane second. No precipitate was formed in this reaction at first. Unfortunately, analysis of the ^{1}H-NMR-spectrum showed a large amount of peaks in the aliphatic region, indicating formation of a (complex mixture of) unsymmetrically substituted products. Attempts to force cage formation by refluxing the crude material in toluene overnight did not work, but did form a white solid in a brown liquid. It was therefore suspected that lithiation occurred at the tertiary carbon of **1** instead of at the nitrogens.

In order to ascertain the litiation position, the reaction of **1** with *n*-butyllithium was carried out, the product isolated and subsequently reacted with D_2O. This resulted in the bottom spectrum in figure 7. The main difference with the top spectrum is the addition of two THF peaks, and a slight shift, most likely because of having some THF in the solution. In particular the peak at 6.15 ppm did not disappear. The spectrum of the lithiated compound is also very different. This proves lithiation occurs at the intended positions, forming compound **5**.

Here, a switch to a different silicon precursor was made. Tris(dimethylamino)silane has been

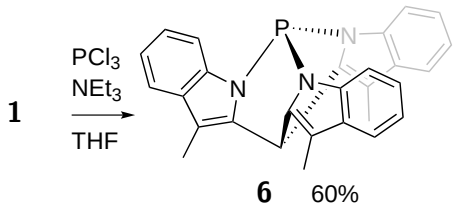

Scheme 6: *Synthesis of* ***6****.*

used before in the synthesis of azasilatranes [32]. The main advantage of using this precursor is that no base is required, and the dimethylamine produced in the reaction is gaseous. The reaction was performed at 100 °C in toluene because $HSi(NMe_2)_3$ is less reactive than $HSiCl_3$. Unfortunately, starting material was observed in ^{1}H-NMR, but in this case no precipitate was formed.

It is possible that the previous reaction did not work because of the very slow reaction of the starting materials. For reaction to occur, either **1** must spontaneously lose a proton, or tris(dimethylamino)silane must spontaneously lose dimethylamide. To circumvent this, the same reaction was carried out with 5 % lithium hexamethyldisilazide as a basic catalyst. Unfortunately after a night of refluxing in toluene again starting material was observed.

Here the silicon source was changed once again to $SiCl_4$. This has been successfully employed in the synthesis of carbazolylsilanes [33] using the lithium salt of carbazole in refluxing 1,2,3,4-tetramethylbenzene (boiling point 203 °C).

A small-scale reaction was tried first, using $SiCl_4$ and **1** in benzene-d_6 without any base. This gave a range of peaks in ^{1}H-NMR, also after heating to 100 °C (oil bath temperature) for two hours, and overnight.

Finally, a full-scale procedure was attempted, using *n*-butyllithium to deprotonate and subsequently adding tetrachlorosilane in toluene. A ^{1}H-NMR was taken of a sample of the liquid layer of the crude mixture (a precipitate was formed), which gave a multitude of peaks in both the aromatic (5.5 to 8 ppm) and aliphatic region. Extraction of the solid with dichloromethane led to starting material, again by ^{1}H-NMR.

From these experiments it can be seen that generally starting material is recovered (perhaps by not using harsh enough conditions), sometimes together with a complex mixture of products, and also ususally with an unidentified solid. Even if the solid is the expected salt byproduct (triethylammonium chloride, sodium chloride or lithium chloride), no hints of a clean reaction were found, while the appearance of this salt is a clear indication of a reaction happening. It is therefore postulated that instead of forming the cages of **3** and **2a,b**, oligomers or polymers are formed instead. This is supported by the DFT calculations described below in section 3.4 and further.

Finally, as a final verification that the lack of synthetic success was not by systematic error, synthesis of **6** following literature procedure [28] was done. This succeeded without any difficulties (59.5 % yield, approx. 83 % purity by ^{1}H-NMR).

Some other synthesis options have been considered, but not performed. The type of aromatic substitution reaction used for the synthesis of **1** is known to be very sensitive to exact starting materials and solvents. Additionally, ethanol is produced as a side product. Therefore, synthesis of tris(methylindolyl)silane, followed by aromatic substitution is likely to fail, both due to the likelyhood of incomplete cage formation and reaction of ethanol with the silicon. Additionally, silicon(II) reagents are rare and direct reaction to the silanide is not known.

3.3. Synthesis of iron precursors and attempted metallation of trispyrrolylsilane

In order to have suitable iron precursors for eventual metallation, two iron compounds were synthesised. First of all, $FeCl_2 \cdot 1.5THF$ **7** was synthesised by soxhlet extraction of the chloride with THF [34]. This was then used to synthesise dimesityliron by reaction with mesitylmagnesium bromide [35].

Metallation of trispyrrolylsilane was attempted with three iron precursors: iron pentacarbonyl, $FeCl_2$ and the previously synthesised dimesityliron. Reaction with iron pentacarbonyl gave no product even after heating to 80 °C overnight. No reaction was oberserved using iron(II) chloride either. Dimesityliron was found to decompose before forming a complex.

Deprotonation of **4** was also attempted. Reaction with lithium hexamethyldisilazane gave a second set of aryl peaks. These two aryl peaks are consistent with deprotonation of **4**, although certain proof was not obtained. It could be confirmed by $^{29}Si\{^1H\}$-NMR or perhaps more completely by hydrogen-coupled ^{29}Si-NMR, which would give a doublet for the unreacted **4** and a singlet for the deprotonated form. Reaction of **4** with *n*-butyllithium gave a mixture of unidentified products.

3.4. DFT: strain in the unmodified cage

As synthesis of the compounds **2a** and **2b** had not succeeded, DFT was used to try and identify possible problems. It was postulated that forming this ring system was unfavourable. Calculations were performed on two series of homodesmotic reactions. The first series uses pyrrole as a simplification for 3-methylindole in order to find the strain energies when the N-bound group was varied. The removed benzene ring and methyl groups are not expected to significantly influence the angles within the ring.

The equilibrium used for the first series of calculations is shown in scheme 7, and the results are shown in table 1. The zero-point energy is the main measure of the strain in the molecule. It can be seen that all of these are negative, which is a logical consequence of locking the molecule in a bicyclo[2.2.2]octane-like conformation. This does however not take into account the entropy factor of having four molecules on the left and only two on the right. Adjusting for this gives the Gibbs free energy shown. Unfortunately, these are still negative (favouring the open form) for the two molecules synthesis was attempted for, but positive once deprotonation happens. They are also positive for phosphorus. Cage formation being unfavourable may mean intramolecular reaction stops after either forming the linear product or monocyclic product, but with these chlorines still available for further reaction, intermolecular reactions are a likely continuation.

Some additional interesting values can be extracted from the optimized structures through bond lengths and angles (table 2). When the N−E−N-angles are measured, it can be seen that

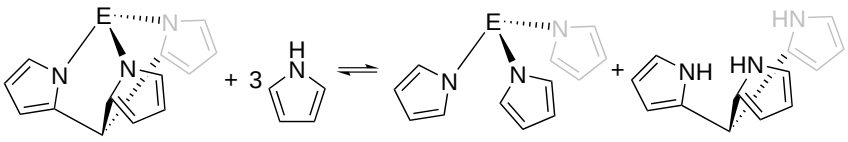

8a E = SiH
8b E = SiCl
8c E = Si^-
8d E = P

9a E = SiH
9b E = SiCl
9c E = Si^-
9d E = P

Scheme 7: *Equilibrium used for strain energy calculations, varying the nitrogen-bound group.*

Compounds	$\Delta E_{\text{Zero-point}}$ (kcal/mol)	ΔG (kcal/mol)
8a and **9a**	−23.4599	−3.3686
8b and **9b**	−24.3958	−4.7435
8c and **9c**	−9.0423	+10.8211
8d and **9d**	−10.9655	+9.2031

Table 1: *Strain energies for compounds **8a**–**d**.*

Compound	N−E−N (°)	N−E (Å)
9a	109.729	1.750
8a	100.730	1.754
Difference	8.999	
9b	109.727	1.740
8b	101.668	1.745
Difference	8.059	
9c	96.753	1.873
8c	90.400	1.874
Difference	6.352	
9d	100.192	1.745
8d	94.437	1.745
Difference	5.756	

Table 2: *Selected angles and distances for compounds **8a**–**d** and **9a**–**d**, and the differences in angles between open compound and cage-like compound.*

the angles for the Si^{-}-structures are remarkably close to 90°. This indicates there is nearly no hybridisation on this silicon atom. Rather the bonds are formed with orbitals of high p-character which allows the lone pair to occupy the s-type orbital. This notion of high p-character is reinforced by the large bond distance when compared to the structures with E = SiH or SiCl, since p-type orbitals' maximum electron density is further away from the nucleus than for an sp^3-type orbital. In the open compounds for the hydrogen- and chloro-substituted silane, they are instead very close to the ideal tetrahedral angle, showing a near-perfect sp^3-hybridisation. This can be explained by the lack of a lone pair and lack of steric hindrance between the substituents (the compounds adapt a propellor-like conformation). The exchange of a substituent for a lone pair with phosphorus and the silanide immediately decrease the angles, in accordance with VSEPR theory.

The difference in angles between the open structure and cage-like structure can also be considered. The open structure can be seen as having the "ideal" angles for this compound, while the cage forces them to be slightly different. In all cases, the angles in the cage are smaller than those in the open structure. It can also be seen that both reactions with a negative Gibbs free energy difference (respectively **9a** and **8a** and **9b** and **8b**) the difference in angles is greater than in those with a positive Gibbs free energy difference. While the relationship is not linear, it is a good indication that the difference in the angles in the open compound compared with the cage-like compound is a good measure of strain in the molecule.

3.5. DFT: varying the lower atom

The second series of calculations was used to give an indication whether or not this strain can be alleviated by changing the lower ring group, which has a CH in **1**. Desired here is not only to have low strain for the silanide as in the previous section, but also for the hydrosilane. Both silicon and phosphorus are bigger than carbon which may help alleviate this strain. For these equilibria, the methyl groups have been placed back onto the pyrrole ring. These may now be important for sterics, as one of the linkers tried has a substituent bigger than hydrogen. Pyrrole is still expected to behave in a similar fashion to indole in this system.

The compounds and equilibrium used are shown in scheme 8, and the results are given in table 3. Again, all zero-point energies are negative, while for the anion (**10d,e,f**) all Gibbs free energies are positive. The Gibbs free energy for the silane with a phosphorus bridging group (**10b**) is also positive, but this compound may give problems when binding to the metal, as phosphorus's lone pair may bind instead.

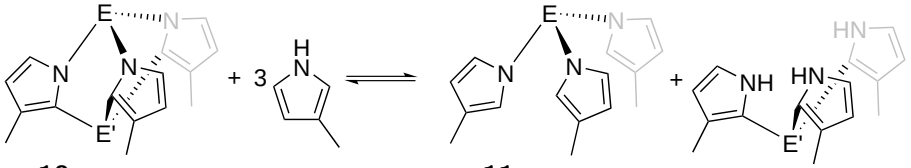

10a E = SiH, E' = CH
10b E = SiH, E' = P
10c E = SiH, E' = SiMe
10d E = Si^-, E' = CH
10e E = Si^-, E' = P
10f E = Si^-, E' = SiMe

11a E = SiH
11b E = Si^-

Scheme 8: *Equilibrium used for strain energy calculations, varying both the nitrogen-bound group and the lower bridging group.*

Reaction	$\Delta E_{\text{Zero-point}}$ (kcal/mol)	ΔG (kcal/mol)
10a and **11a**	−22.9756	−2.0012
10b and **11a**	−15.8422	+3.7178
10c and **11a**	−25.9698	−4.9200
10d and **11b**	−8.6541	+12.5785
10e and **11b**	−2.4798	+16.1726
10f and **11b**	−15.9835	+5.0933

Table 3: *Strain energies for compounds **10a–f**.*

Compound	N-E-N avg	N-E avg
10a	100.832	1.752
Difference	8.918	
10b	103.502	1.751
Difference	6.248	
10c	104.288	1.755
Difference	5.462	
10d	90.406	1.872
Difference	6.465	
10e	92.735	1.869
Difference	4.136	
10f	94.101	1.876
Difference	2.770	
11a	109.750	1.749
11b	96.872	1.871

Table 4: *Selected (average) angles and distances for **10a–f** and **11a,b**, and differences between open and cage-like compounds.*

Again comparing the angles in the ring, it can be seen that the decision to remove the methyl groups for the calculations done in section 3.4 was justified. Comparing the angles of the analogous compounds with and without methyl groups, the biggest difference in angles is found in the open silanide (**9c** and **11b** at 0.12°). This shows the deformation caused by the methyl groups is very small.

The trend for bond angles and energies indicated for **8a–d** continues for **11a–b** and **10a–f**. Again, the angles for the anions are very close to 90°, the N−E bond lengths are much greater than for the neutral Si−H, and the lone pair occupies an orbital relatively low in energy with large s-character.

Here, the differences in angles show less correlation with energies. For the silanide with methylsilane bottom group the angle difference is only 2.8°, while its associated energy is the least favourable amongst the silanides. This higher energy may be caused by steric interaction between the methyl group on the bottom silicon and the three methyl groups on the pyrroles adjacent to it, which is greater in the cage-like molecule than in the free ligand, which can adopt a propellor-like structure to minimize this steric hindrance.

3.6. DFT: methylene bridges in the cage

As a final set of structures, methylene bridges were added between the indoles and the bottom carbon. The idea here is similar to that presented in the previous section, in that increasing the size of the bottom bridging group may result in a less strained system for the hydrosilane, perhaps making it synthesisable.

The equilibrium and compounds used are shown in scheme 9, and the energies are given in table 5. It is set up completely analogously to the previous two.

Interesting here is that the Gibbs energy for all compounds except the unmodified hydrosilane is positive, and the zero-point energy is negative. This is due to the different number of molecules on either sides of the arrow. All hydrosilanes with extra methylene bridge however have more positive Gibbs and zero-point energy than the parent molecule, which means they favour the caged compound more. Important here is that the molecule with a single extra bridge has a higher stabilisation for the silanide than the parent molecule, while also stabilising the hydrosilane. This compound would be an interesting synthesis target. The rest of the molecules with extra methylene bridges destabilise the silanide. While the molecule with two extra methylene bridge also still has a very much positive Gibss energy for the silanide, it is less positive than

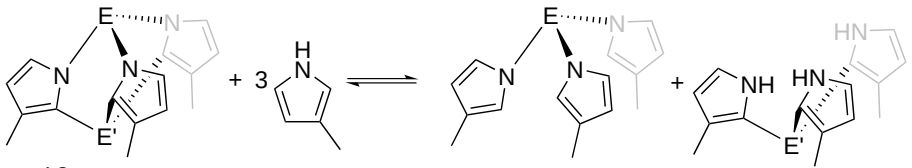

10a E = SiH, E' = CH
12a E = SiH, E' = $HCCH_2$
12b E = SiH, E' = $HC(CH_2)_2$
12c E = SiH, E' = $HC(CH_2)_3$
10d E = Si^-, E' = CH
12d E = Si^-, E' = $HCCH_2$
12e E = Si^-, E' = $HC(CH_2)_2$
12f E = Si^-, E' = $HC(CH_2)_3$

11a E = SiH
11b E = Si^-

Scheme 9: *Equilibrium used for the effect of methylene bridges on the strain energies.*

Reaction	$\Delta E_{\text{Zero-point}}$ (kcal/mol)	ΔG (kcal/mol)
10a and **11a**	−22.9756	−2.0012
12a and **11a**	−15.4528	+5.3672
12b and **11a**	−15.4590	+5.9903
12c and **11a**	−19.2817	+2.9615
10d and **11b**	−8.6541	+12.5785
12d and **11b**	−6.9287	+14.9176
12e and **11b**	−13.1382	+8.5963
12f and **11b**	−20.8131	+0.4058

Table 5: *Strain energies for compounds **10a,d** and **12a–f**.*

the parent molecule. This may still be an interesting molecule to synthesise. The molecule with three extra methylenes is very destabilised in the silanide form and only slightly stabilised in the hydrosilane and is therefore not a useful target.

While actual synthesis of the molecule with a single extra methylene in the bridge may not prove as straightforward as the original target **1**, based on the results presented here it seems a very interesting target and may allow the synthesis of both the hydrosilanes and the silanide.

4. Conclusions

Synthesis of both both the hydrosilane and chorosilane of tris(3-methylindol-2-yl-1-ide)methane did not succeed in all conditions attempted. Synthesis of the phosphorus analogue has succeeded following literature procedure. DFT indicates the reason is the large strain in the cage, which may lead to polymerisation instead of cage formation. A new synthesis target using a 1,1,2-tris(3-methylindol-2-yl-1-ide)ethane scaffold has been proposed.

Deprotonation and metallation of trispyrrolylsilane also did not succeed.

5. Experimental

All reactions except the synthesis of **1** were performed under an atmosphere of dry nitrogen using standard Schlenk and glovebox techniques. All reagents were purchased from commercial sources and used as received unless stated otherwise. THF was distilled over sodium/benzophenone before use, degassed by bubbling nitrogen through it and stored over molecular sieves. Pyrrole and triethylamine were stirred over CaH_2 overnight, vacuum transferred and degassed before use. Triethylamine was also stored over molecular sieves. Hexane and toluene were dried using an MBRAUN MB SPS-80 solvent purification system and degassed before use. Tetrachlorosilane was degassed before use by three freeze-pump-thaw cycles. All other reagents were used as recieved. ^{1}H-, ^{13}C- and ^{31}P-NMR-spectra (resp. 400, 100 and 161 MHz) were recorded on a Varian AS400 or an Agilent MRF400 spectrometer at 25 °C. Chemical shifts are reported relative to TMS using the residual solvent resonance as internal standard for hydrogen and carbon, and relative to 85 % phosphoric acid as external standard for phosphorus. Infrared spectra were recorded using a Perkin Elmer Spectrum One FT-IR spectrometer equipped with a general liquid cell accessory.

Density functional theory results were obtained using the Gaussian 09 software package [36], using the B3LYP functional and the 6-31g(d) basis set for all atoms. The structures were

optimized without any symmetry restraints, except for **10a–f** and **11a–b** which include the methyl groups. These were optimized within C_3-symmetry. Frequency analysis was performed for all calculations, where the absence of a negative frequency indicated a minimum was reached. Surfaces are drawn to isovalue 0.06 a.u..

5.1. Tris(3-methylindol-2-yl)methane (1)

Procedure from ref [26]. Skatole (15.27 g, 0.116 mmol) was added to methanol (25 mL) giving a suspension. To this suspension $HC(OEt)_3$ (6.4 mL, 0.038 mmol) was added, immediately dissolving the skatole. After addition of H_2SO_4 (6 drops), the inside of the flask was scratched with a spatula and the mixture was heated to 60 °C for two hours. After cooling down, it was filtered and and the dark solid washed with MeOH. The resulting green powder was obtained in 12.6 g (82 %) yield, and was pure enough for further reactions. ^{1}H-NMR (400 MHz, $CDCl_3$), $\delta = 2.12$ (s, 9H, Me), 6.15 (s, 1H, $C_{bridge}H$), 7.10 (m, 6H, Ar-H), 7.16 (m, 3H, Ar-H), 7.51 (d, 3H, $^3J_{HH} = 8.1$ Hz, Ar-H), 7.67 (s, br, 3H, NH). $^{13}C\{^1H\}$-NMR (100 MHz, $CDCl_3$), $\delta = 8.5$ (Me), 33.8 (bridging), 109.0, 111.2, 118.7, 119.8, 122.2, 129.7, 131.7, 135.5 (aromatics).

5.2. Phosphorus tris(3-methylindol-2-yl)methane (6)

Procedure from ref [28]. Tris(3-methylindol-2-yl)methane (1.002 g, 2.48 mmol) was suspended in dry THF (18 mL) and triethylamine (1.1 mL, 7.90 mmol) was added, turning the solution orange. This was cooled to approximately −78 °C. PCl_3 (0.25 mL, 2.86 mmol) was added. After addition the cold bath was removed. This was refluxed for 24 hours. After cooling down, it was filtered, washed with THF (6×3 mL) until the filtrate and residue were colourless. The THF was removed in vacuo and the solid suspended in 10 mL cold technical methanol and filtered in air. It was then washed with cold methanol (4×2.5 mL) and cold hexanes (4×2.5 mL). This gave crude product **6** (0.637 g, 59.5 %). Purity is estimated by comparing the integrals of product peaks with those of the other peaks in ^{1}H-NMR, which gives an 83 % purity. This is enough to unambiguously assign the spectrum. ^{1}H-NMR (400 MHz, $CDCl_3$), $\delta = 2.38$ (s, 9H, CH_3), 5.89 (s, 1H, $C_{bridge}H$), 7.10 (t, 3H, $^3J_{HH} = 7.5$ Hz, H5), 7.21 (t, 3H, $^3J_{HH} = 7.6$ Hz, H6),7.40 (d, 3H, $^3J_{HH} = 7.8$ Hz, H4), 7.65 (d, 3H, $^3J_{HH} = 8.1$ Hz, H7). $^{13}C\{^1H\}$-NMR (100 MHz, $CDCl_3$), $\delta =$ 8.5, 31.5, 109.1, 110.3 (d, $^3J_{PC} = 4.0$ Hz), 119.4, 120.9, 122.9, 130.1 (d, $^3J_{PC} = 4.4$ Hz), 134.6, 137.1 (d, $^2J_{PC} = 19.7$ Hz). ^{31}P-NMR (161 MHz, $CDCl_3$), $\delta = 21.46$.

5.3. Lithium tris(3-methylindol-2-yl-1-ide)methane (5)

In THF was dissolved **1** (498 mg, 1.24 mmol) and cooled to −100 °C. To this purple solution *n*-butyllithium was added (2.325 mL, 1.6 M, 3.72 mmol), turning the solution a bright orange/yellow immediately. Upon complete addition a precipitate formed. It was allowed to slowly heat up to room temperature overnight. The solvent was then removed. No further purification was done, and no yield was determined. ^{1}H-NMR (400 MHz, C_6D_6), $\delta = 1.06$ (s), 2.80 (s),3.07 (s), 6.73 (s), 7.6 (br). Upon addition of H_2O/AcOH the spectrum of **1** was regenerated. Reaction with D_2O gave the spectrum of **1** minus the pyrrole peaks, and no coupling in the carbon spectrum.

5.4. 2a using triethylamine (failed)

In THF was dissolved **1** (1.00 g, 2.49 mmol) and cooled to −78 °C. Triethylamine (1.24 mL, 8.89 mmol) was added, turning the solution pink. This colour was removed with the first few

drops of trichlorosilane (0.25 mL, 2.47 mmol), but on full addition it turned an opaque yellow. The cold bath was removed and a reflux condenser added. It was refluxed for two hours. A small sample was taken and dried for NMR, which showed large amounts of starting material, so an additional 2 mL of triethylamine and 1 mL of trichlorosilane was added to force the reaction to occur. This was allowed to reflux overnight. Again ^{1}H-NMR was taken, in addition to TLC's. Both indicated no reaction.

5.5. 2a using NaH (failed)

NaH (95.8 mg, 3.99 mmol) was suspended in THF. The solution was cooled down to −25 °C.**1** (498 mg, 1.2 mmol) was added. No bubbles were observed, but the suspension turned yellow-green. The cold bath was removed and the mixture left to stir for two hours. At this point it was cooled down −78 °C and trichlorosilane (0.118 mL, 1.16 mmol) was added. It was left to slowly heat up to room temperature overnight. The THF was removed in vacuo and ^{1}H-NMR was taken in benzene-d_6. No aromatic protons were visible at both room temperature or approximately 80 °C.

5.6. 2a using nBuLi (failed)

In THF was dissolved **1** (501 mg, 1.24 mmol) and cooled down to −100 °C. To this purple solution *n*-butyllithium (2.4 mL, 1.6 M, 3.84 mmol) was added, turning the solution yellow-green. This was left to stir for 30 minutes, after which the cold bath was removed and the solution allowed to warm up. The cold bath was placed back (90 °C) and trichlorosilane (1.3 mL, 1.29 mmol) added. In about half an hour the solution turned opaque and it was allowed to slowly warm up overnight. The solvent of the then clear-green solution was removed in vacuo, and NMR taken. This showed a lot of uninterpretable peaks. In an attempt to clean this up, toluene was added and refluxed for 20 hours. It then formed a brown liquid and a white solid. NMR showed no peak in the silane region and unclear peaks in the aromatic and aliphatic regions, mainly resembling **1**.

5.7. 2a using tris(dimethylamino)silane (failed)

In toluene (approx. 25 mL) was suspended **1** (505 mg, 1.25 mmol). Tris(dimethylamino)silane (0.20 mL, 1.03 mmol) was added, turning the white suspension pinkish. This was heated to 100 °C and left there for half an hour. Bubble-formation was observed during approximately three minutes. The mixture was then heated to reflux overnight. The toluene was removed in vacuo and a ^{1}H-NMR taken of the pinkish solid. Here, the region between 4 and 6 ppm is empty and the NMR resembled **1**.

5.8. 2a using tris(dimethylamino)silane and base catalysis (failed)

Lithium hexamethyldisilazane (24.7 mg, 0.12 mmol) was dissolved in toluene. This solution was added to 1.00 g **1** (2.48 mmol), and the Schlenk tube washed with some more toluene. To this mixture 0.55 mL tris(dimethylamino)silane (2.75 mmol) was added and heated to 100 °C and kept there for two hours. It was then refluxed overnight, the solvent removed and starting material (**1**) recovered as shown by ^{1}H-NMR.

5.9. 2b using $SiCl_4$ (failed)

Tetrachlorosilane (11 mg, 0.064 mmol) and **5** (18.4 mg, 0.047 mmol) were mixed in benzene-d_6. ^{1}H-NMR after one hour indicated a reaction and ^{1}H-NMR after 6 days gave a lot of uninterpretable peaks. Attempts to equilibriate the mixture by heating to 100 °C had no effect.

5.10. 2b using nBuLi (failed)

In toluene was suspended **1** (1.00 g, 2.48 mmol). *n*-butyllithium (4.65 mL, 1.6 M, 7.44 mmol) was added at −78 °C. This bright orange powder in a yellow liquid was heated to 100 °C to ensure completion. The solution turned red after one hour. It was allowed to cool down overnight. Tetrachlorosilane (0.30 mL, 2.62 mmol) was added and the solution brought back to reflux for one day. A sample of the liquid phase was taken for ^{1}H-NMR, which showed a lot of uninterpretable peaks. The liquid was filtered off, a sample of the solid extracted with deuterated DCM and filtered. This ^{1}H-NMR indicated starting material.

5.11. Trispyrrolylsilane (4)

Procedure from [15]. Pyrrole (8.5 mL, 0.123 mmol) and triethylamine (20 mL, 143 mmol) were added to THF (approx. 50 mL). This mixture was cooled to −78 °C, upon which trichlorosilane (4.1 mL, 40 mmol). Five minutes after addition, the cold bath was removed and left to stir for half an hour. Approximately 50 mL hexane was added and the suspension filtered. The filtrate was dried in vacuum. The product was purified by distillation. Trispyrrolylsilane was isolated in 0.1943 g (36 %) yield. ^{1}H-NMR (400 MHz, C_6D_6), $\delta = 5.53$ (s, 1H, SiH), 6.33 (t, 6H, $^3J_{HH} = 2.0$ Hz, β-H) 6.56 (s, 6H, $^3J_{HH} = 2.0$ Hz, α-H). ^{13}C{^{1}H}-NMR (100 MHz, C_6D_6), $\delta = 113.9$, 123.7.

5.12. Lithium trispyrrolylsilanide using nBuLi (failed)

4 (0.19 g, 0.85 mmol) was dissolved in THF. This was brought to −78 °C and *n*-butyllithium (0.55 mL, 1.6 M, 0.88 mmol) was added. This mixture was allowed to warm up overnight. A sample was taken and prepared for NMR, which showed a variety of peaks, indicating some decomposition.

5.13. Sodium trispyrrolylsilanide (failed)

4 (18.4 mg, 0.065 mmol) was dissolved in thf-d_8. A small amount of sodium was added and the mixture stirred overnight. This was filtered into an NMR-tube and measured (^{1}H-NMR). This showed at least three products, possibly more.

5.14. Iron trispyrrolylsilylide using iron pentacarbonyl(failed)

Iron pentacarbonyl (14 μl, 0.106 mmol) and **4** (19.2 mg, 0.084 mmol) were mixed in benzene-d_6. ^{1}H-NMR showed no reaction, even after heating to 80 °C overnight.

5.15. Iron trispyrrolylsilylide using iron(II) chloride (failed)

Iron(II) chloride (8.3 mg, 0.065 mmol) and **4** (13.0 mg, 0.057 mmol) were mixed in benzene-d_6 with a small amount of thf-d_8. No reaction was observed in ^{1}H-NMR.

Number	**13** (mg/mmol)	**4** (mg/mmol)	PPh_3 (mg/mmol)
1	19.1/0.032	0	0
2	19.4/0.033	15.6/0.069	0
3	22.4/0.038	15.0/0.066	18.3/0.070

Table 6: *Small-scale test for synthesis of iron trispyrrolylsilylide.*

5.16. $FeCl_2 \cdot 1.5$THF (7)

Procedure adapted from ref [34]. A soxhlet was filled with dry iron(II) chloride (20.90 g, 165 mmol) and THF (150 mL). This was left to reflux for two weeks. Due to problems with solvent leaks, THF had to be refilled several times. The product is slightly soluble in THF and accumulated in the bottom flask. At the end of the reaction, the THF was filtered off and the solid washed with THF until the liquid was no longer yellow. The desired product was obtained in 14 % yield (5.4416 g). IR (ν, cm^{-1}, KBr): 1026 (s), 878 (s).

5.17. Dimesityliron (13)

Procedure from ref [35]. In a mixture of THF (130 mL) and dioxane (25 mL), **7** (5.42 g, 23.1 mmol) was suspended. This was cooled to −30 °C and kept under −25 °C while mesitylmagnesium bromide solution (50 mL, 1.0 M) was slowly added with stirring and occasional shaking. When the addition was complete, the mixture was allowed to come up to room temperature and left to stir for two hours. The thick deep-red slurry was filtered and all solvent removed in vacuo. The solid was dissolved in ether (150 mL). This solution was then concentrated to approximately 20 mL and upon filtration deep-red crystals of Fe_2Mes_4 were isolated (1.58 g, 2.69 mmol). These heat- and air-sensitive crystals were stored at −20 °C in closed Schlenk tubes. ^{1}H-NMR (400 MHz, C_6D_6), δ = −6.68 (s, 6H), 10.21 (s, 6H), 17.96 (s, 3H), 17.96 (s, 3H), 21.42 (s, 3H), 23.17 (s, 2H), 23.70 (2H).

5.18. Lithium trispyrrolylsilanide using LiHMDS

4 (19.1 mg, 0.084 mmol) and lithium hexamethyldisilazane (16.1 mg, 0.096 mmol) were mixed in benzene-d_6 in an NMR tube. Two new peaks were observed. ^{1}H-NMR (400 MHz, C_6D_6), δ = 6.37, 6.79. To check for deprotonation or substitution IR was used in THF (resp. 13.0 mg, 9.0 mg). A silane peak was observed, therefore reaction was incomplete or in equilibrium.

5.19. Iron trispyrrolylsilylide using dimesityiron and triphenylphosphine(failed)

Three NMR-tubes in benzene-d_6 were prepared as in table 6. These were kept in an oil bath at 50 °C, with ^{1}H-NMR and $^{13}C\{^1H\}$-NMR taken the next day and the two days thereafter. Day 1: two peaks appeared in tube 2 at −11.9 and −12.3 ppm. On day 2 these shifted to −15.4 and −15.8 ppm. On day 3 these peaks also appeared in tube 1, so no complexation took place.

Part III.
Aryliminopyrrole

6. Introduction

Because of the failure of the synthesis as described in the previous part, we decided to investigate a different type of silylene instead. The eventual goal of the project to make high-field ligands has not changed.

Some interesting known compounds are shown in figure 8. All of them use $\varkappa^3$-ligands. Two examples of pentacoordinate silanes are shown in figures 8a and 8b. These both use a similar amino-imine framework to coordinate to silicon, although they respectively use an aminomethylpyridine and a pyrrolylimide, and they both add another anionic ligand, respectively an oxygen [16] or a sulfur [24]. There is also a hexacoordinate silane known, shown in figure 8c. None of these silanes have two easily removable groups, and they are therefore not very interesting starting materials for the synthesis of silylenes.

If however the third coordinating group (either the oxygen or the sulfur) is removed, two groups of compounds can be synthesised: pentacoordinate ligand-alkyl-chlorohydrosilane or a hexacoordinate bisligand-chlorohydrosilane using trichlorosilane, or the corresponding dichlorosilanes with tetrachlorosilane. The first group can be deprotonated with additional loss of a chloride to the silylene, while the last group can be reduced. These are interesting synthesis targets.

6.1. Aim

In scheme 10 the route to the silylene is summarised. The condensation reaction in the first step is well known [37, 38, 39]. This ligand can then be reacted with either trichlorosilane or tetrachlorosilane to form the hexacoordinate silylene. This compound may or may not have the imines coordinated to silicon. The actual silylene may be synthesised by reduction of the hexacoordinate silicon by for example potassium graphite. This may again not have one or both of the imines bound to silicon. If it does not, this free imine can bind to iron for extra stabilisation.

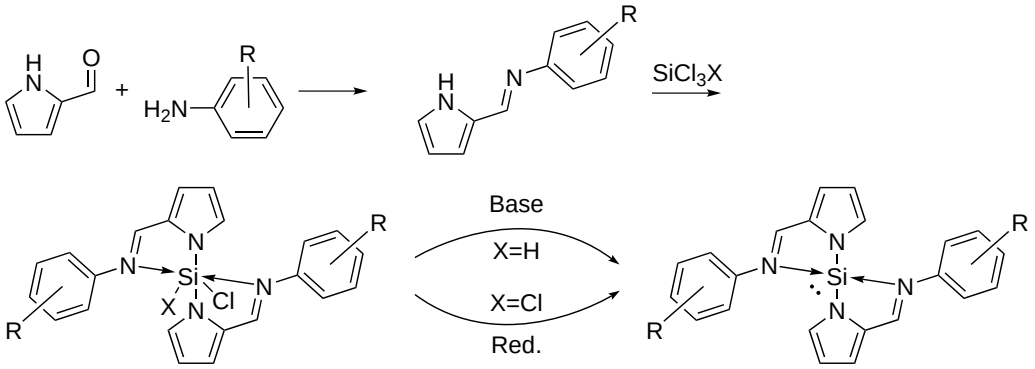

Scheme 10: *The general plan for the synthesis of novel N-heterocyclic silylene precursors, R is H or 2,6-diisopropyl. X is H or Cl.*

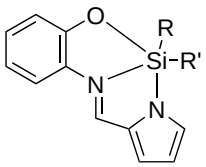

(a) *Pentacoordinate silane using κ^3-ONN-ligand from [16]. R, R' are a variety of alkyls and aryls.*

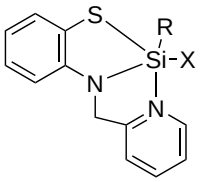

(b) *Pentacoordinate silane using one κ^3-SNN-ligands from [24]. R is alkyl, X is (pseudo)halide.*

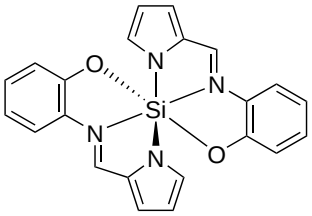

(c) *Hexacoordinate silane using two κ^3-ONN-ligands from [16].*

Figure 8: *Some known compounds similar to the target.*

7. Results and discussion

Two ligands were chosen for experimental work: N-phenyl-2-formiminopyrrole **14** and N-(2,6-diisopropylphenyl)-2-formiminopyrrole **15**. These ligands were synthesised according to literature procedures. The reactions of these ligands with both trichloro- and tetrachlorosilane were also performed. Additionally, some experiments were done on the reduction of the products of those reactions, and DFT was utilised to explain certain observations and predict differences between the ligands. For the DFT-work, N-mesityl-2-formiminopyrrole was added as a ligand, with bulk inbetween **14** and **15**.

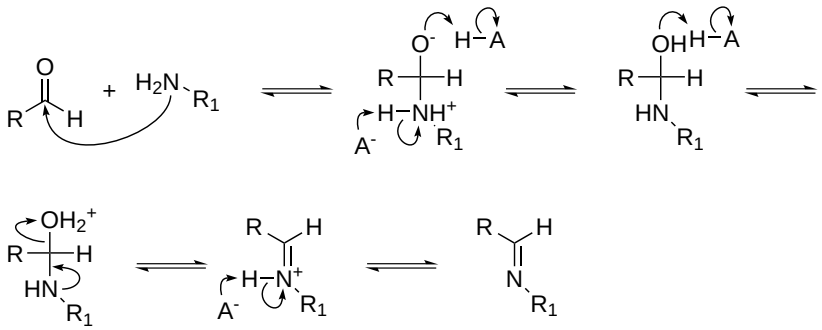

Scheme 11: *The general mechanism for imine formation.*

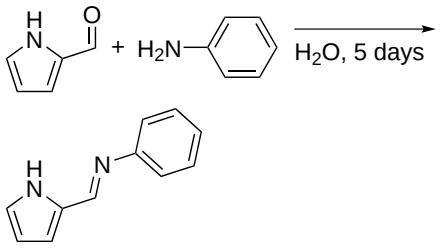

14

Scheme 12: *Synthesis of N-phenyl-2-formiminopyrrole **14**.*

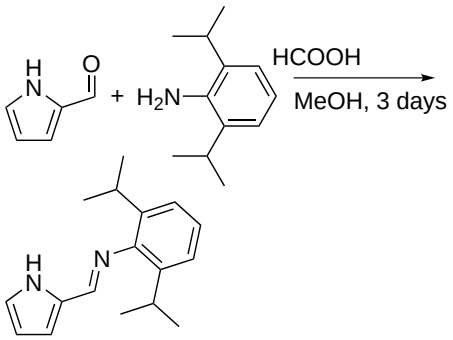

15
59% (crude)

Scheme 13: *Synthesis of N-(2,6-diisopropyl)-2-formiminopyrrole **15**.*

7.1. Ligand synthesis

The general mechanism for imine formation is given in scheme 11 [30]. The amine attacks the aldehyde and forms a tetrahedral intermediate. After some proton shifts and protonation of the resulting alcohol by an acid catalyst, water is expelled and an iminium cation is formed. This can then regenerate the acid catalyst and give the product.

Generally for imines, the reverse reaction readily takes place. Here it does not, which is easily seen as one of the imine syntheses given here uses water as a solvent, while the other uses technical (wet) methanol and no water removal. The apparent lack of reactivity towards water can be explained by noting that both products are solid and will precipitate. This solid is still in equilibrium with both dissolved product and starting materials, giving a less than quantitative yield.

The phenyl-substituted ligand **14** has been synthesised [38] as shown in scheme 12, by simply mixing the two starting materials in water and stirring for 5 days. This results in ^{1}H-NMR and ^{13}C{^{1}H}-NMR pure product. No yield has been determined.

The diisopropylphenyl-substituted **15** was synthesised by direct reaction of analogous starting materials as in the synthesis of **14**, but with methanol as solvent (scheme 13). It was also recrystallised from methanol.

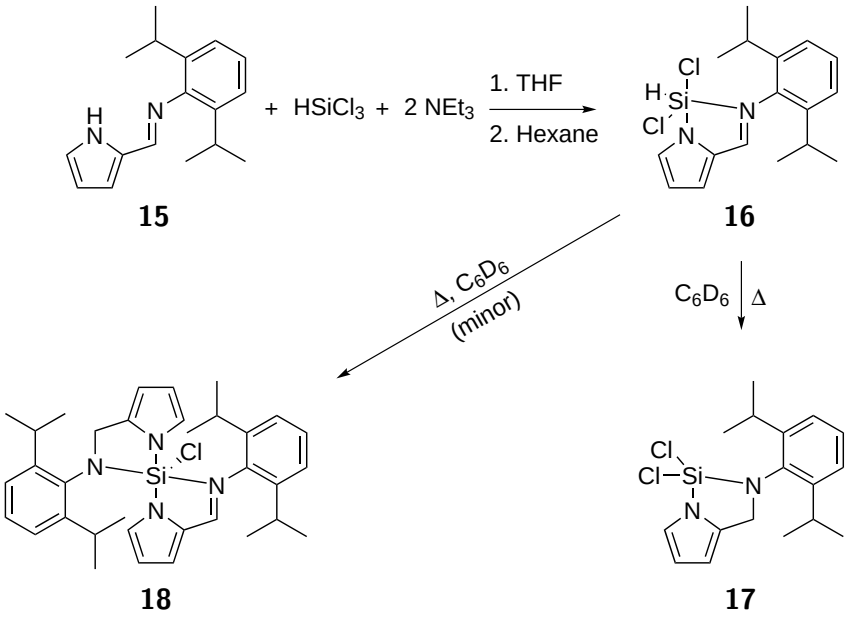

Scheme 14: *Reaction scheme of the reaction of **15** with $HSiCl_3$, and the proposed structures of the first and final products.*

7.2. Reactions with $HSiCl_3$

7.2.1. Diisopropyl-based ligand

The reaction of **15** with $HSiCl_3$ is quite well-defined and gives some interesting products. It can very nicely be followed by ^{1}H-NMR and ^{29}Si$\{^1$H$\}$-NMR. The crude product is light-sensitive, and even in solid state it will react to a complex mixture. If it is kept cold and dark it can be stored without any issues. Two main products are observed: **16**, **17**, in addition to some impurities.

The first product **16** is most likely the direct adduct of the ligand with trichlorosilane (figure 14, **16**, top NMR in figure 9). This has a single type of isopropyl group due to symmetry, but two different methyl groups with hindered rotation around the Ph$-$CHMe$_2$-bond, due to steric interaction with the chlorines and hydrogen on silicon. Having two different methyl groups on the isopropyl can be confirmed using COSY. It also has an Si$-$H-bond, making it possible to see a peak in ^{29}Si$\{^1$H$\}$-NMR without the addition of a relaxation agent at -92.8 ppm. Additionally, this peak splits into a doublet in non-decoupled ^{29}Si-NMR with $^1J_{\mathrm{HSi}} = 383$ Hz.

After taking an ^{29}Si$\{^1$H$\}$-NMR, involving a night of measuring, a new ^{1}H-NMR was taken, which is the middle spectrum in figure 9. The peaks corresponding to the first product have gone down, and one new major set of peaks emerges. This can be sped up by keeping the NMR-tube at elevated temperatures.

At the end of the reaction, another product **17** is formed. This again has a single peak for the tertiary carbon in the isopropyl group, and two different methyl groups. It also has a singlet at 4.2 ppm. HSQC combined with DEPT-135 shows this peak is instead due to a CH$_2$-group. Additionally, analysis of the COSY shows the pyrrole system is intact. ^{29}Si$\{^1$H$\}$-NMR of the mixture indicates it not to have a hydrogen bonded to silicon because a relaxation agent (Cr(acac)$_3$) is required to get any peaks. This is confirmed using non-decoupled ^{29}Si-NMR, where the peak remains a singlet. Therefore, it seems likely the structure of this compound

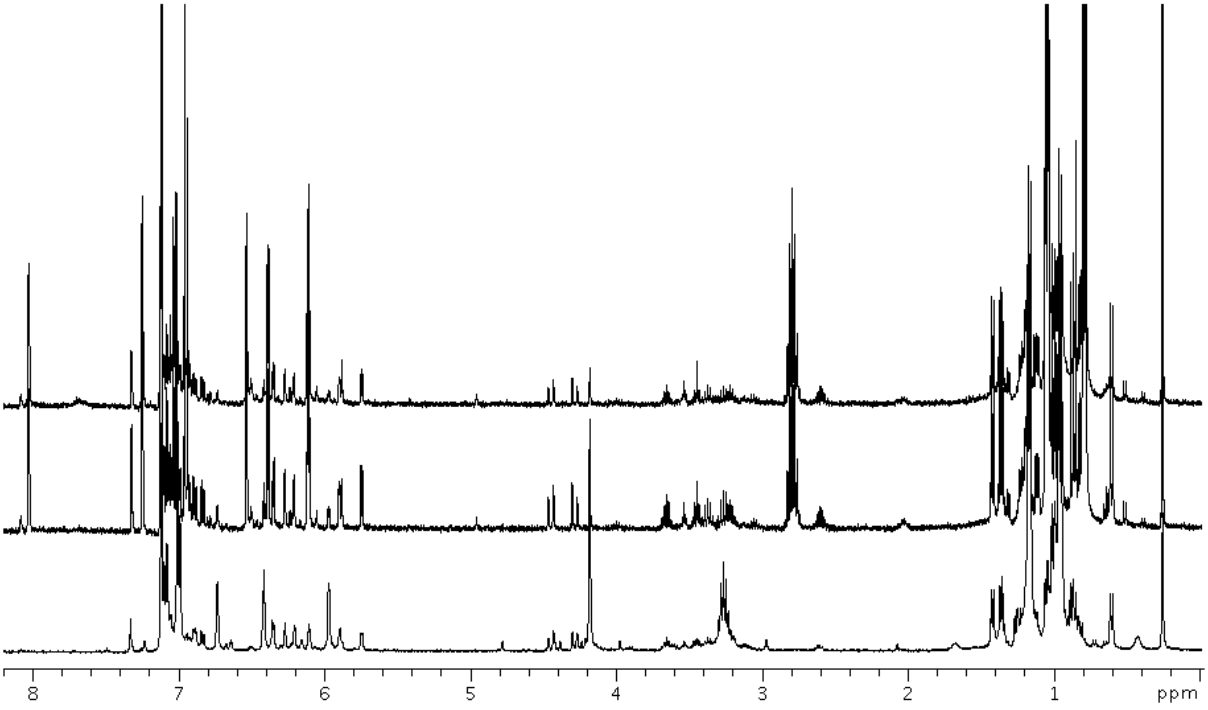

Figure 9: *Evolution of products visible in ^{1}H-NMR. Top to bottom: directly after reaction, one night in the NMR-tube, four days at 80°*C.

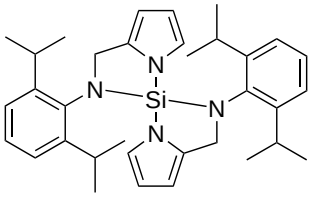

Figure 10: *Structure of **19** as used for DFT.*

Compound	^{1}H (DFT)	^{1}H (Exp)	^{29}Si (DFT)	^{29}Si (Exp)	Si−H (DFT)	Si−H (Exp)[a]
16	6.82	7.00[b]	−81.56	−92.80	−400	383
17	-	-	−31.74	−36.70[c]	-	-
19	-	-	−56.51	−36.70[c]	-	-
18	-	-	−116.87	−116.5	-	-

[a] No sign has been determined.
[b] Only singlet of required size. NMR crowded.
[c] Highest peak in ^{29}Si{^{1}H}-NMR.

Table 7: *Results for calculated NMR-shifts and couplings of the expected products of the reaction of **15** with trichlorosilane.*

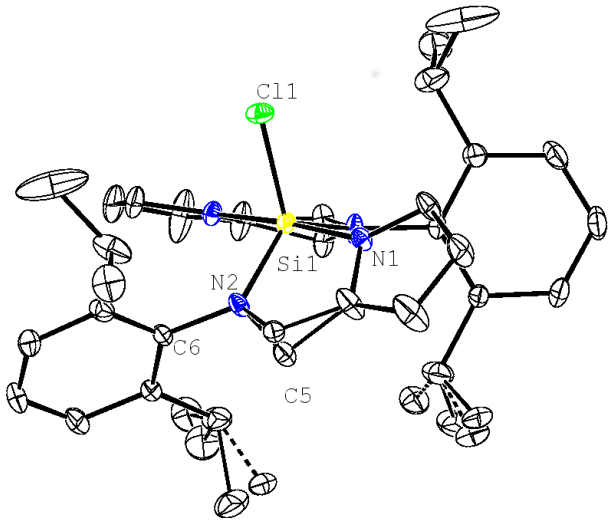

Figure 11: *Ellipsoid plot of **18**. Hydrogen atoms are omitted for clarity. As drawn, the molecule is C_2-symmetrical. Ellipsoids are drawn at the 50 % probability level. For C5, two positions are visible, one constrained to a single C(5)−N(2)-bond, one to a double bond.*

C(5)−N(2)	1.3890(19)[a]
C(6)−N(2)	1.4457(16)

[a] Unconstrained

Table 8: *Selected bond lengths (Å) for compound **18**.*

either the hydrosilylated product **17**, or the doubly substituted product **19** shown in figure 10. These two compounds cannot be distinguished by a qualitative interpretation of the silicon chemical shift or by peak count and multiplicities in ^{1}H-NMR, but can by calculating chemical shifts by DFT. It can be seen in table 13 that while the calculated shift of **17** is within 5 ppm of the experimental value, the calculated shift of **19** is 20 ppm below the experimental value. This is much greater than any compound used for calibration, which are consistently calculated to be 5 to 10 ppm higher (see section 10.1). This is evidence against **19** being the final compound, and it seems likely that **17** is formed instead.

The clearly-visible side product in NMR has a somewhat more complex structure. There are two doublets visible at both sides of 4.4 ppm. These can be shown in COSY to couple only with each other, with $^{n}J_{HH} = 14$ Hz. This coupling constant is typical for either a *trans*-alkene coupling, which is very unlikely here, or a geminal coupling. Additionally HSQC shows that both hydrogens belong to the same carbon.

In order to have a geminal coupling, the two hydrogens must be diastereotopic, which means the compound as a whole must be chiral. There are two similarly-sized pyrrole systems visible in ^{1}H-NMR, and these also match with the two doublets. Unfortunately some other contaminants are of similar size.

On crystallisation attempts, one of the contaminants formed crystals and was analysed by single-crystal X-ray diffraction, and its structure is shown in figure 11.

The structure shown in figure 11 fits the NMR-data mentioned above with some additional interpretation. It is intentionally shown with two differently constrained C(5)−N(2)-bonds. When fitted without this constraint, a bond which is halfway between fully single (for example C(6)−N(2)) and fully double (as in **20** or free ligand [40]) is obtained. These can be treated

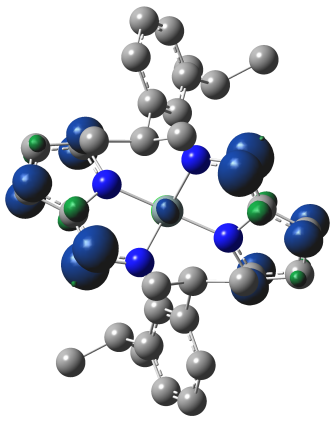

Figure 12: *Spin-density plot of the radical interpretation of the crystal structure shown in figure 11. Hydrogen atoms omitted for clarity. View aligned with the Si−Cl-bond.*

in two ways: as an unordered crystal structure with one single and one double bond, or as a ligand-centred radical. This last compound (spin-density shown in figure 12) would most likely not give an interpretable NMR-signal, and while it cannot be ruled out, the model using one single and one double bond fits the available NMR-data.

One last indication that this compound is indeed formed can be gained through ^{29}Si{^{1}H}-NMR. When this spectrum of final mixture is recorded, a peak appears at −116.87 ppm. This peak is typical for a pentacoordinate silane, shows no splitting in proton-coupled ^{29}Si-NMR, and is the only clearly-visible peak in the pentacoordinate region. It is also very close to the calculated chemical shift of −116.5 ppm. While this is still not proof, it is evidence for **18** having the suggested SiLL'Cl-structure with one reduced and one unreduced ligand.

The rest of the mixture is more intricate than originally thought: taking an ^{29}Si{^{1}H}-NMR with Cr(acac)$_3$ of the final mixture reveals at least 7 peaks, possibly 9.

7.2.2. Phenyl-based ligand

Reaction of the phenyl-based ligand with trichlorosilane unfortunately does not give a clean reaction, or even a clean set of reactions. ^{1}H-NMR shows a multitude of aromatic peaks, and also 5 to 7 in the aliphatic region, and some 4 in the same region as the CH_2NRSi obtained above. It is therefore proposed that hydrosilylation is occurring at least to some extent. Unfortunately the origin of the peaks in the aliphatic region is unknown.

7.3. Reactions with $SiCl_4$

$SiCl_4$ shows reactivity the other way around: a very clean reaction with the phenyl-based ligand, and an incomplete reaction with a not fully identified product using the diisopropylphenyl-based ligand.

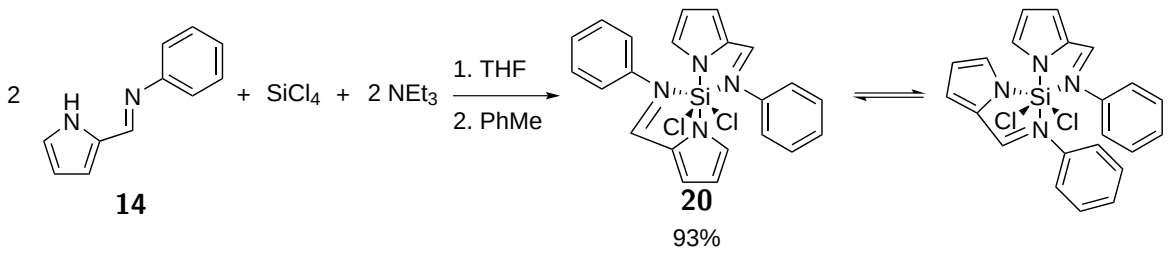

Scheme 15: *Synthesis of* cis*-dichlorodi(N-phenyl-2-formiminopyrrolide)-λ⁶-silane (**20**) and its isomer.*

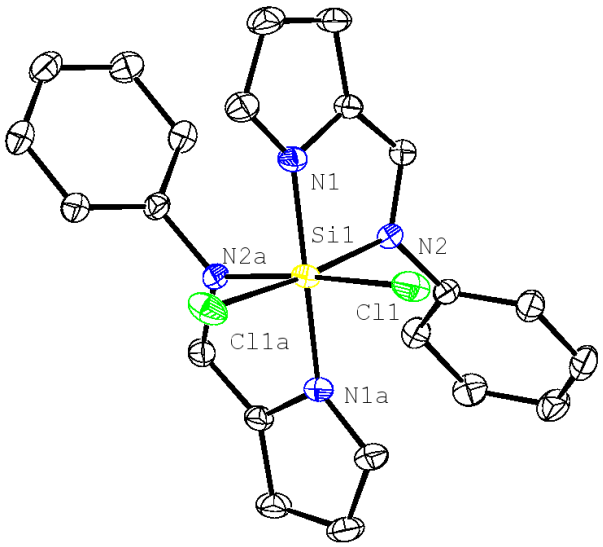

Figure 13: *Ellipsoid plot of the Λ-isomer of **20**. The unit cell also contains one Δ-isomer. Hydrogen atoms are omitted for clarity. The molecule is C_2-symmetrical. Ellipsoids are drawn at the 50% probability level.*

7.3.1. Phenyl-based ligand

The hexacoordinate silane **20** was synthesised by the global route shown in scheme 15. The three reactants were mixed in THF at −70 °C, after which they were stirred at room temperature overnight. The THF was evaporated under reduced pressure, and replaced with toluene. This solution was filtered and the toluene evaporated at 60 °C under reduced pressure. This yields the product **20**.

Table 9 shows the Si−Cl and Si−N bond lengths obtained from the crystal structure shown in figure 13. These are quite typical for N_4Cl_2-coordinated silicon. For example, silicon bis(amidinato) complexes have average Si−Cl bond lengths of 2.191 Å [41] and 2.1936 Å [42] (average because these compounds do not have the C_2-symmetry found here). These also respectively have axial Si−N bond lengths of 1.839 Å and 1.8703 Å, and equatorial Si−N-lengths of 1.915 Å and 1.9024 Å, close to the measured lengths. When the sums of the angles around silicon are calculated, it can be seen these are very close to the planar 360°, showing the environment around silicon is almost perfectly octahedral.

While in the solid state the product of this reaction only contains the same isomer found using X-ray analysis, a second set of peaks is visible in ^{1}H-NMR when this solid is dissolved in benzene-d_6 and left to stand (equilibrium mixture ^{1}H-NMR in figure 14). The equilibrium is

Si(1)−N(1)	1.8410(10)
Si(1)−N(2)	1.9540(9)
Si(1)−Cl(1)	2.1770(4)
N(1)−Si(1)−N(2)	82.42(4)
N−N−N−Cl	359.82
N−N−Cl−Cl	360.42

Table 9: *Selected bond lengths (Å), angles (°) and sum of plane angles (°) around silicon for compound **20**.*

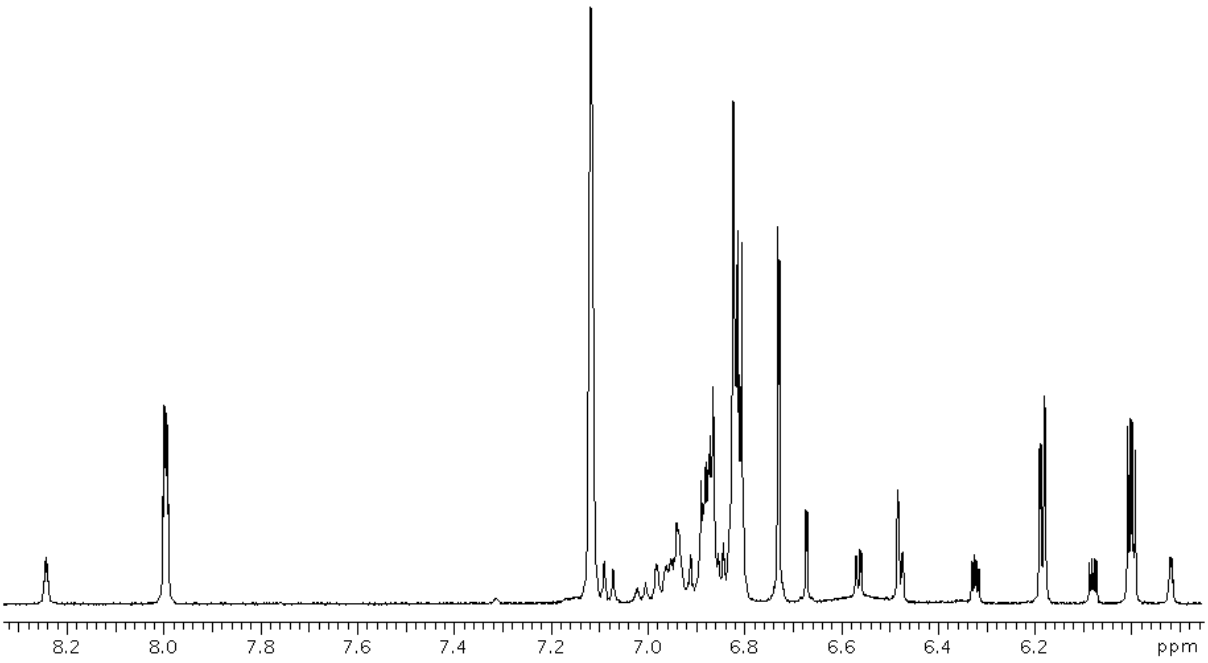

Figure 14: *^{1}H-NMR of the equilibrium mixture of **20** and its isomer in benzene-*d_6.

Isomer	ΔG (kcal/mol)	K
20	0[a]	1[a]
all-cis	1.903173169	$4.0200 \cdot 10^{-02}$
5-coordinate	19.15735369	$8.92263 \cdot 10^{-15}$
4-coordinate	10.69796879	$1.42688 \cdot 10^{-08}$

[a] By definition.

Table 10: *Energy differences and equilibrium constants for different isomers of **20**. Energies and equilibrium constants given for **20** ⇌ Isomer at 298 K.*

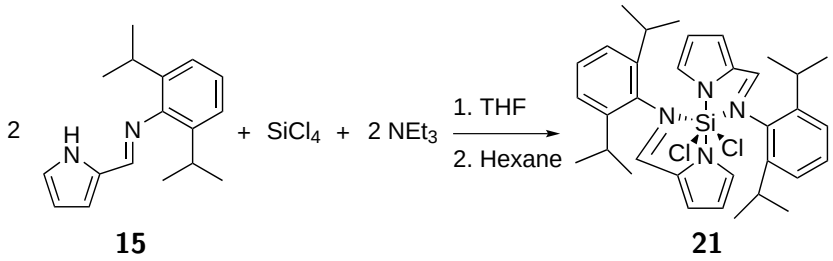

15 **21**

Scheme 16: *Reaction of **15** with tetrachlorosilane. Expected product (by analogy with **20**) shown.*

an approximately 10:1 mixture. An approximately 1:1 mixture is obtained in synthesis when the heating step (see experimental) is omitted. When this is left to stand for approximately a week or heated to 60 °C to 80 °C for three days the same 10:1 mixture is obtained. There is no free ligand visible, ruling out a dissociation. The number of peaks visible in ^{1}H-NMR means it cannot be a symmetrical species, which eliminates the 4-coordinate isomer with both imines dissociated. It therefore seems likely that either a 5-coordinate species is formed, or that in a 6-coordinate species one of the ligands has its pyrrolyl and imine positions swapped. DFT was used to calculate the relative energies and equilibrium constants.

From these equilibrium constants, it is not unresonable to assume that the unknown isomer seen in ^{1}H-NMR is the *all-cis* isomer. It is however reversibly formed, so it may be possible that the five-coordinate form is accessible as an intermediate. This way the isomer encountered in the solid state may dissociate one imine, enter a distored trigonal bipyramidal geometry, rotate along the pyridine-silicon bond, and recoordinate the imine on the other side. This intermediate is not visible in ^{1}H-NMR. The high energy of the five-coordinate species may also explain the slow equilibration. The four-coordinate isomer, already ruled out on the basis of the ^{1}H-NMR-spectrum, is also much higher in energy than both **20** and its *all-cis* isomer.

7.3.2. Diisopropyl-based ligand

This reaction (scheme 16) is relatively clean by ^{1}H-NMR. Two major compounds are visible, one of which increases heavily when more ligand is added. The other clearly shows two different isopropyl groups. Additionally, when this same reaction is done with only one equivalent of ligand the same spectrum is obtained. Unfortunately, this does not prove whether the mono-ligand trichlorosilane or bis-ligand dichlorosilane is formed. While it can be proven with X-ray diffraction, crystallisation attempts did not succeed. Therefore, the product is drawn in analogy with **20**.

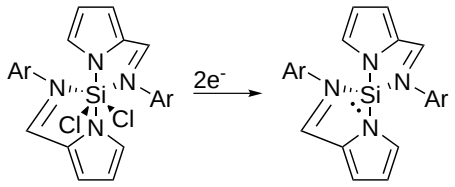

Scheme 17: *General expected product for reduction.*

7.4. Reduction attempts

After successful synthesis of **20**, the next step is reduction to the silylene (scheme 17). Two reductants were used: sodium naphtalide and potassium graphite. The latter has been successfully employed in the reduction of chlorosilanes to silylenes [43, 44]. Potassium metal can also reduce chlorosilanes [10, 45, 46, 47, 13] but for ease of use potassium graphite was employed here.

Two solvents were tried in the reduction of **20**: THF as a coordinating solvent which may facilitate a faster reaction by coordinating the potassium, and toluene which may give a cleaner reaction by not coordinating the potassium. The difference in reaction speed was experimentally verified. After a reaction period of four days, using ^{1}H-NMR, it was determined that the reaction using toluene still contained mostly starting material while the reaction using THF did not show any. Even after 10 days, this was still the case. Unfortunately the reaction with THF did show peaks in the aliphatic region, indicating side reactions. Here, detection of paramagnetic products by ^{1}H-NMR was attempted, but none were found. It is possible that paramagnetic material was still formed, but that its peaks are broad enough to be undetectable by NMR. A new reaction was set up using THF, which was checked after one day, where there was still mainly starting material present.

7.5. DFT: reduction predictions

Two types of reduction can be imagined for the hexacoordinate silanes: reduction to a lone pair on silicon (singlet state), or single-electron reduction of both ligands (overall triplet state). While triplet carbenes exist, the difference in energy between the 3s and 3p orbital is much more than the electron pairing energy and therefore triplet silylenes are unknown. These can both quite simply be modeled by DFT.

Three things must be taken into account here. First of all, only the fully reduced, non-stabilised structures are considered here. It is not unreasonable to assume that instead one chlorine stays in the structure and forms a negatively-charged species. Comparison of these structures with those without a chlorine is not straightforward. Additionally, single-electron reduction of one of the ligands to form a negatively-charged radical might be the most stable structure. These are also not considered. Finally, the energy differences given here are somewhat unreliable because comparing a closed-shell system with an open-shell system is problematic. The trend predicted here will howver most likely be correct.

Table 11 shows the energies related to the equilibrium shown in scheme 18. The preference for the singlet silylene state increases as the bulk of the aryl ring decreases. This can be explained by looking at the distances between closest *ortho*-carbons as a measure for the difference in steric hindrance. While in all cases these are closer together in the silylene, using the phenyl ligand allows them a much less hindered triplet state, hence a greater difference, which is reflected in the energy. On the other hand, the mesityl and diisopropylphenyl-based ligands have a much

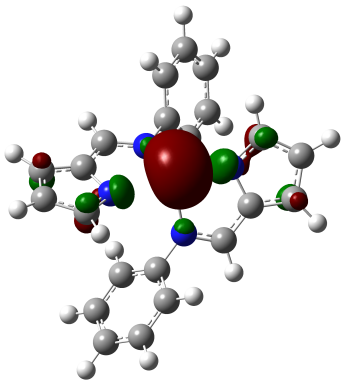

(a) *Singlet silylene from **20**, HOMO (lone pair) shown.*

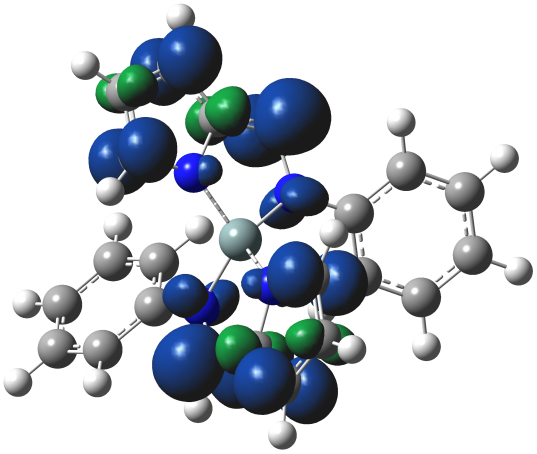

(b) *Triplet state spin density of the silylene from **20**.*

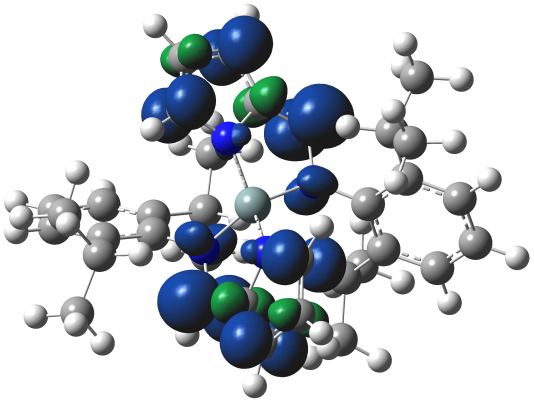

(c) *Triplet state spin density of the silylene from **21**.*

Figure 15: *The singlet silylene derived from **20**, and comparison of the spin density plots of the triplet states derived from **20** and **21**.*

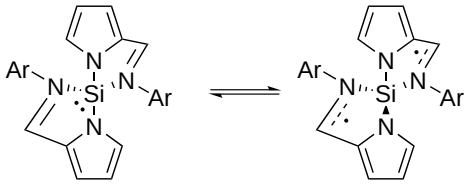

Scheme 18: *The equilibrium used for determining the favoured reduction for non-stabilised hexacoordinate silanes.*

Ar =	$\Delta E_{Zero\text{-}point}$	ΔG	Distance difference [a]
Ph	−11.7877	−12.3888	0.9108
Mes	−1.1306	−0.5622	0.2888
Dip	2.4358	2.3661	0.3058

[a] Singlet larger in all cases.

Table 11: *Energy differences in kcal/mol and difference in difference between ortho-carbons in Åfor the equilibrium shown in scheme 18.*

lesser distance difference which leads to a disfavoured triplet state.

For all ligands, the spin density resides exclusively on the pyrrolylimine π-system (figures 15b and 15c show phenyl and diisopropylphenyl respectively). The orientation required of the aryl rings prevents overlap of it with the pyrrolylimine, which could stabilise the triplet state.

8. Conclusions

Both N-phenyl-2-formiminopyrrolyl (pfp) and N-(2,6-diisopropylphenyl)-2-formiminopyrrolyl (dipfp) have been synthesised according to literature prodedure. The hexacoordinate silance $Si(pfp)_2Cl_2$ has also been successfully synthesised. For the second ligand, a mixture of free ligand and hexacoordinate silane were obtained using trichlorosilane, and using tetrachlorosilane first a direct 1:1 adduct $Si(dipfp)Cl_2H$ was observed, which hydrosilylates into the final product $SiLCl_2$, where L is (2,6-diisopropylphenyl)(2-pyrrolylmethyl)amide..

Reduction of $Si(pfp)_2Cl_2$ was unsuccessful. DFT calculations showed that the biradical formed by placing two electrons in the ligands may be more stable than the silylene.

9. Outlook

Reduction of the silylenes can be attempted. Results on **20** with potassium graphite are not yet conclusive. Other methods of reduction could be tried, for example potassium metal or lithium naphtalide.

With silanes containing a labile hydrogen, deprotonation may be the easiest route. This hydrogen need not be situated on silicon. Deprotonation of the hydride **16** and the amide **17** may result in the same product.

Of course, after the silylenes have been obtained, reaction with an iron precursor may be attempted. If the silylenes are unstable in free form, oxidative addition to iron would be an option, without external reductant or base. There exist also iron precursors like tetramesityldiiron [35] which might act as their own base.

For ligand scope, the mesityl-substituted ligand may be synthesised [48] and reaction with tri- and tetrachlorosilane attempted. Its properties can be compared to the predictions done by DFT.

10. Experimental

All reactions involving air-sensitive reagents or products were done under an atmosphere of nitrogen using standard Schlenk and glovebox techniques. All reagents were purchased from commercial sources and used as received unless stated otherwise. THF was distilled over sodium/benzophenone before use, degassed by bubbling nitrogen through it and stored over molecular sieves. Triethylamine was stirred over CaH_2 overnight, vacuum transferred and degassed before use. Triethylamine was also stored over molecular sieves. Hexane and toluene were dried using an MBRAUN MB SPS-80 solvent purification system and degassed before use. Tetrachlorosilane was degassed before use by three freeze-pump-thaw cycles. Graphite was dried by placing it at 150 °C under high vacuum overnight. All other reagents were used as recieved. ^{1}H- and ^{13}C{^{1}H}-NMR-spectra (resp. 400 and 100 MHz) were recorded on either a Varian AS400 or an Agilent MRF400 spectrometer and reported relative to TMS using the residual solvent resonance as internal standard. All ^{29}Si{^{1}H}-NMR- and ^{29}Si-NMR-spectra (75 MHz) were recorded on a Varian AS400 spectrometer relative to TMS using hexamethyldisiloxane as external reference. All NMR-spectra were recorded at 25 °C unless stated otherwise.

10.1. Computational methods

Density functional theory results were obtained using the Gaussian 09 software package [36], using the B3LYP functional and the 6-31g(d) basis set for all atoms for optimisations, and the IGLO-III basis set for subsequent NMR calculations. The structures were optimized without any symmetry restraints. Frequency analysis was performed for all calculations, where the absence of a negative frequency indicated a minimum was reached. MO-surfaces are drawn to isovalue 0.06 a.u., spin densities to 0.004 a.u..

For the NMR-calculations, three basis sets were tried: 6-31+G(d,p), IGLO-II and IGLO-III [49], and their accuracy checked with the experimental measurements of the hydrochlorosilane-series, for which all shifts and couplings are known [50]. The calibration data is shown in table 12. Because IGLO-III resulted in values closest to experimental, and all calculations still completed in a reasonable time, this basis set was used. While the couplings are less precise, the SpinSpin method is much faster than the Mixed method.

After this test on the hydrochlorosilanes, the applicability on these penta- and hexacoordinate silanes was determined. For this the previously-synthesised hexacoordinate **20** and compound **22** were used, where the last one is shown in figure 16 and was synthesised within the group [51]. These shifts and couplings are shown in table 13, and are within 0.5 ppm for hydrogen, 12 ppm for silicon and 4 Hz for the Si−H-coupling.

10.2. N-phenyl-2-formiminopyrrole (14)

Procedure from ref [38]. 2-formylpyrrole (5.01 g, 52.6 mmol) and aniline (5.0 mL, 55 mmol) were mixed in 50 mL water. This was stirred for 5 days. Filtration and washing with water yielded ^{1}H-NMR and ^{13}C{^{1}H}-NMR pure **14**. It was dried under vacuum for approx. 24 hours. NMR consistent with literature [38]. ^{1}H-NMR (400 MHz, $CDCl_3$), $\delta = 8.27$ (1H, s, HC=N), 7.38 (2H,

Compound	6-31+G(d,p)	IGLO-II	IGLO-III	Experimental
		^{1}H-NMR-shifts		
$HSiCl_3$	6.1572	6.6175	6.5084	6.09
H_2SiCl_2	5.6437	6.2302	6.0267	5.32
H_3SiCl	4.8736	5.4024	5.201	4.48
H_4Si	3.5216	3.851	3.6934	3.14
		^{29}Si{^{1}H}-NMR-shifts		
$SiCl_4$	18.0384	10.1378	6.0684	−18.55
$HSiCl_3$	19.5349	9.3063	4.4286	−9.52
H_2SiCl_2	12.3888	−2.3585	−6.8497	−16.83
H_3SiCl	−17.2454	−38.3992	−42.2287	−50.87
H_4Si	−78.7189	−108.8125	−112.4755	−95.84
		H−Si-coupling		[a]
$HSiCl_3$	−380.47	−385.60	−368.44	377.5
H_2SiCl_2	−292.80	−296.89	−282.77	308.0
H_3SiCl	−242.17	−242.17	−229.95	257.4
H_4Si	−208.76	−208.76	−197.58	203.0

[a] Experimental coupling constant is absolute value.

Table 12: *Calibration data for NMR-calculations. All shifts in ppm relative to TMS, calculated within the respected basis set. Couplings in Hz. Using the Mixed option for 6-31+G(d,p) and IGLO-II, and the SpinSpin option for IGLO-III. Experimental data in thf-*d_8*, from [50].*

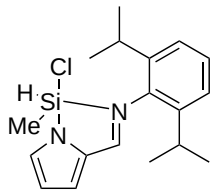

22

Figure 16: *Structure of **22** as used for DFT.*

Compound	^{1}H (DFT)	^{1}H (Exp)	^{29}Si (DFT)	^{29}Si (Exp)	Si−H (DFT)	Si−H (Exp)[a]
20	-	-	−171.63	−177	-	-
22	6.37	6.11	−56.87	−65.30	−315.42	312

[a] No sign has been determined.

Table 13: *Results for calculated NMR-shifts and couplings of known and expected compounds.*

t, $^3J_{HH}$ = 7.4 Hz), 7.20 (3H, t, $^3J_{HH}$ = 7.4 Hz), 6.93 (1H, d, $^3J_{HH}$ = 27.7 Hz), 6.70 (1H, d, $^3J_{HH}$ = 3.2 Hz), 6.32-6.28 (1H, m).

10.3. cis-dichlorobis-κ²-(N-phenyl-2-formiminopyrrolide)-λ⁶-silicon (20)

Tetrachlorosilane (1.0 mL, 1.48 g, 8.7 mmol), triethylamine (3.0 mL, 2.72 g, 21.5 mmol) and **14** (3.00 g, 17.6 mmol) were mixed in THF (60 mL) at −70 °C. The mixture was stirred at low temperature for one hour, after which the cold bath was removed and the mixture stirred overnight. From this yellow-white suspension all volatiles were removed under reduced pressure. In order to remove all THF, toluene (10 mL) was added and removed in vacuo, twice. To the resulting solid toluene 600 mL was added, and the suspension filtered. The toluene was reduced in volume to approx. 10 mL at 60 °C by transferring it under static vacuum into an ethanol/liquid nitrogen-cooled Schlenk flask. The remaining toluene was cannula-filtered off, and the yellow solid was the desired product **20** (3.59 g, 8.2 mmol, 93 %). It was contaminated with a low amount (approx. 5 % by NMR) of Et_3NHCl. Crystals suitable for X-ray analysis were grown by diffusion of n-hexane into a solution of **20** in benzene-d_6. The $^{13}C\{^1H\}$-NMR-spectrum was recorded at 60 °C. The $^{29}Si\{^1H\}$-NMR-spectrum was recorded at 70 °C with approx. 10 % $Cr(acac)_3$ as relaxation agent. Peak assignments were done using COSY and HSQC. This compound is air- and water-sensitive, but can be handled in solid state under normal atmosphere for short amounts of time. ^{1}H-NMR (400 MHz, C_6D_6), δ = 6.04 (2H, dd, $^3J_{HH}$ = 3.8 Hz, $^4J_{HH}$ = 2.1 Hz, pyrrole-4), 6.22 (2H, dd, $^3J_{HH}$ = 3.8 Hz, $^4J_{HH}$ = 0.8 Hz, pyrrole-5), 6.76 (2H, d, $^4J_{HH}$ = 0.8 Hz, imine-H), 6.83-6.92 (10H, m, Ph-H), 8.05 (2H, m, pyrrole-3). $^{13}C\{^1H\}$-NMR (100 MHz, C_6D_6), δ = 115.1 (pyrrole-4), 119.6 (pyrrole-5), 124.1 (Ph), 127.1 (Ph), 128.4 (Ph), 130.5 (pyrrole-2), 138.4 (pyrrole-3), 144.3 (Ph 4°, 154.0 (C=N). $^{29}Si\{^1H\}$-NMR (79 MHz, C_6D_6), δ = −170.0. IR (ν, cm^{-1}, ATR): 3121 (w), 3102 (w), 3058 (w), 3032 (w), 1577 (s), 1400 (s), 1043 (m), 749 (m).

10.4. N-(2,6-diisopropyl)phenyl-2-formiminopyrrole (15)

Procedure from [52]. 2-formylpyrrole (1.88 g, 19.7 mmol) and 2,6-diisopropylaniline (3.7 mL, 3.5 g, 20 mmol) were dissolved in methanol (30 mL). Formic acid (0.5 mL) was added as a catalyst. This mixture was stirred over the weekend. The suspension was filtered and washed with cold methanol. This gave the desired product **15** in 59 % yield (2.93 g). This product was recrystallised from hot methanol in 64 % yield, for an overall yield of 37 % (1.86 g). ^{1}H-NMR (400 MHz, C_6D_6), δ = 1.13 (12H, d, $^3J_{HH}$ = 6.9 Hz, Me−H), 3.19 (2H, sept, $^3J_{HH}$ = 6.9 Hz, Ph−$CHMe_2$), 6.08 (1H, dd, $^3J_{HH}$ = 2.6 Hz, $^3J_{HH}$ = 6.5 Hz), 6.12 (1H, m), 6.42 (1H, dd, $^3J_{HH}$ = 1.4 Hz, $^3J_{HH}$ = 3.6 Hz), 7.11-7.19 (2H, m), 7.78 (1H, d, $^3J_{HH}$ = 0.7 Hz), 10.42 (1H, br). $^{13}C\{^1H\}$-NMR (100 MHz, C_6D_6), δ = 23.71, 28.36, 110.38, 117.04, 123.56, 124.19, 124.91, 130.42, 139.04, 149.44, 152.95.

10.5. Dichloro-hydrido-κ²-(N-(2,6-diisopropylphenyl)-2-formiminopyrrolyl)-λ⁵-silicon (16)

Triethylamine (0.41 mL, 2.95 mmol) and **15** (0.5040 g, 1.98 mmol) were dissolved in THF (10 mL) in a brown Schlenk flask. Trichlorosilane (0.21 mL, 1.98 mmol) was added at −75 °C. This was stirred at low temperature for 45 minutes and at room temperature overnight. Hexane (30 mL) was added, the mixture filtered, and the residue washed with two times 10 mL hexane.

This compound was not purified, and the crude reaction mixture is light-sensitive even in solid state. It was stored in the dark at −20 °C. For ^{1}H-NMR, coupling distances and partners are unknown, $3 < n < 5$.

^{1}H-NMR (400 MHz, C_6D_6), δ = 0.83 (6H, Me, d, $^3J_{HH}$ = 6.9 Hz), 1.09 (6H, Me, d, $^3J_{HH}$ = 6.9 Hz), 2.83 (2H, *i*-Pr, sept, $^3J_{HH}$ = 6.9 Hz), 6.15 (1H, pyrrole, dd, $^nJ_{HH}$ = 2.7 Hz, $^nJ_{HH}$ = 3.5 Hz), 6.43 (1H, pyrrole, dd, $^nJ_{HH}$ = 1.0 Hz, $^nJ_{HH}$ = 3.5 Hz), 6.58 (1H, d, $^nJ_{HH}$ = 1.0 Hz), 6.98 (1H, d, $^nJ_{HH}$ = 0.8 Hz), 7.00 (1H, s, Si−H), 7.29 (1H, dd, $^nJ_{HH}$ = 0.8 Hz, $^nJ_{HH}$ = 1.4 Hz). ^{29}Si{^{1}H}-NMR (79 MHz, C_6D_6), δ = −92.8 (d, $^1J_{HSi}$ = 383 Hz).

10.6. Dichloro-κ²-((2,6-diisopropylphenyl)-(pyrrol-2-ylmethyl)amide)-λ⁴-silicon (17)

A sample of **16** in benzene-d_6 was kept at 80 °C in the dark for 4 days.

This compound was not isolated, ^{1}H-NMR data omits phenyl peaks which due to overlap cannot be clearly assigned. Peaks at 6.10, 6.46 and 6.78 ppm were assigned to this compound due to integrals.

^{1}H-NMR (400 MHz, C_6D_6), δ = 1.00 (6H, Me, d, $^3J_{HH}$ = 6.7 Hz), 1.21 (6H, Me, d, $^3J_{HH}$ = 6.7 Hz), 3.31 (2H, *i*-Pr, sept, $^3J_{HH}$ = 6.7 Hz), 4.22 (2H, CH_2, s), 6.10 (1H, m), 6.46 (1H, t, $^3J_{HH}$ = 2.9 Hz), 6.78 (1H, d, $^3J_{HH}$ = 2.3 Hz).

10.7. Chloro-κ²-(N-(2,6-diisopropylphenyl)-2-formiminopyrrolyl)-κ²-((2,6-diisopropylphenyl)-(pyrrol-2-ylmethyl)amide)-λ⁵-silicon (18)

Crystals suitable for X-ray analysis were gained from crude **16** by diffusion of hexane into a THF-solution, diethyl ether into a toluene-solution, and diffusion of dichloromethane out of a dichloromethane/hexane-solution. These were carried out in the dark. All methods gave the same solvent-free unit cell. Unfortunately this compound is air-sensitive and a clean, complete ^{1}H-NMR could not be obtained as the crystals could not be placed back into an oxygen- and moisture-free environment.

^{29}Si{^{1}H}-NMR (79 MHz, C_6D_6), δ = −116.5 (assigned based on coordination and DFT (−116.87)).

10.8. Potassium graphite

Potassium metal (0.88 g, 22.5 mmol) and graphite (2.16 g, 179.8 mmol) were mixed in a Schlenk tube at 120 °C for 2.5 hours under constant stirring until a homogeneous brown powder had formed.

10.9. Reduction of 20

In both THF and toluene (approx. 3 mL) **20** (resp. 106.2 mg, 0.24 mmol and 97.2 mg, 0.22 mmol) and KC_8 (resp. 77.3 mg, 0.57 mmol and 67.7 mg, 0.50 mg) were mixed in a glass vial and left to stir for four days and a ^{1}H-NMR taken. One week later another ^{1}H-NMR was taken.

Part IV.
Conclusions and outlook

11. Conclusions

The aim of the project as described in section 1.6 has been successfully realised.

The aim of the project is the synthesis of pyrrole-based silanes as potential precursors for Si-centred ligands. First, the pyrrole-containing organic moieties will be synthesised. These will then be reacted with a suitable silicon precursor.

12. Outlook

Synthesis of the proposed scaffold 1,1,2-tris(3-methylindol-2-yl)ethane can be attempted, and the product silylated. Afterwards removal of either a proton or a chloride (depending on the method of silylation) can be tried.

Reduction of the obtained $Si(pfp)_2Cl_2$ can be attempted. While unsuccessful here, reduction agents like potassium metal or lithium naphtalide can be used. It appears the time for which the reduction is ran is important, and *in-situ* reduction could be used to monitor the progress by ^{1}H-NMR.

Afterwards, complexation of both the silanide and silylene to iron could be attempted.

Part V.
Appendix

A. Acknowledgements

First of all, I thank Dr. Marc-Etienne Moret for his supervision, for always being available for discussing this spectrum, that result, those energies, and for teaching me most if not all the practical work, ranging from Schlenk techniques to the synthesis of KC_8. You also taught me how to do all those DFT-calculations used in this thesis, which gave some very nice insights.

I would also like to thank Prof. Bert Klein Gebbink for giving me the chance to do my Master thesis in this group. It has given me a clearer view on what I would like to do when I finish my studies.

Dr. Johann Jastrzebski I thank for all his help with the NMR, especially the silicon- and high-temperature NMR, and the help with the interpretation of the more tricky spectra.

Henk Kleijn I don't thank for ESI-MS (for a change), but for his help on the lab with some little things and the discussions about both my research and his own.

I would not have any X-ray structures without Dr. Martin Lutz, thank you for measuring them.

Finally, I would like to thank the OCC group for being always friendly and always helpful.

B. References

[1] Heck, R. F.; Nolley, J. P. *J. Org. Chem.* **1972** 37, 14, 2320.

[2] Tamao, K.; Sumitani, K.; Kumada, M. *J. Am. Chem. Soc.* **1972** 94, 12, 4374.

[3] Milstein, D.; Stille, J. K. *J. Am. Chem. Soc.* **1978** 100, 11, 3636.

[4] Lee, M.-t.; Hu, C.-h. *Organometallics* **2004** 23, 5, 976.

[5] Boehme, C.; Frenking, G. *Organometallics* **1998** 17, 26, 5801.

[6] Bourissou, D.; Guerret, O.; Gabbaï, F. P.; Bertrand, G. *Chem. Rev.* **2000** 100, 1, 39.

[7] Arduengo, A. J.; Harlow, R. L.; Kline, M. *J. Am. Chem. Soc.* **1991** 113, 1, 361.

[8] Arduengo, A. J.; Davidson, F.; Dias, H. V. R.; Goerlich, J. R.; Khasnis, D.; Marshall, W. J.; Prakasha, T. K. *J. Am. Chem. Soc.* **1997** 119, 52, 12742.

[9] Scholl, M.; Ding, S.; Lee, C. W.; Grubbs, R. H. *Org. Lett.* **1999** 1, 6, 953.

[10] Denk, M.; Lennon, R.; Hayashi, R.; West, R.; Belyakov, A. V.; Verne, H. P.; Haaland, A.; Wagner, M.; Metzler, N. *J. Am. Chem. Soc.* **1994** 116, 6, 2691.

[11] West, R.; Denk, M. *Pure Appl. Chem.* **1996** 68, 4, 785.

[12] Driess, M.; Yao, S.; Brym, M.; van Wüllen, C.; Lentz, D. *J. Am. Chem. Soc.* **2006** 128, 30, 9628.

[13] So, C.-W.; Roesky, H. W.; Magull, J.; Oswald, R. B. *Angew. Chem. Int. Ed. Engl.* **2006** 45, 24, 3948.

[14] Zybill, C.; Müller, G. *Angew. Chemie Int. Ed. English* **1987** 26, 7, 669.

[15] Hübler, K.; Roper, W. R.; Wright, L. J. *Organometallics* **1997** 16, 12, 2730.

[16] Gerlach, D.; Ehlers, A. W.; Lammertsma, K. *Z. Naturforsch* **2009** , IV, 1571.

[17] Siriwardane, U.; Islam, M. S.; West, T. A.; Hosmane, N. S.; Maguire, J. A.; Cowley, A. H. *J. Am. Chem. Soc.* **1987** 109, 15, 4600.

[18] Albright, T. A.; Burdett, J.; Whangbo, M. *Orbital interactions in chemistry* Wiley**1985**.

[19] White, M. C. *Science (80-.).* **2012** 335, 6070, 807.

[20] Tamura, M.; Kochi, J. *Synthesis (Stuttg).* **1971** 1971, 06, 303.

[21] Jana, R.; Pathak, T. P.; Sigman, M. S. *Chem. Rev.* **2011** 111, 3, 1417.

[22] Sonogashira, K.; Tohda, Y.; Hagihara, N. *Tetrahedron Lett.* **1975** 16, 50, 4467.

[23] Koch, W.; Holthausen, M. C. *A Chemists Guide to Density Functional Theory* vol. 3 Wiley-VCH, Weinheim, Weinheim**2001** second edi ed.

[24] Kobelt, C.; Burschka, C.; Bertermann, R.; Fonseca Guerra, C.; Bickelhaupt, F. M.; Tacke, R. *Dalton Trans.* **2012** 41, 7, 2148.

[25] Friebolin, H. *Basic One- and Two-Dimensional NMR Spectroscopy* Wiley-VCH, Weinheim, Weinheim**1998** third revi ed.

[26] von Dobeneck, H.; Prietzel, H. *Hoppe-Seylers Zeitschrift für Physiol. Chemie* **1955** 299, Jahresband, 214.

[27] Armbruster, F.; Fernández, I.; Breher, F. *Dalton Trans.* **2009** , 29, 5612.

[28] Barnard, T. S.; Mason, M. R. *Organometallics* **2001** 20, 1, 206.

[29] Hübler, K.; Hübler, U.; Roper, W. R.; Schwerdtfeger, P.; James Wright, L. *Chem. - A Eur. J.* **1997** 3, 10, 1608.

[30] Clayden, J.; Greeves, N.; Warren, S.; Wothers, P. *Organic Chemistry* Oxford University Press, Oxford**2001**.

[31] Ciclosi, M.; Lloret, J.; Estevan, F.; Lahuerta, P.; Sanaú, M.; Pérez-Prieto, J. *Angew. Chem. Int. Ed. Engl.* **2006** 45, 40, 6741.

[32] Gudat, D.; Verkade, J. G. *Organometallics* **1989** 8, 12, 2772.

[33] Appler, H. *J. Organomet. Chem.* **1988** 350, 2, 217.

[34] Kern, R. *J. Inorg. Nucl. Chem.* **1962** 24, 9, 1105.

[35] Klose, A.; Solari, E.; Ferguson, R.; Floriani, C.; Chiesi-Villa, A.; Rizzoli, C. *Organometallics* **1993** 12, 7, 2414.

[36] Frisch, M. J.; Trucks, G. W.; Schlegel, H. B.; Scuseria, G. E.; Robb, M. A.; Cheeseman, J. R.; Scalmani, G.; Barone, V.; Mennucci, B.; Petersson, G. A.; Nakatsuji, H.; Caricato, M.; Li, X.; Hratchian, H. P.; Izmaylov, A. F.; Bloino, J.; Zheng, G.; Sonnenberg, J. L.; Hada, M.; Ehara, M.; Toyota, K.; Fukuda, R.; Hasegawa, J.; Ishida, M.; Nakajima, T.; Honda, Y.; Kitao, O.; Nakai, H.; Vreven, T.; Montgomery, Jr., J. A.; Peralta, J. E.; Ogliaro, F.; Bearpark, M.; Heyd, J. J.; Brothers, E.; Kudin, K. N.; Staroverov, V. N.; Kobayashi, R.; Normand, J.; Raghavachari, K.; Rendell, A.; Burant, J. C.; Iyengar, S. S.; Tomasi, J.; Cossi, M.; Rega, N.; Millam, J. M.; Klene, M.; Knox, J. E.; Cross, J. B.; Bakken, V.; Adamo, C.; Jaramillo, J.; Gomperts, R.; Stratmann, R. E.; Yazyev, O.; Austin, A. J.; Cammi, R.; Pomelli, C.; Ochterski, J. W.; Martin, R. L.; Morokuma, K.; Zakrzewski, V. G.; Voth, G. A.; Salvador, P.; Dannenberg, J. J.; Dapprich, S.; Daniels, A. D.; Farkas, O.; Foresman, J. B.; Ortiz, J. V.; Cioslowski, J.; Fox, D. J. Gaussian 09 Revision A.02.

[37] Bellabarba, R. M.; Gomes, P. T.; Pascu, S. I. *Dalt. Trans.* **2003** 2, 23, 4431.

[38] Grushin, V. V.; Marshall, W. J. *Adv. Synth. & Catal.* **2004** 346, 12, 1457.

[39] Carabineiro, S. A.; Silva, L. C.; Gomes, P. T.; Pereira, L. C. J.; Veiros, L. F.; Pascu, S. I.; Duarte, M. T.; Namorado, S.; Henriques, R. T. *Inorg. Chem.* **2007** 46, 17, 6880.

[40] Gomes, C. S. B.; Suresh, D.; Gomes, P. T.; Veiros, L. F.; Duarte, M. T.; Nunes, T. G.; Oliveira, M. C. a. *Dalton Trans.* **2010** 39, 3, 736.

[41] Karsch, H. H.; Schlüter, P. A.; Reisky, M. *Eur. J. Inorg. Chem.* **1998** 1998, 4, 433.

[42] Junold, K.; Burschka, C.; Bertermann, R.; Tacke, R. *Dalton Trans.* **2010** 39, 39, 9401.

[43] Gehrhus, B.; Hitchcock, P. B.; Pongtavornpinyo, R.; Zhang, L. *Dalton Trans.* **2006** , 15, 1847.

[44] Kong, L.; Zhang, J.; Song, H.; Cui, C. *Dalton Trans.* **2009** 750, 28, 5444.

[45] Gehrhus, B.; Lappert, M. F.; Heinicke, J.; Boese, R.; Blser, D. *J. Chem. Soc. Chem. Commun.* **1995** , 19, 1931.

[46] Gehrhus, B.; Hitchcock, P. B.; Lappert, M. F.; Heinicke, J.; Boese, R.; Bläser, D. *J. Organomet. Chem.* **1996** 521, 1-2, 211.

[47] Heinicke, J.; Oprea, A.; Kindermann, M. K.; Karpati, T.; Nyulászi, L.; Veszprémi, T. *Chem. - A Eur. J.* **1998** 4, 3, 541.

[48] Liu, C.; Zhou, S.; Wang, S.; Zhang, L.; Yang, G. *Dalton Trans.* **2010** 39, 38, 8994.

[49] Kutzelnigg, W.; Fleischer, U.; Schindler, M. *The IGLO-Method: Ab Initio Calculation and Interpretation of NMR Chemical Shifts and Magnetic Susceptibilities* Springer-Verlach, Heidelberg**1990**.

[50] Thorshaug, K.; Swang, O.; Dahl, I. M.; Olafsen, A. *J. Phys. Chem. A* **2006** 110, 32, 9801.

[51] Shu, Z. Master thesis Utrecht University **2014**.

[52] Li, Y.-S.; Li, Y.-R.; Li, X.-F. *J. Organomet. Chem.* **2003** 667, 1-2, 185.

C. Spectra

Spectra given here are given a compound number where applicable, and the section of the experimental they can be found in.

C.1. Compound 1, section 5.1

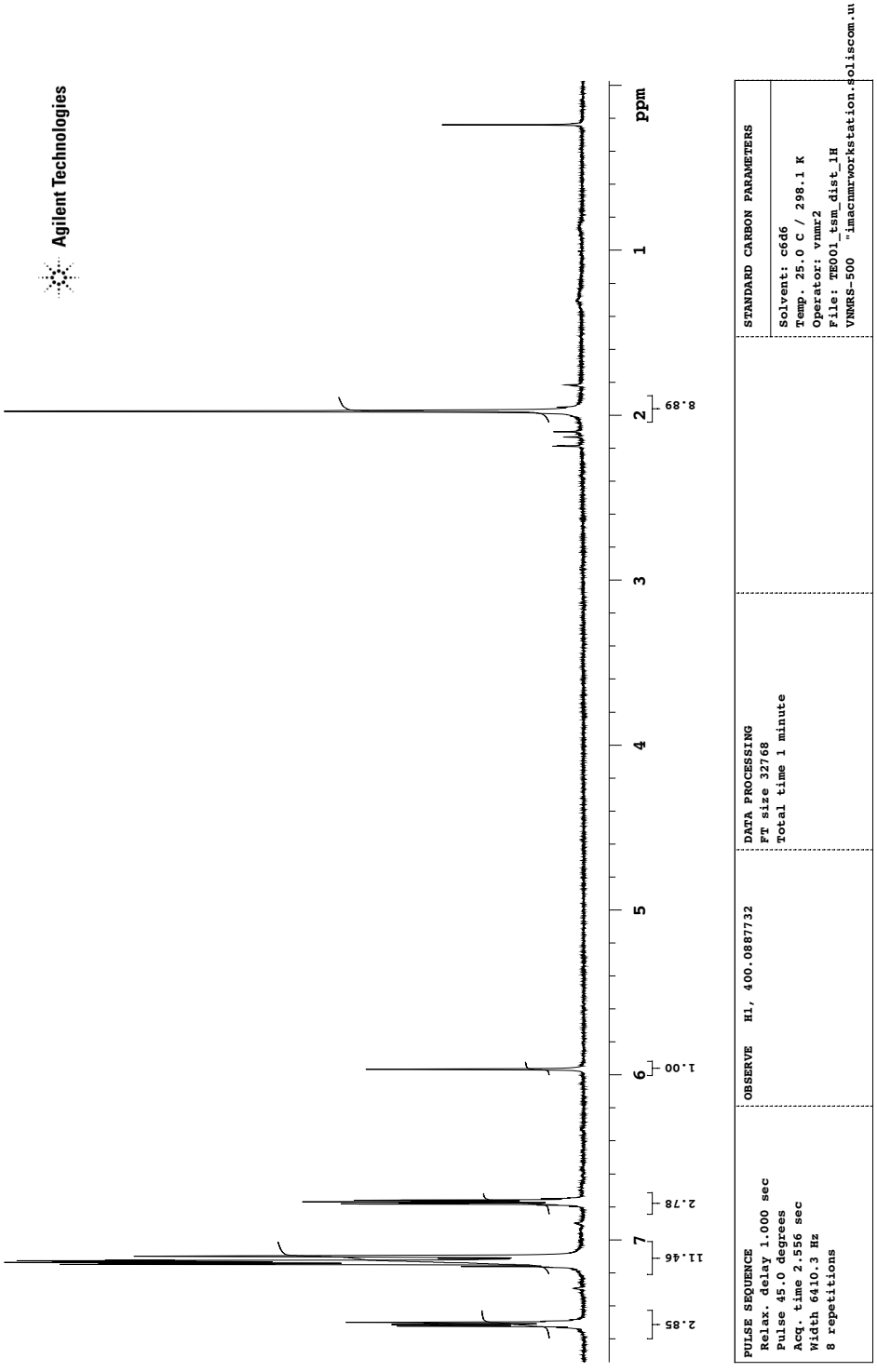

C.2. Compound 6, section 5.2

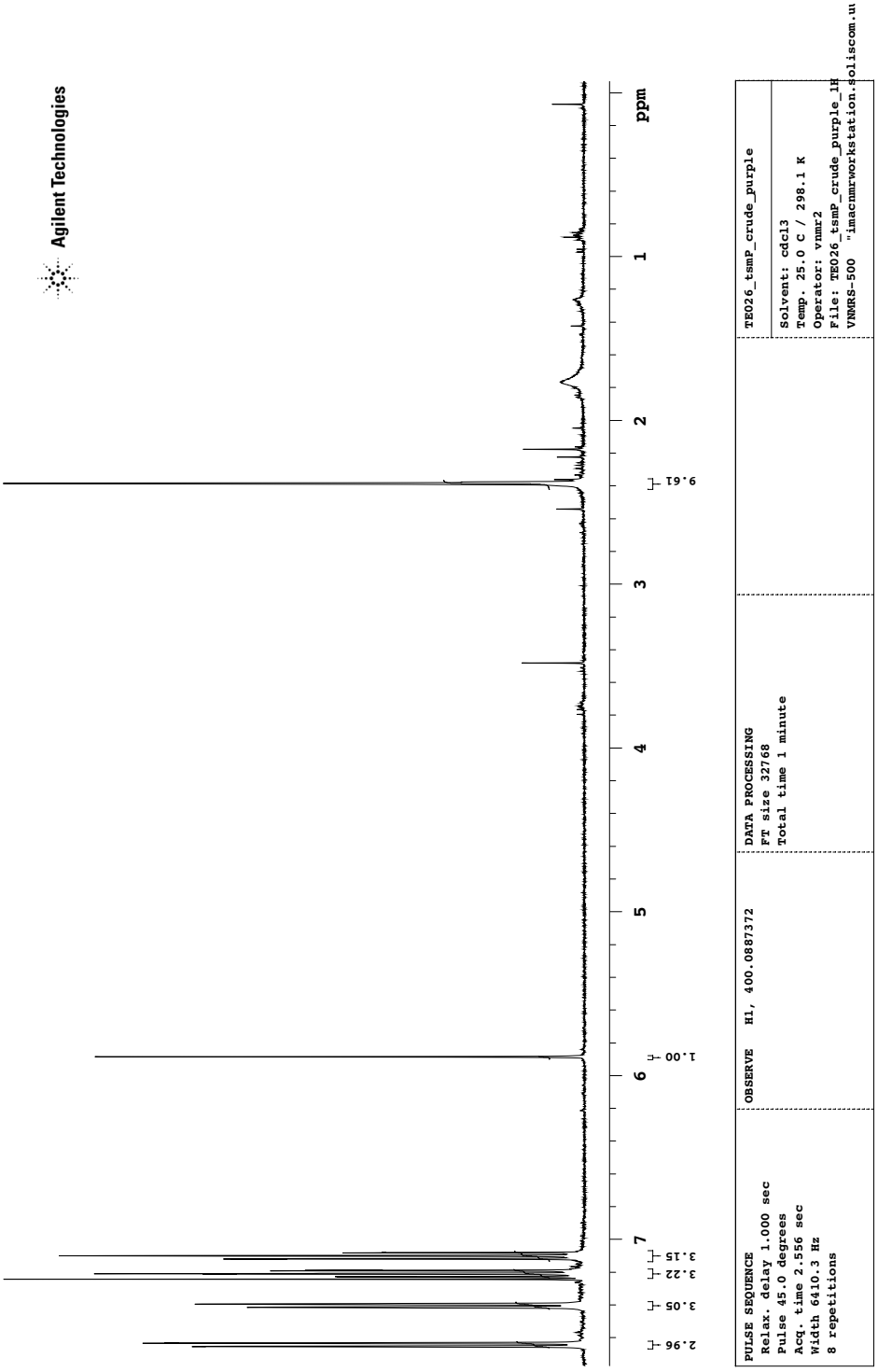

C.3. Compound 5, section 5.3

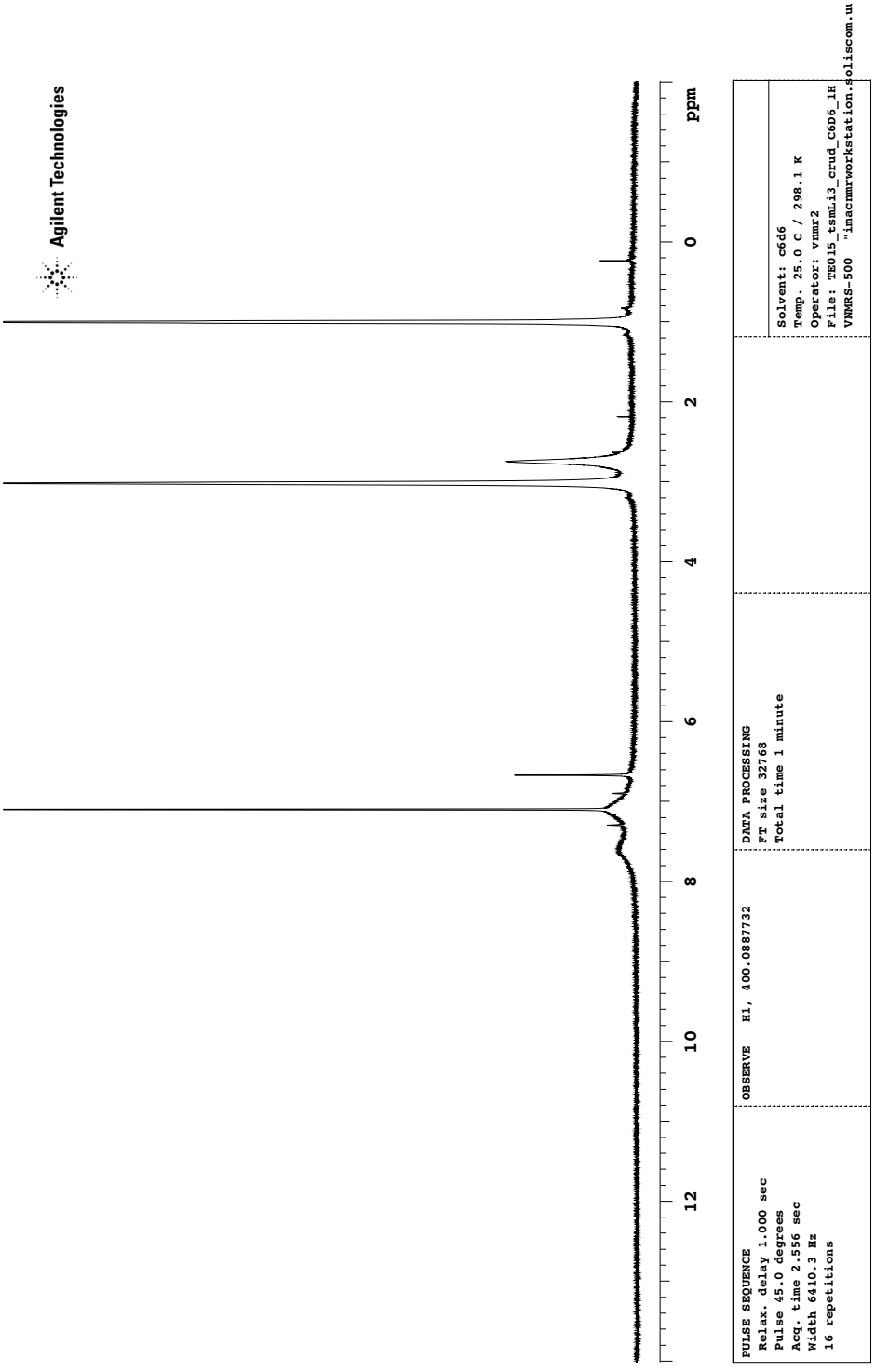

C.4. Section 5.4

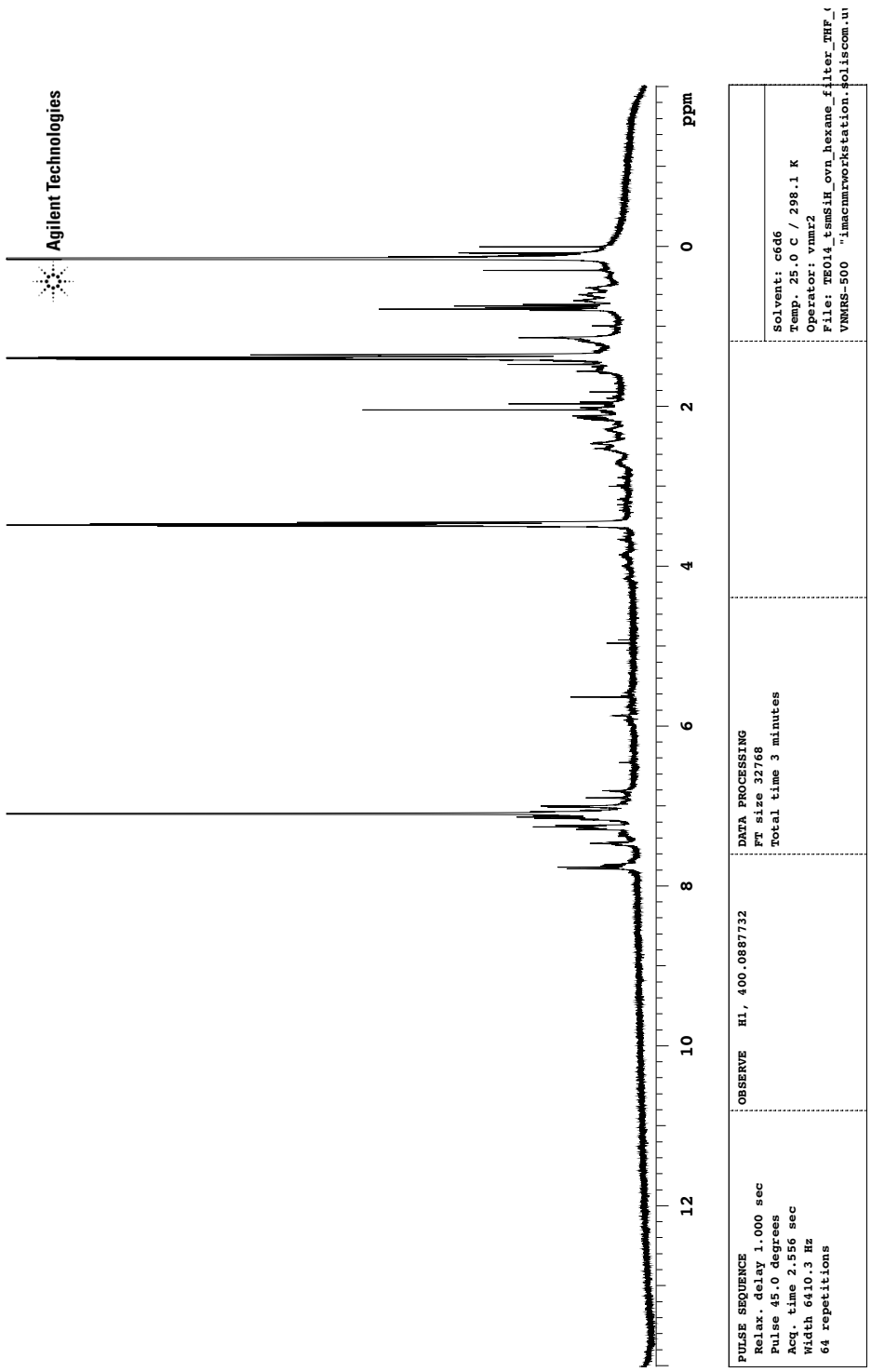

C.5. Section 5.6

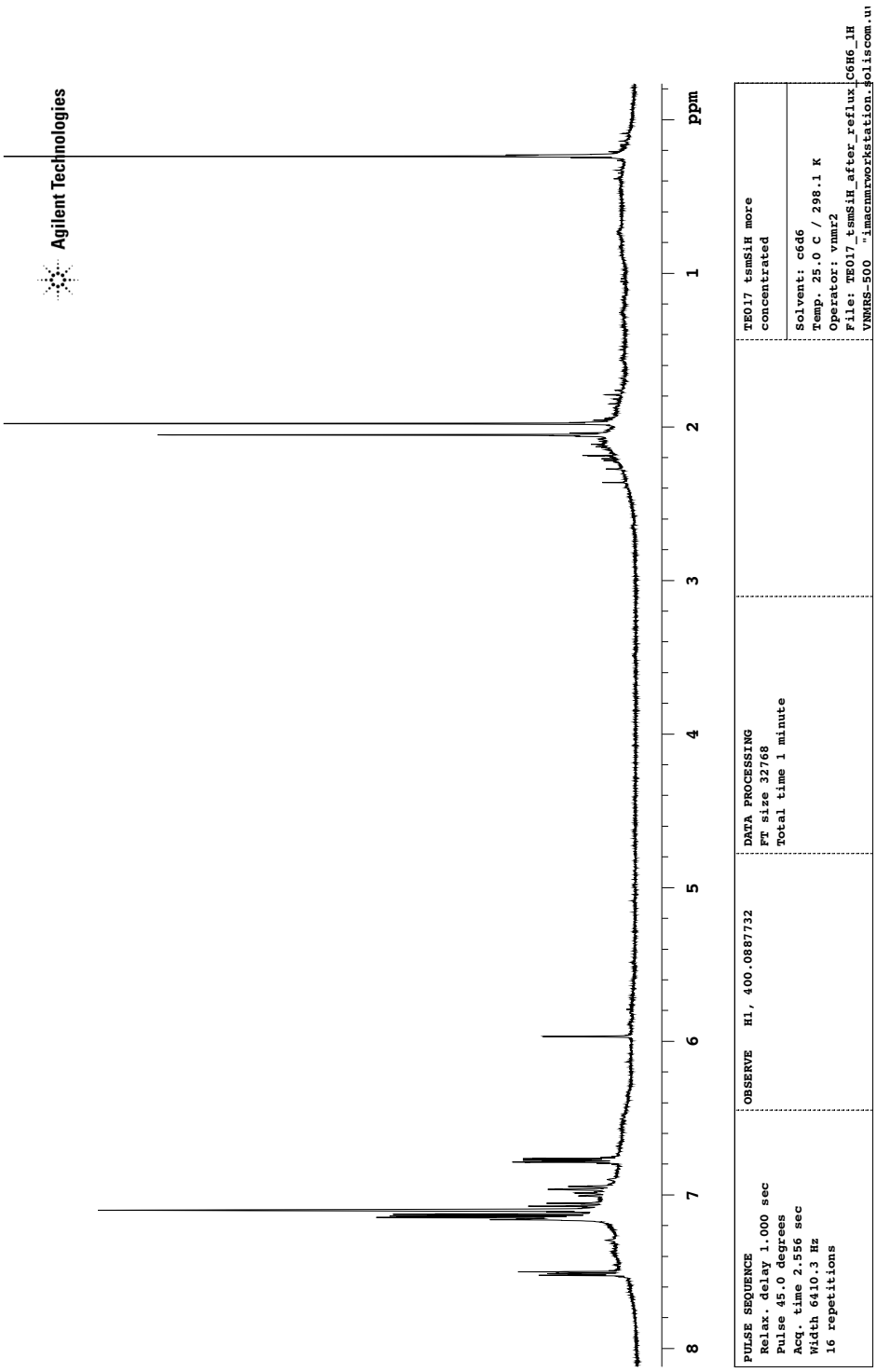

C.6. Section 5.7

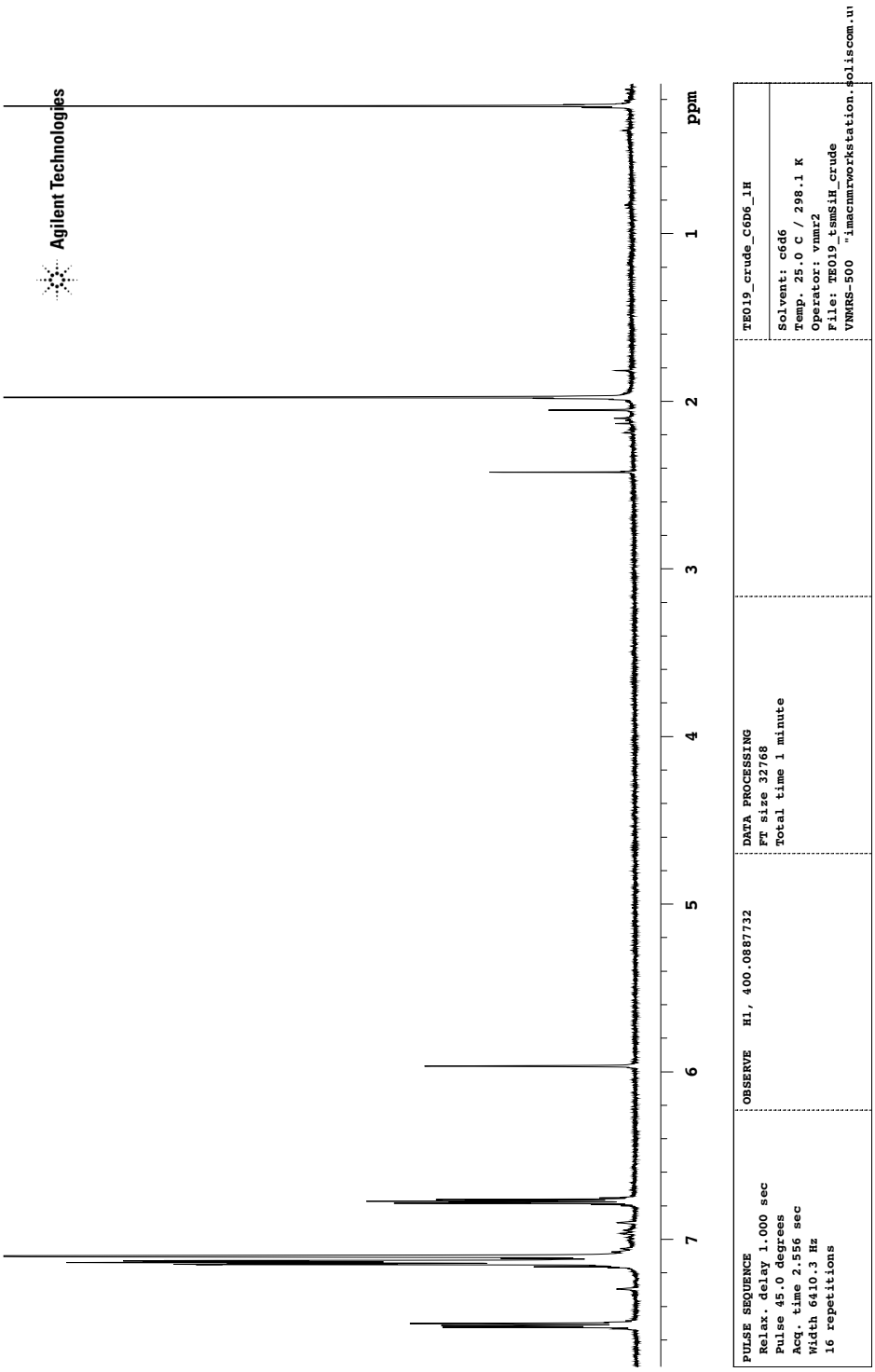

C.7. Section 5.8

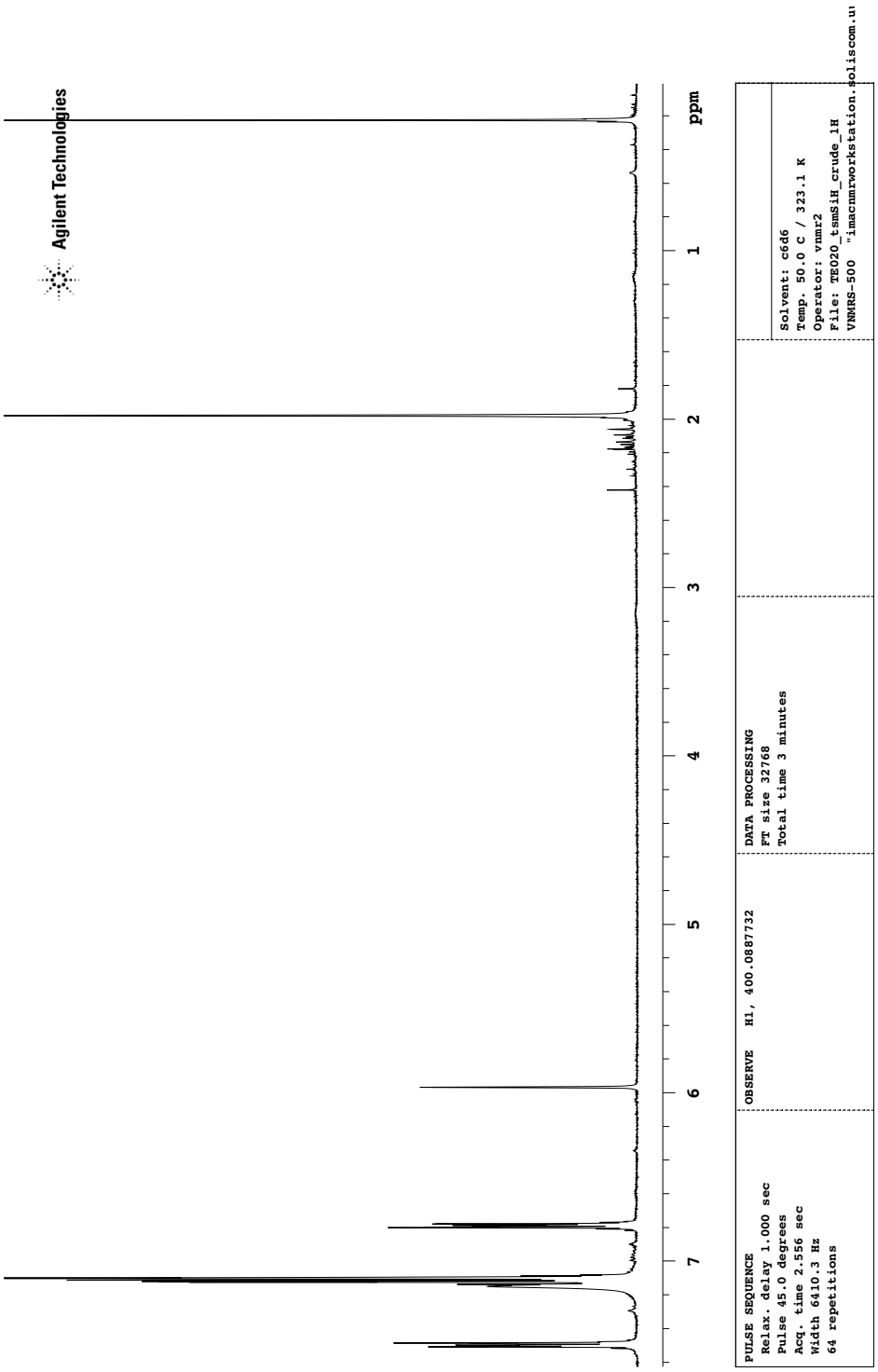

C.8. Section 5.10, liquid phase

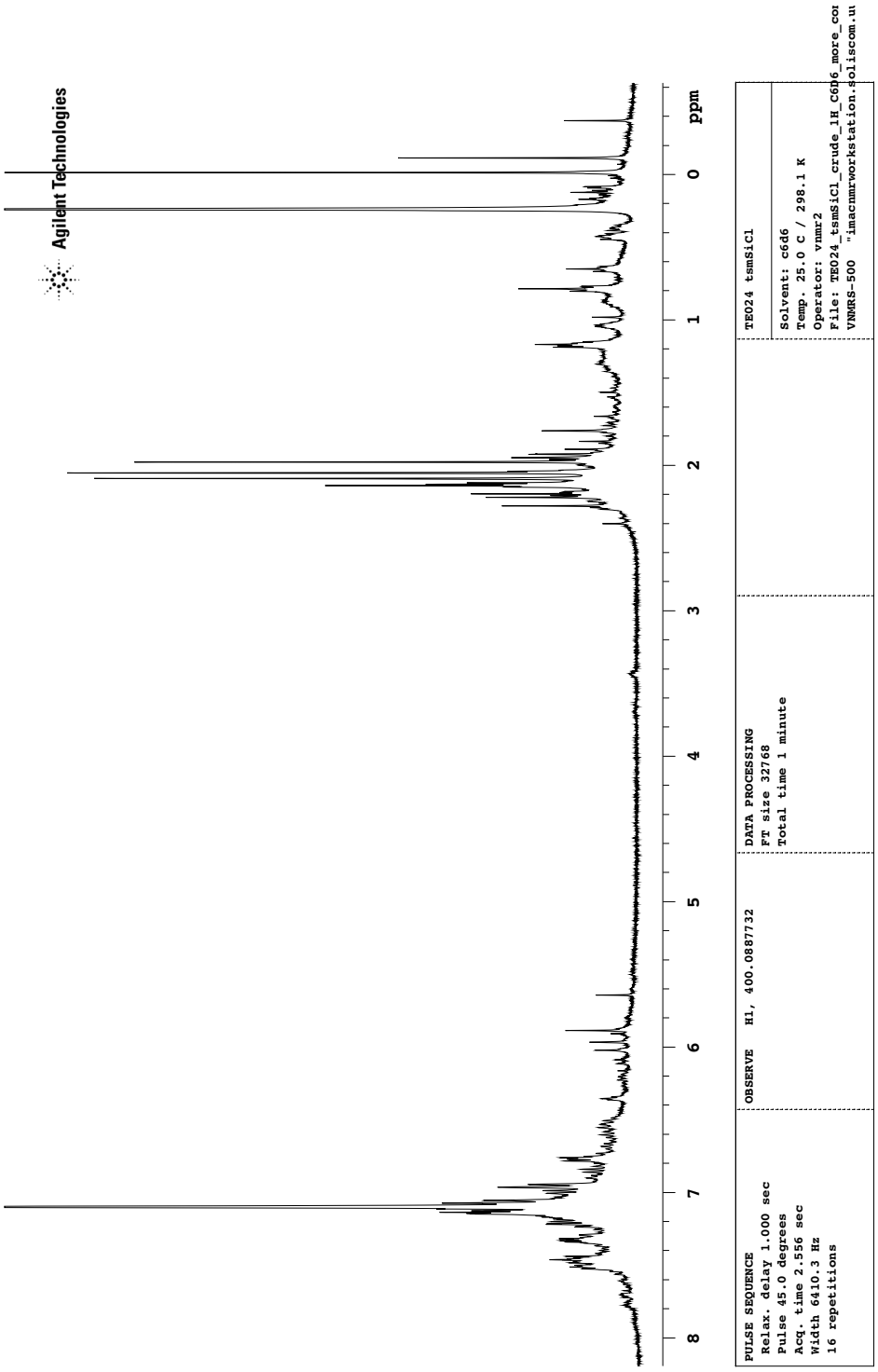

C.9. Compound 4, section 5.11

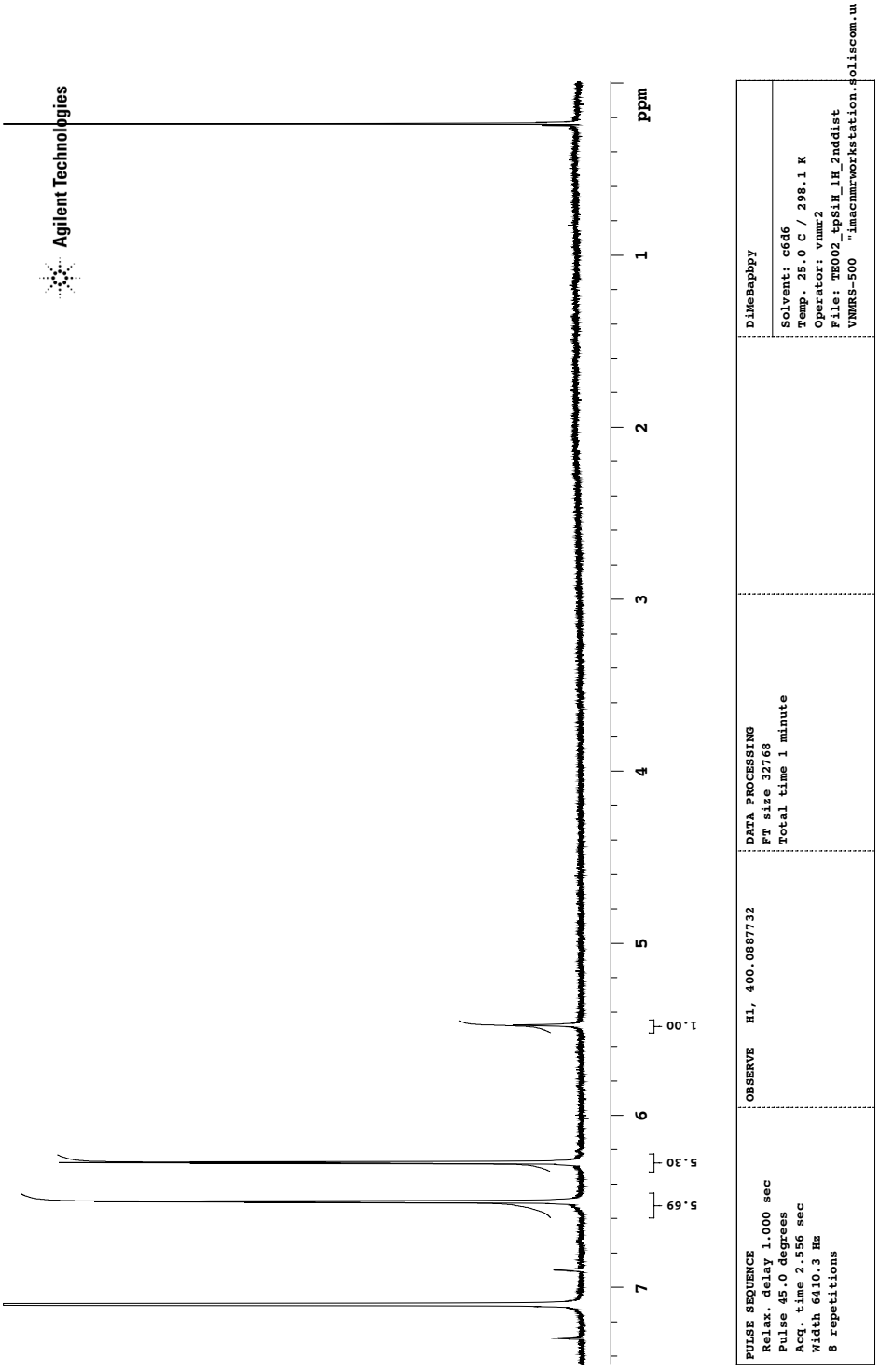

C.10. Section 5.18

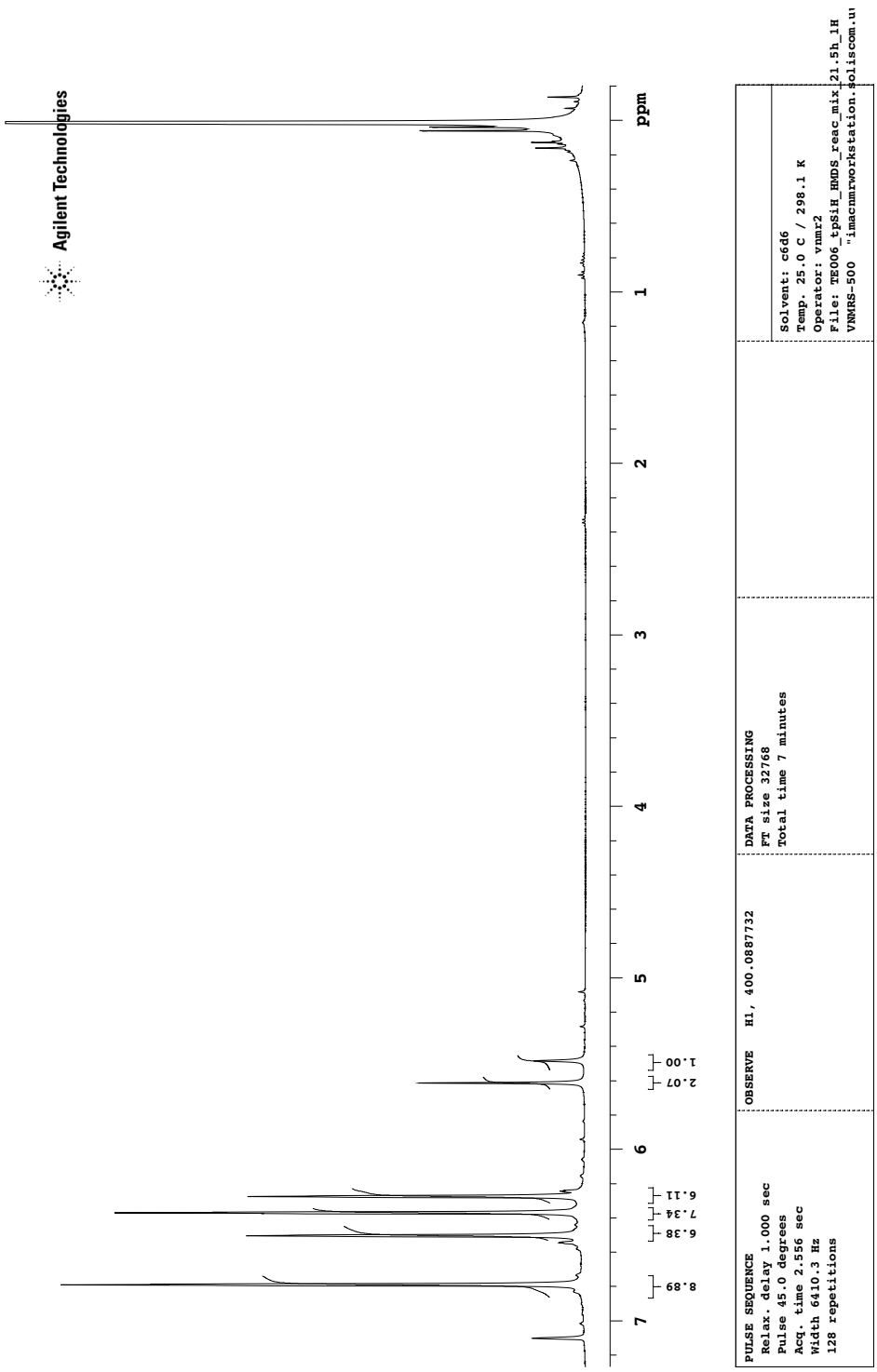

C.11. Section 5.14

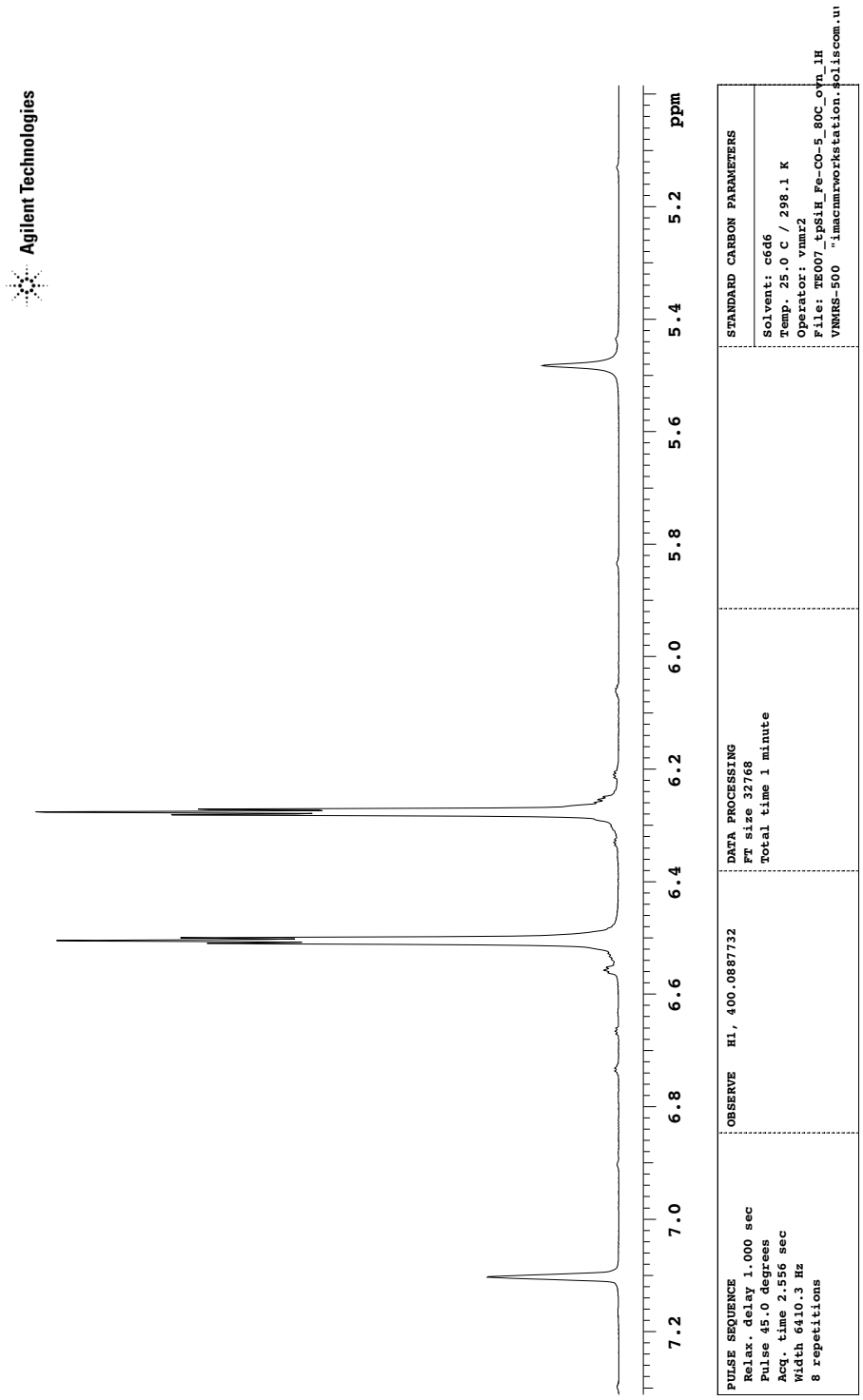

C.12. Compound 13, section 5.17

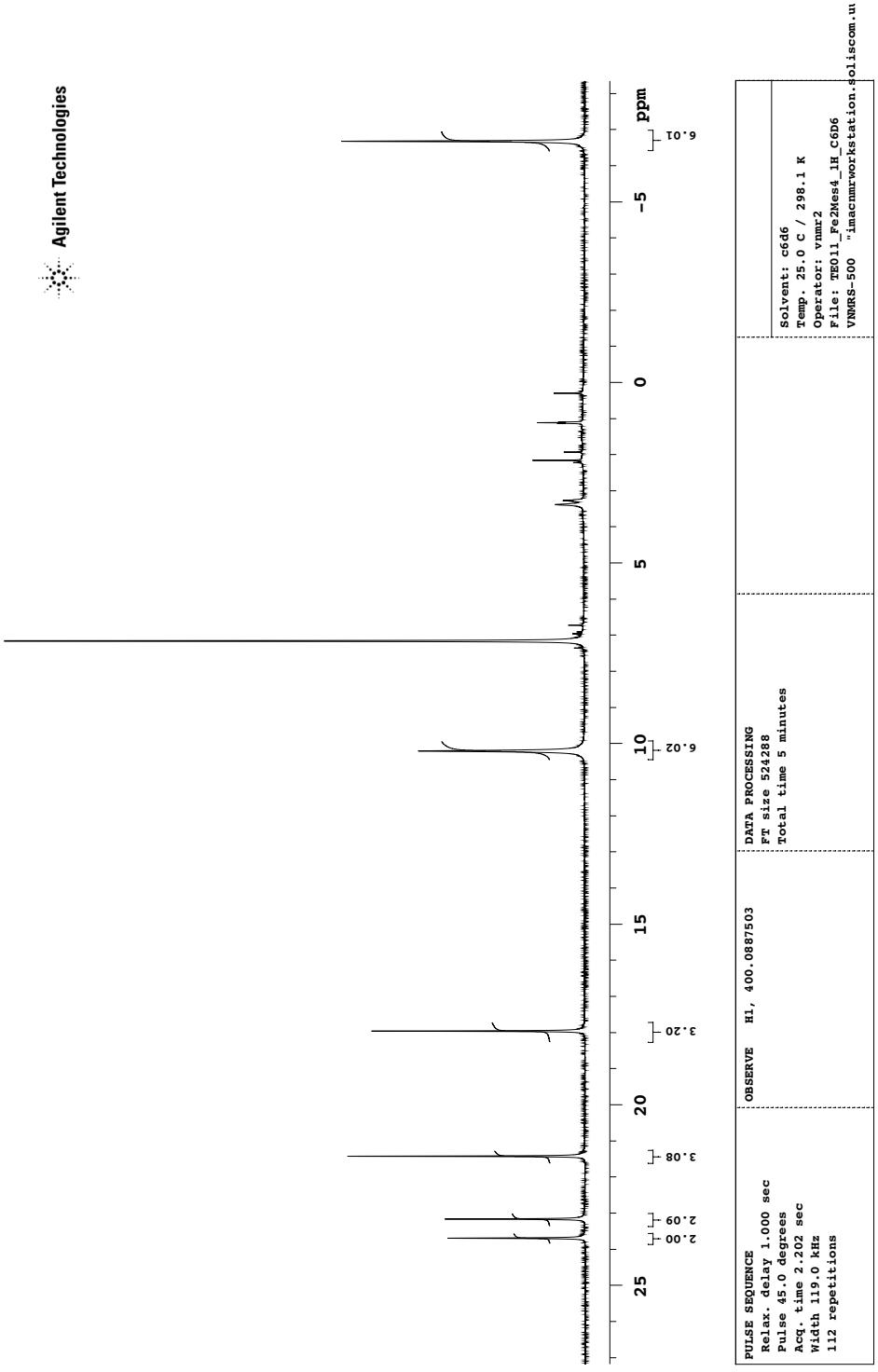

C.13. Section 5.19, 1, final

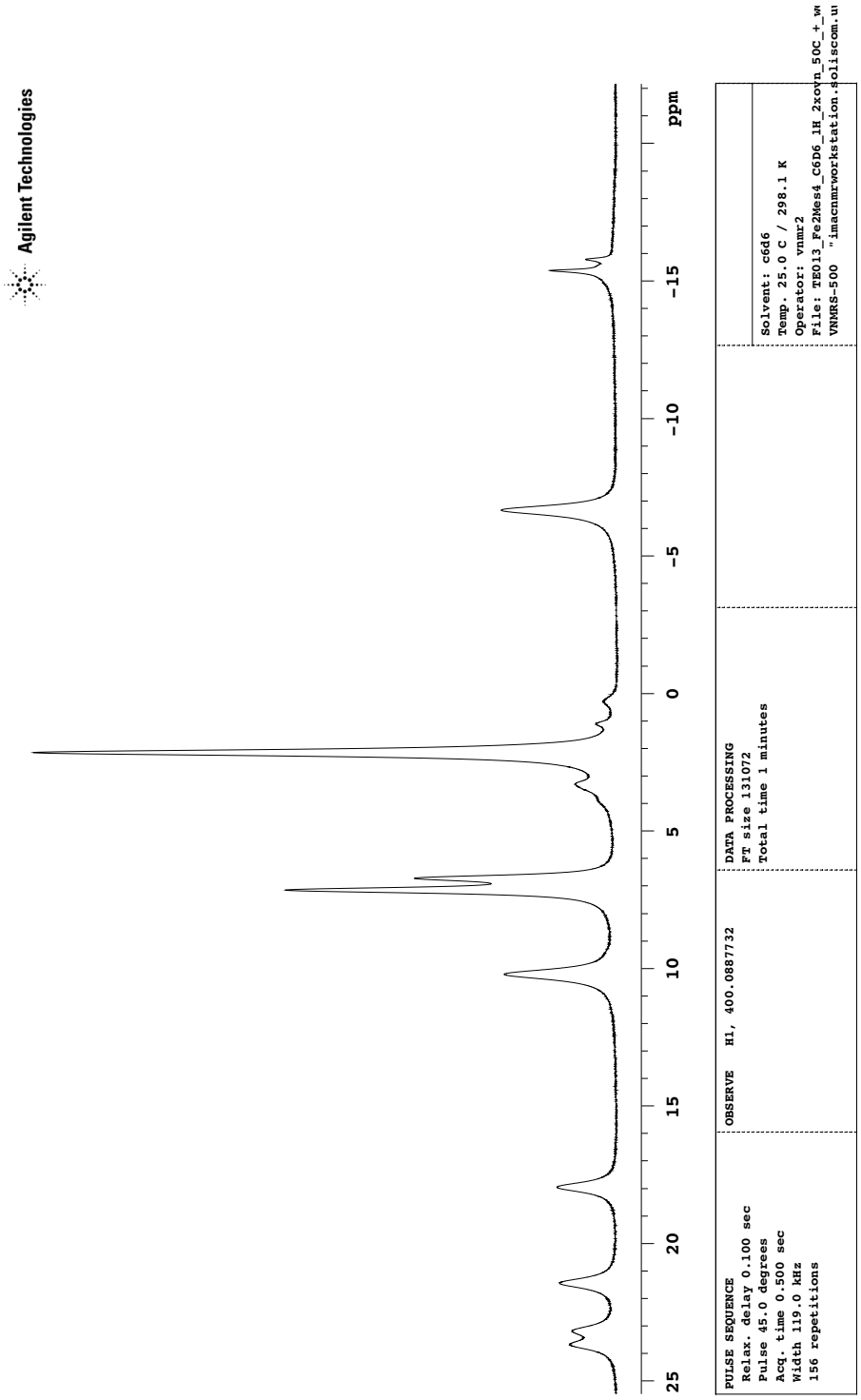

C.14. Section 5.19, 2, final

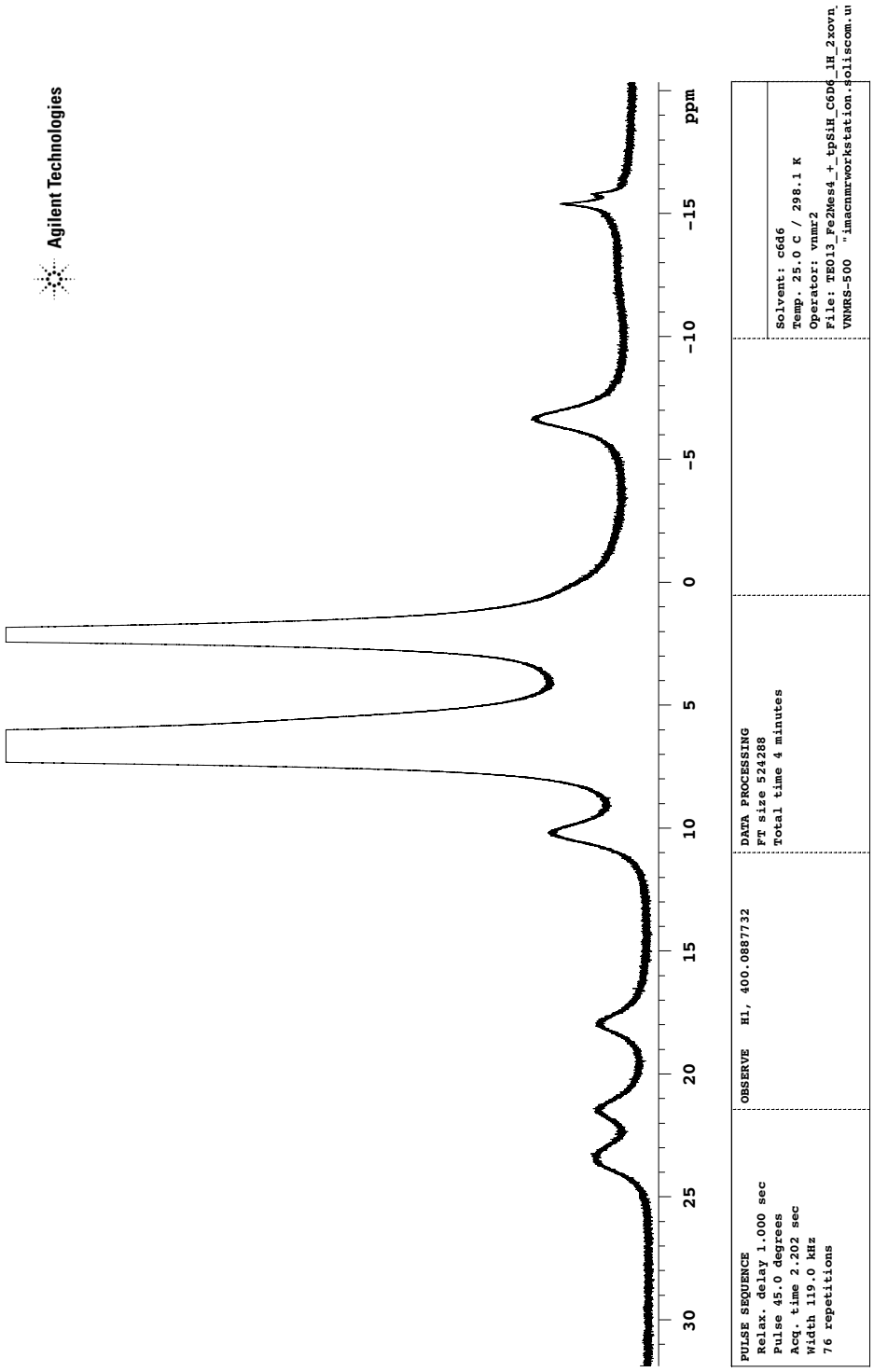

C.15. Section 5.19, 3, final

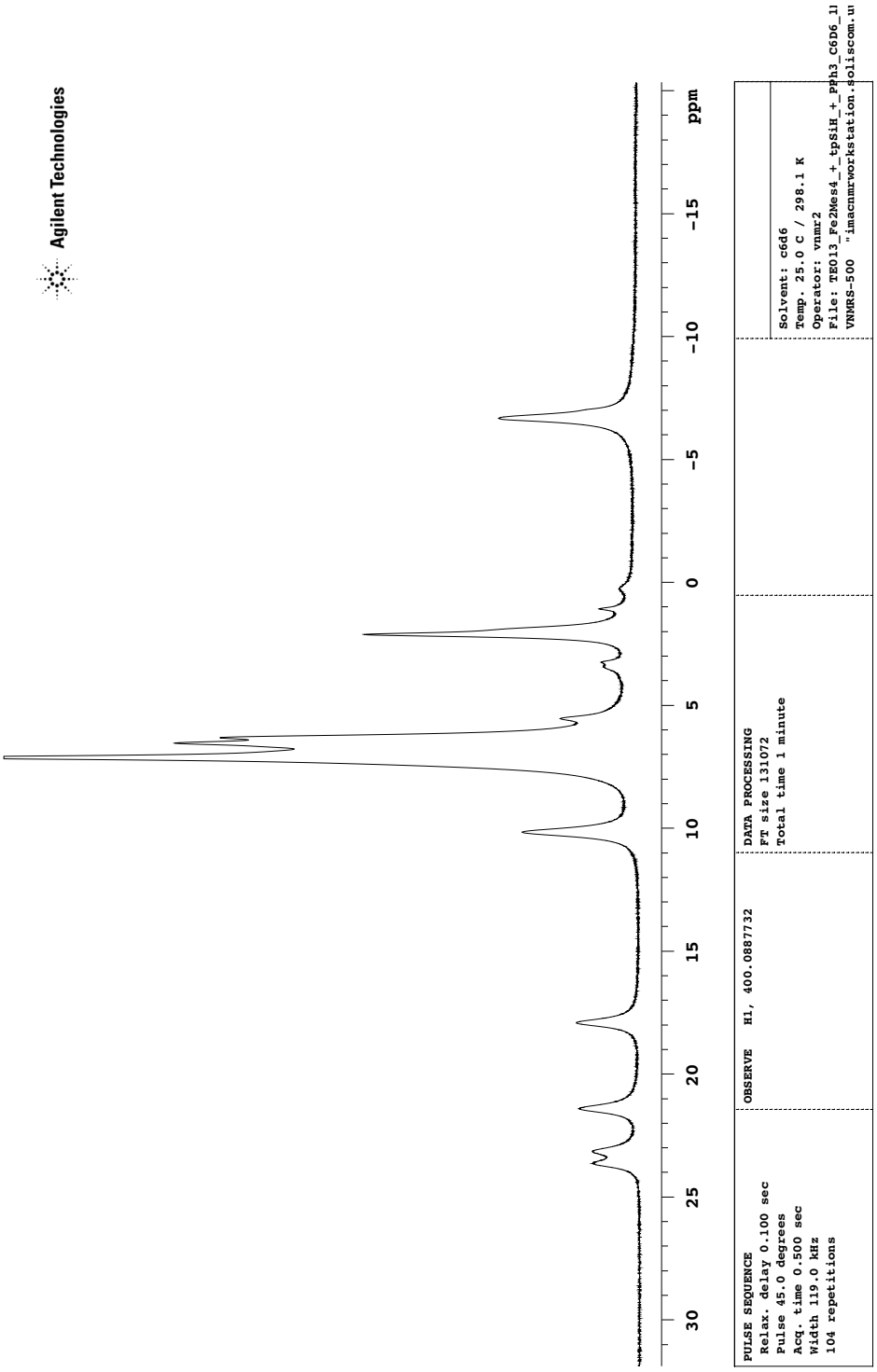

C.16. Compound 14, section 10.2

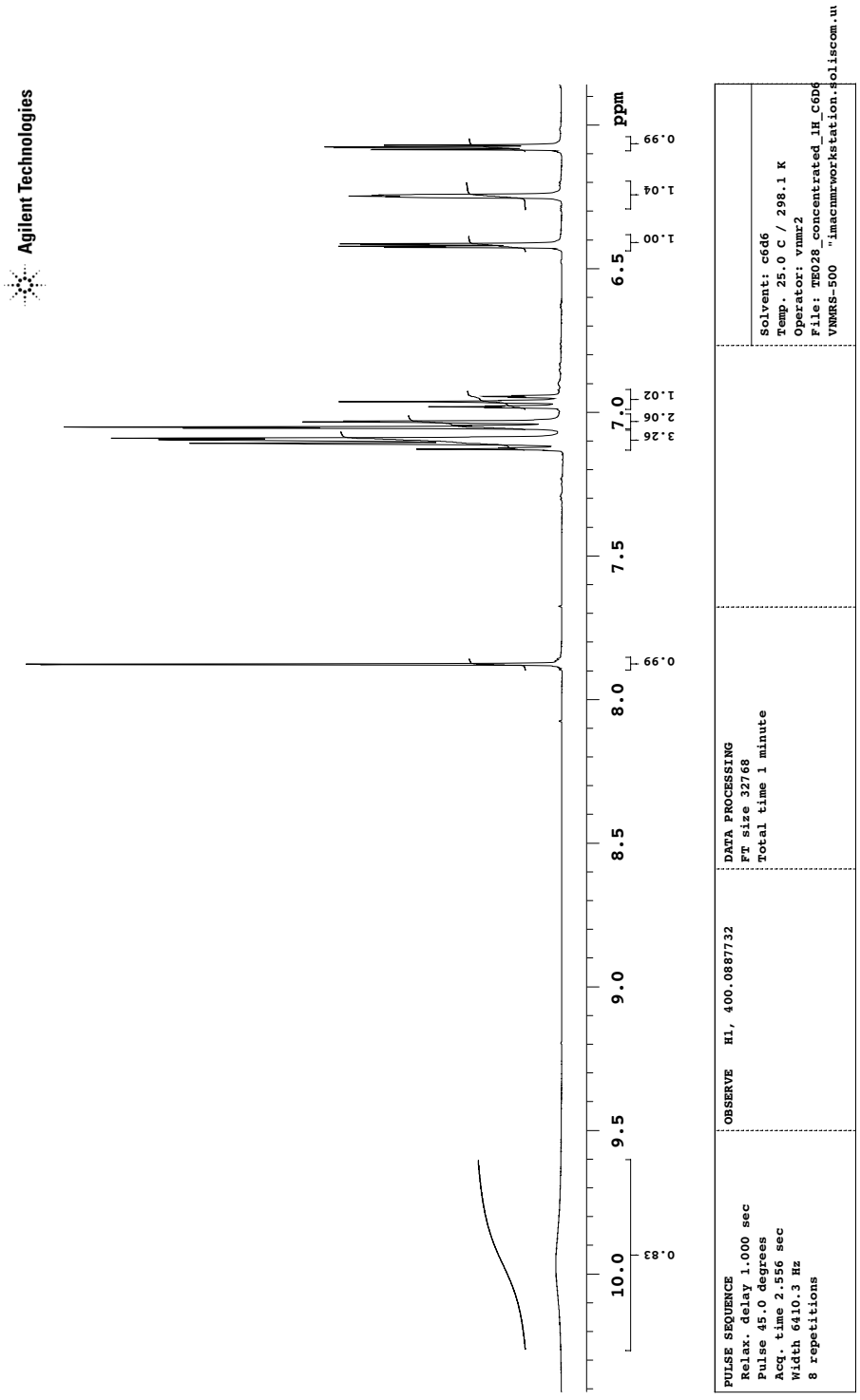

C.17. Compound 20, section 10.3, ^{1}H-NMR

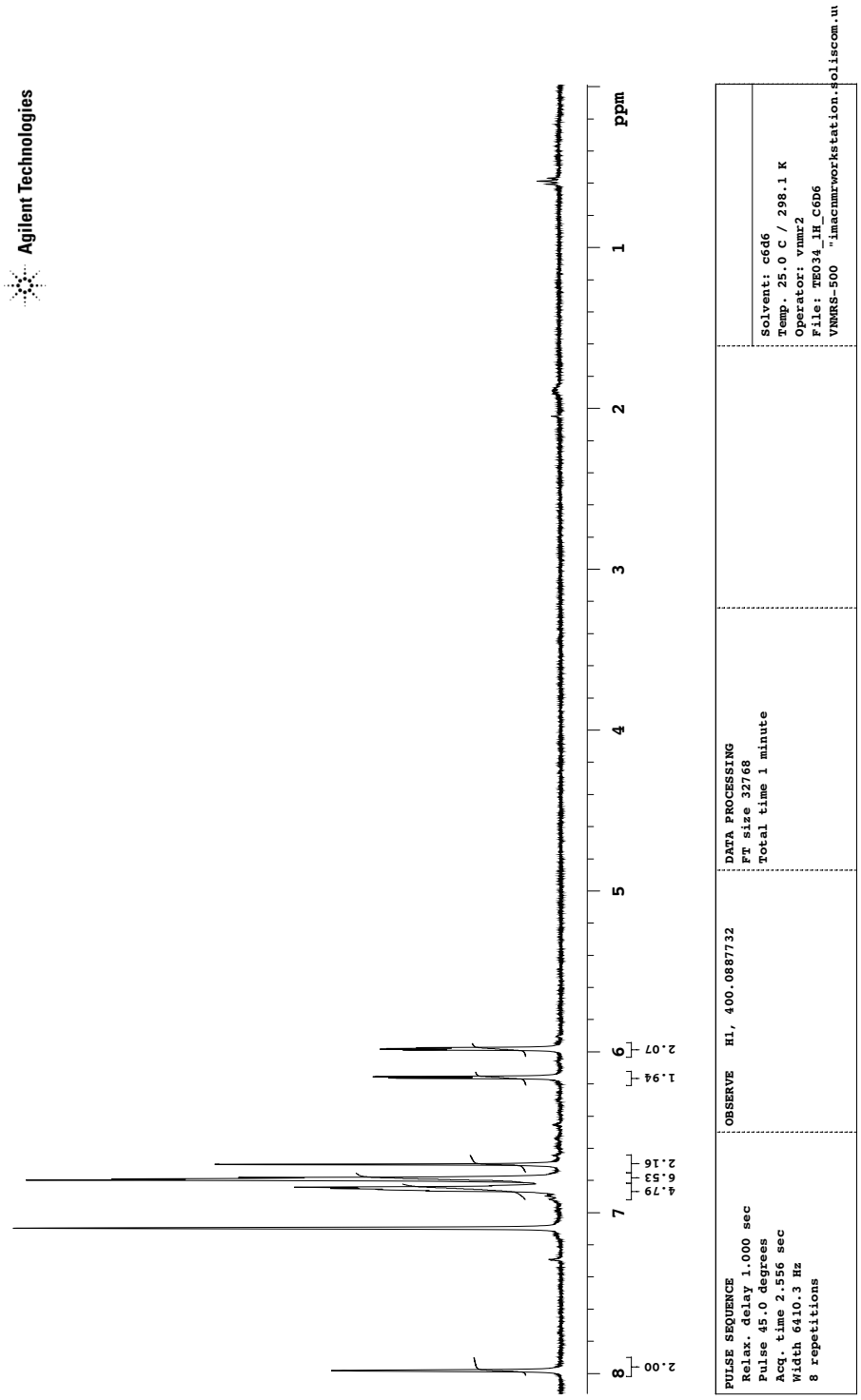

C.18. Compound 20, section 10.3, COSY

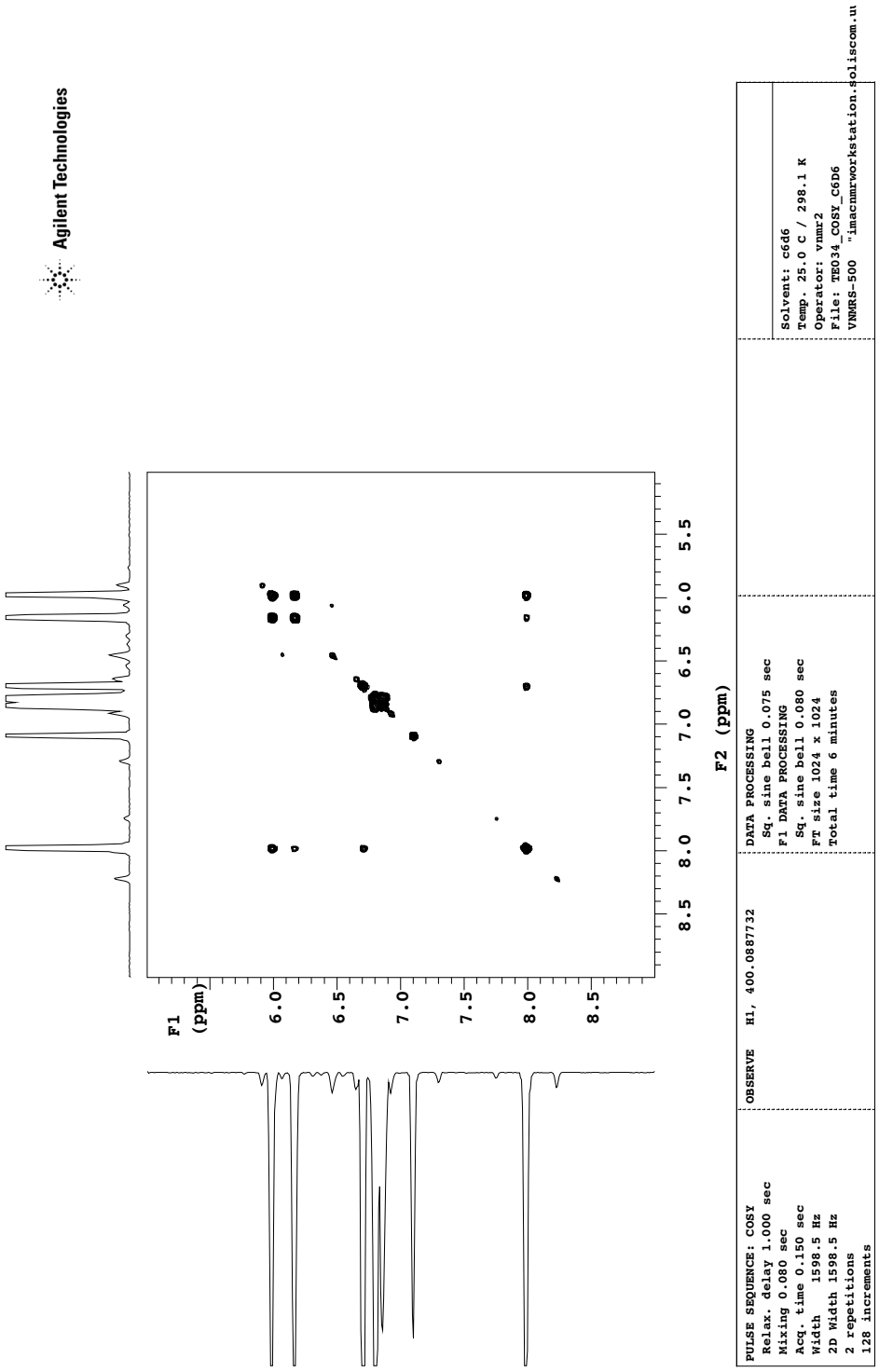

C.19. Compound 20, section 10.3, $^{13}C\{^{1}H\}$-NMR, equilibrium mixture

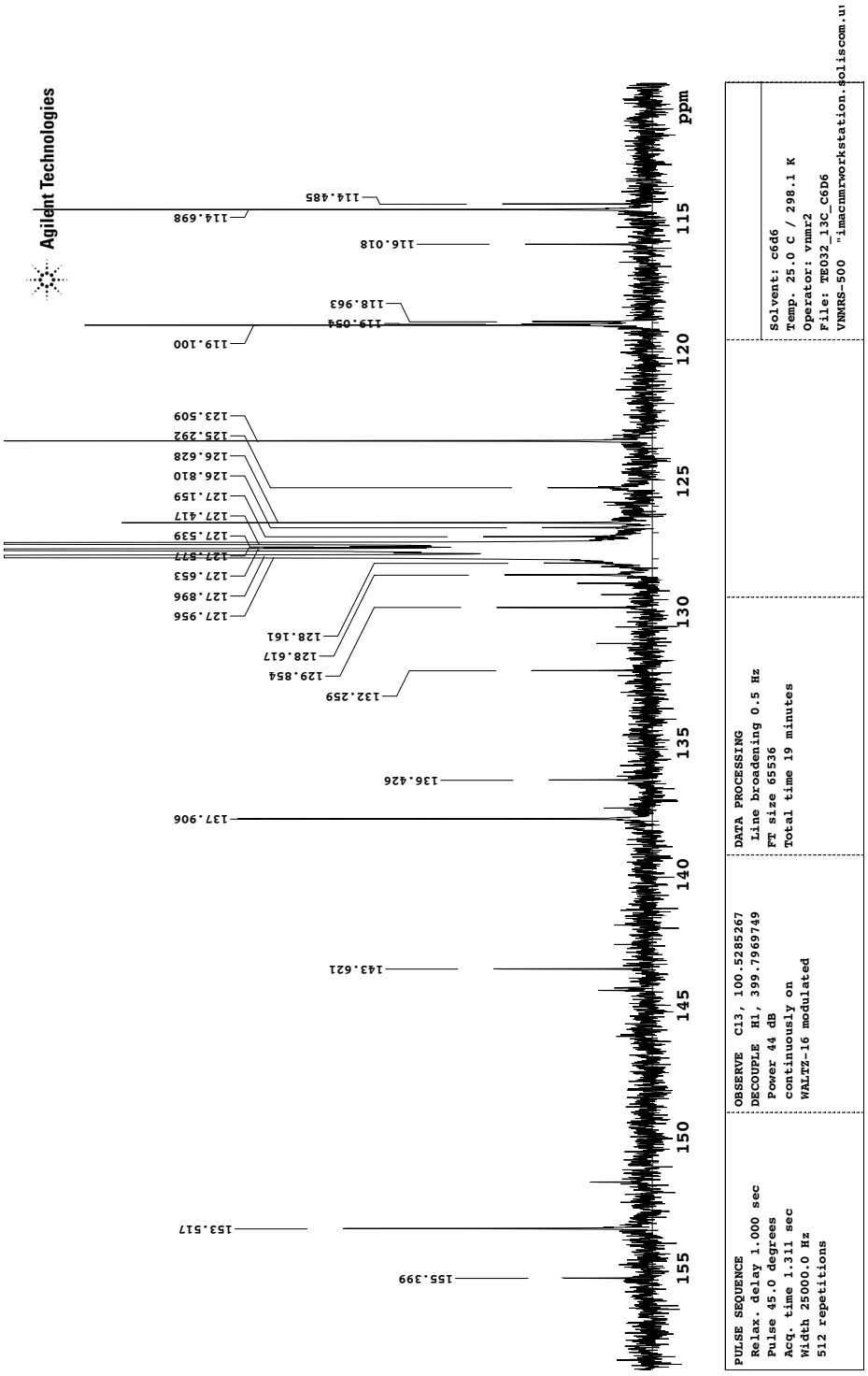

C.20. Compound 20, section 10.3, HSQC, equilibrium mixture

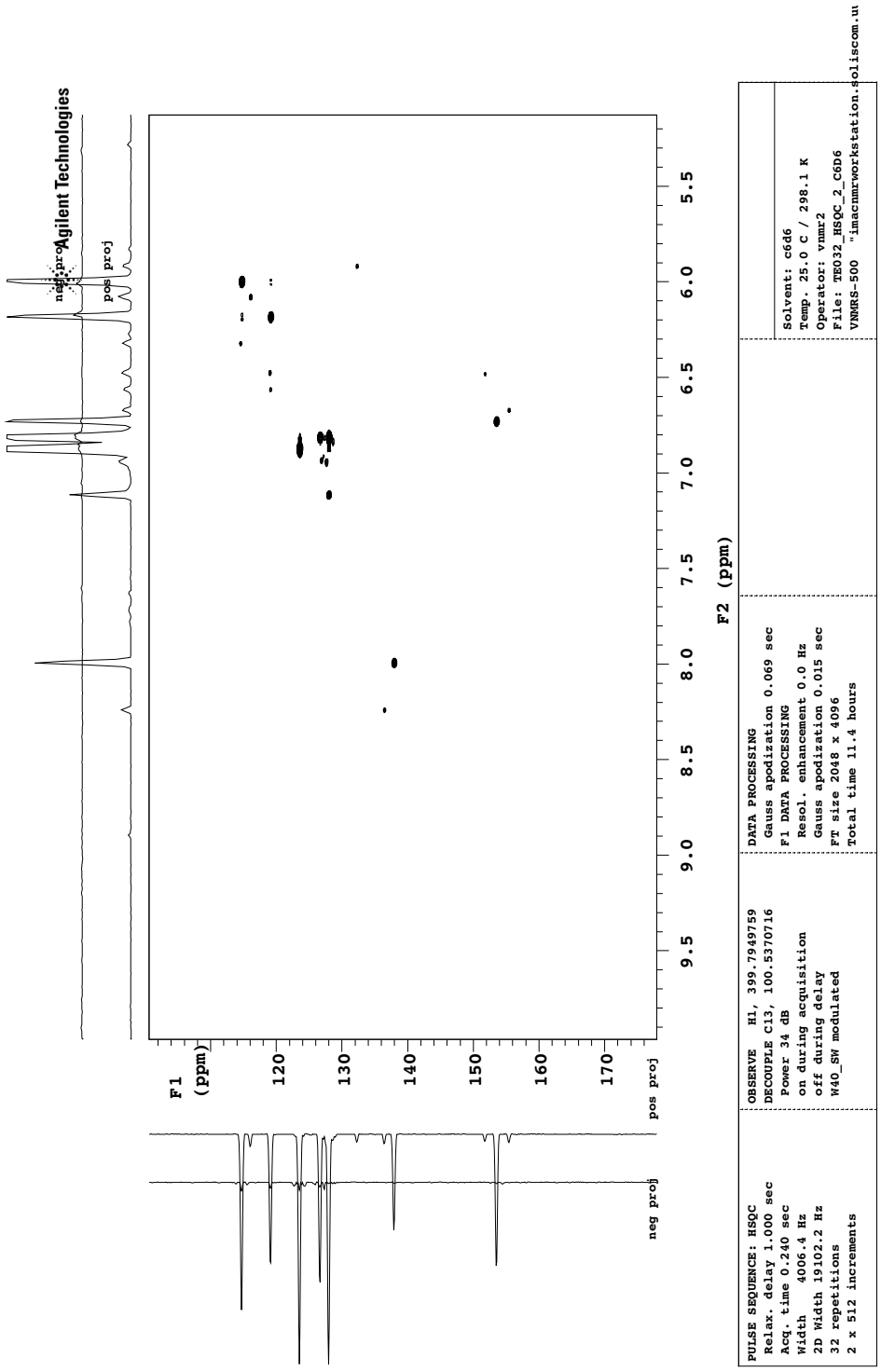

C.21. Compound 20, section 10.3, $^{29}Si\{^{1}H\}$-NMR

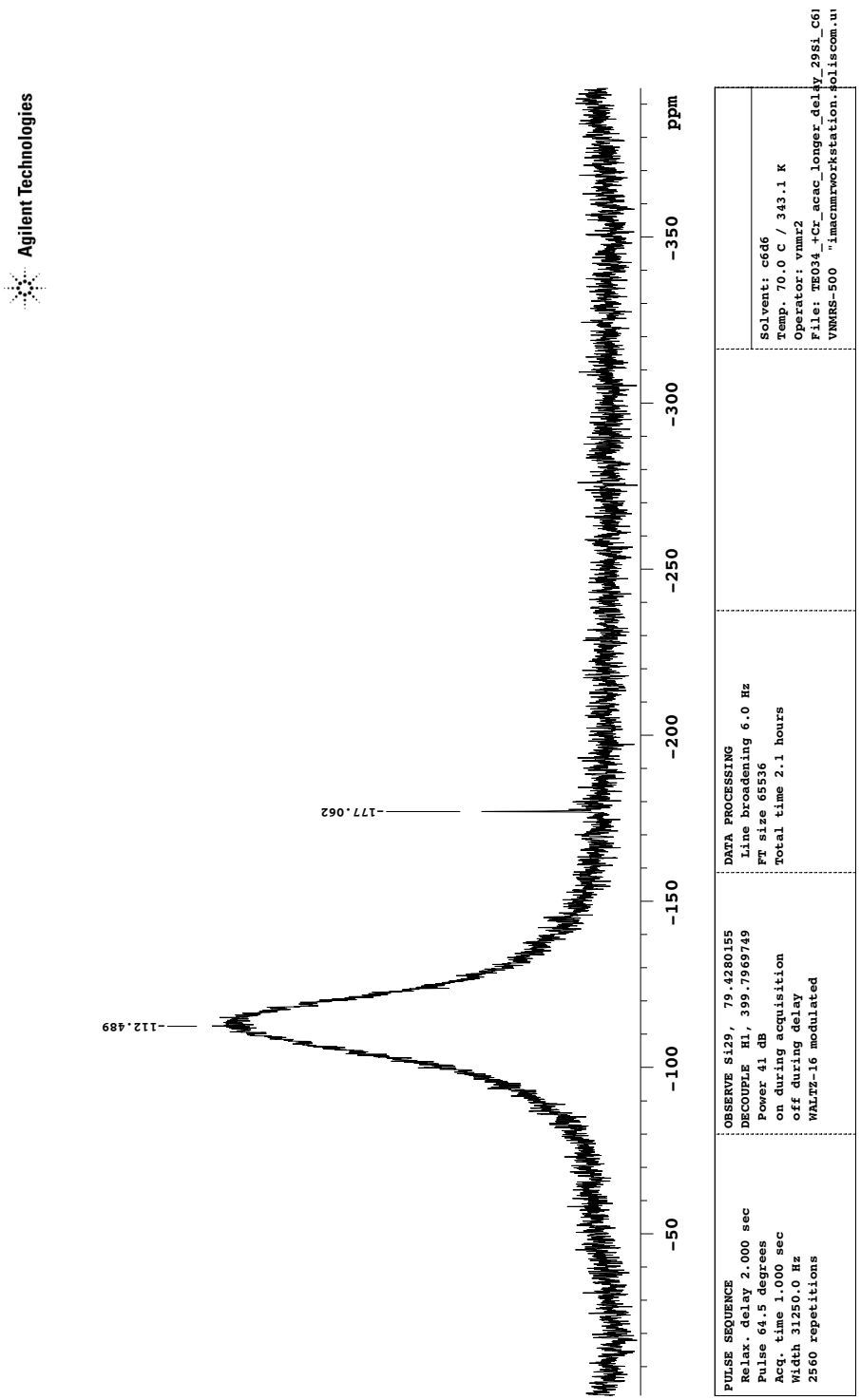

C.22. Compound 15, section 10.4

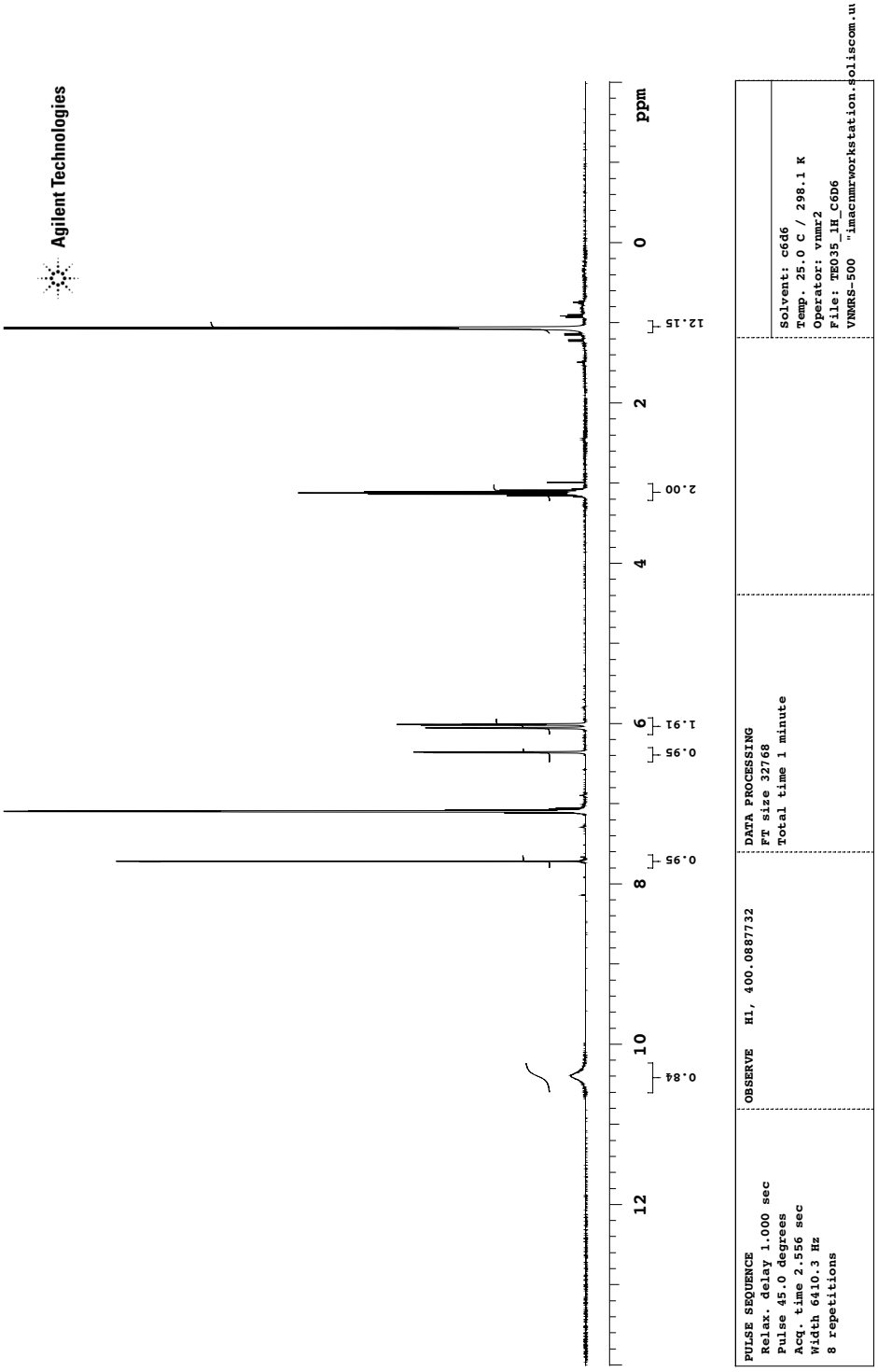

C.23. Section 10.5 to 10.7, crude $^{29}Si\{^{1}H\}$-NMR

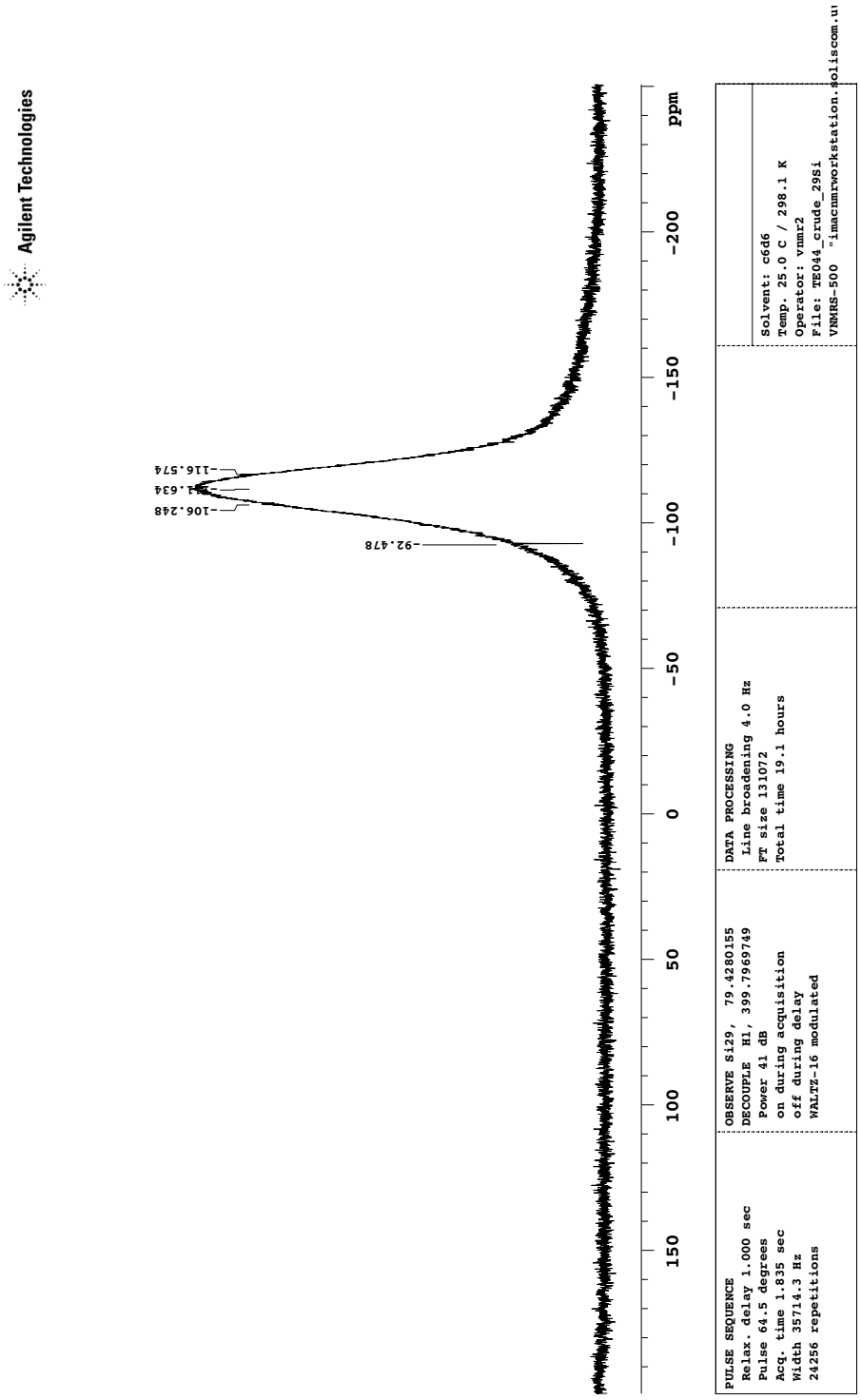

C.24. Section 10.5 to 10.7, crude coupled ^{29}Si-NMR

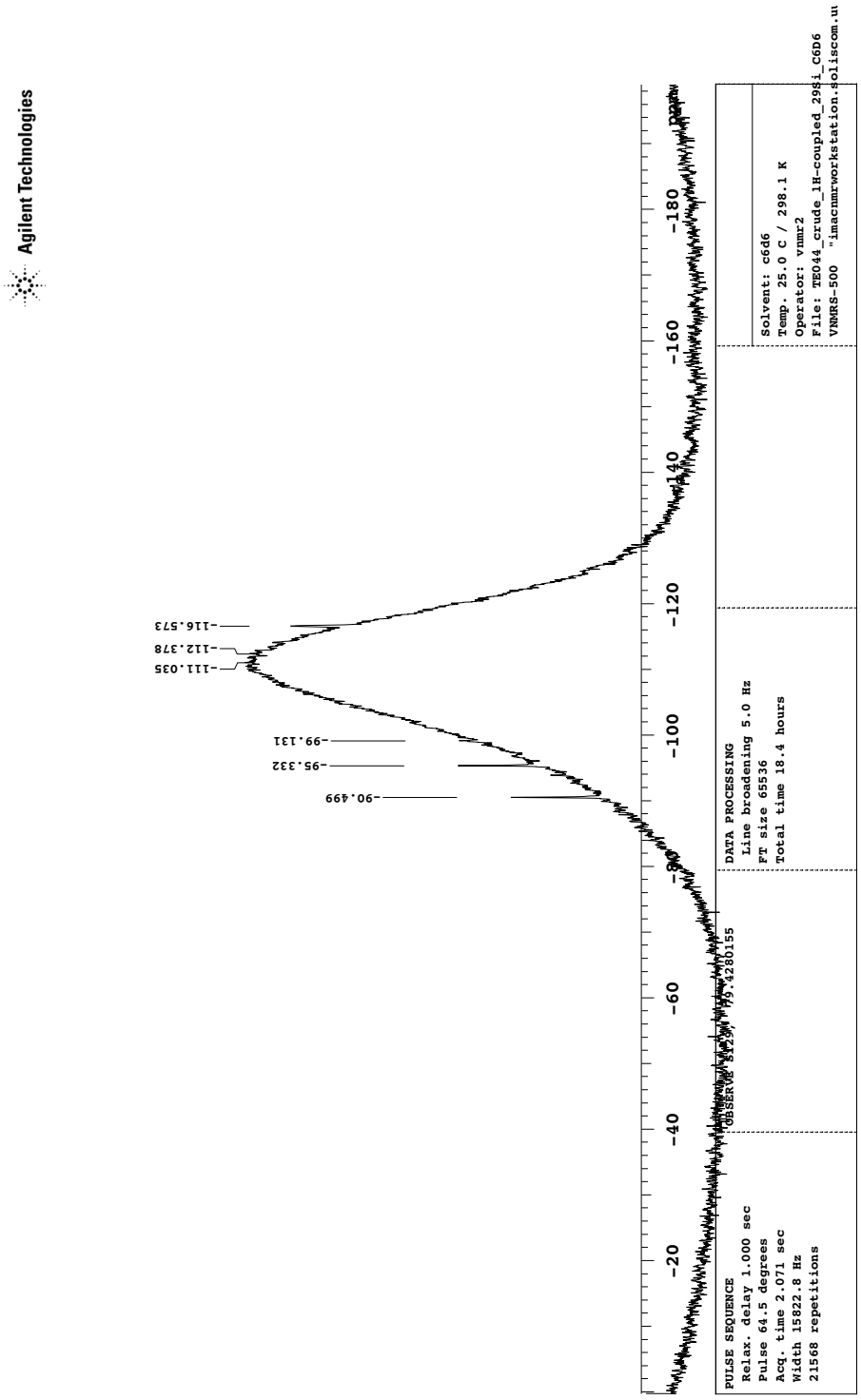

C.25. Section 10.5 to 10.7, ^{1}H-NMR after above

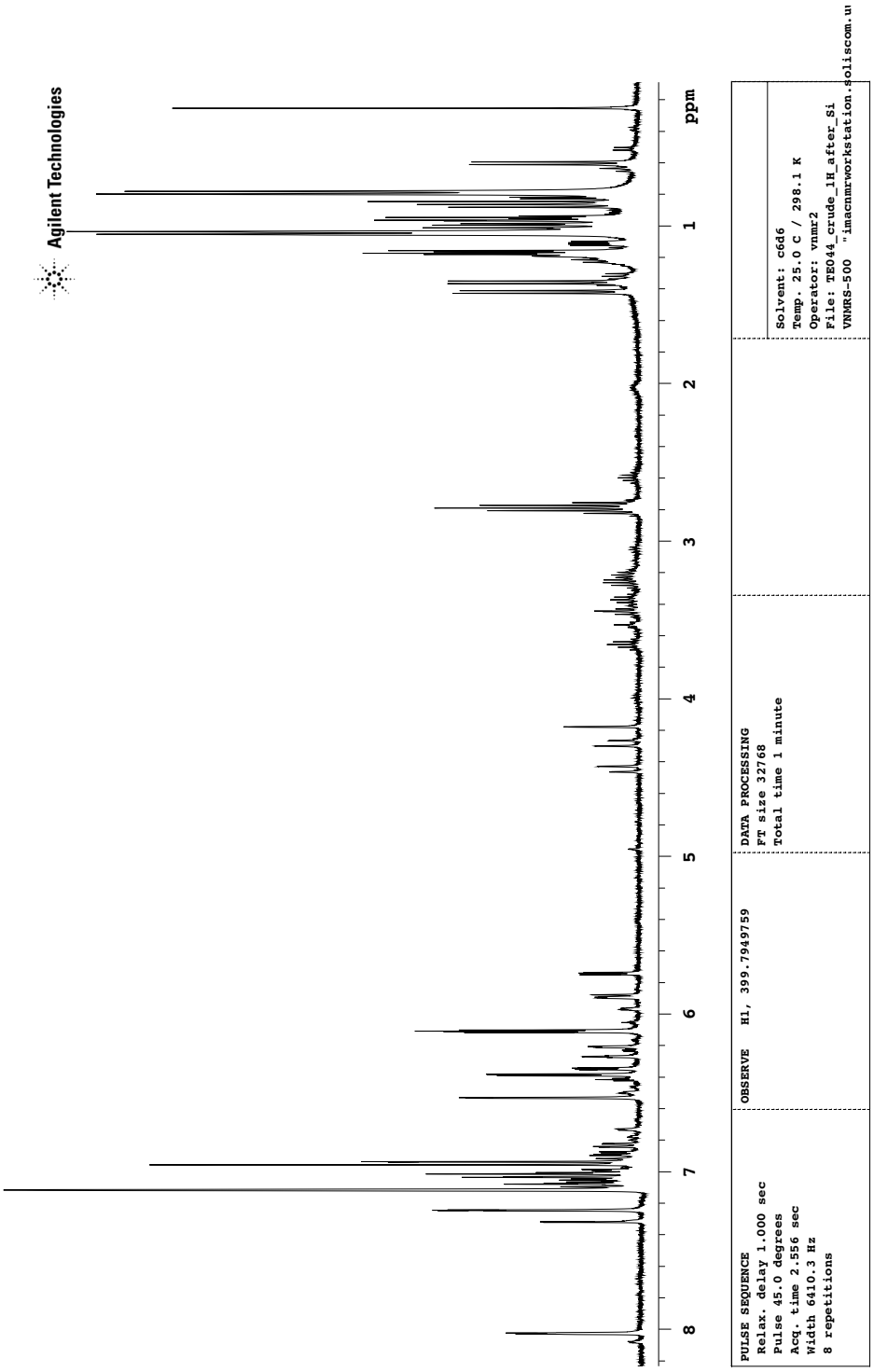

C.26. Section 10.5 to 10.7, final mixture, ^{1}H-NMR

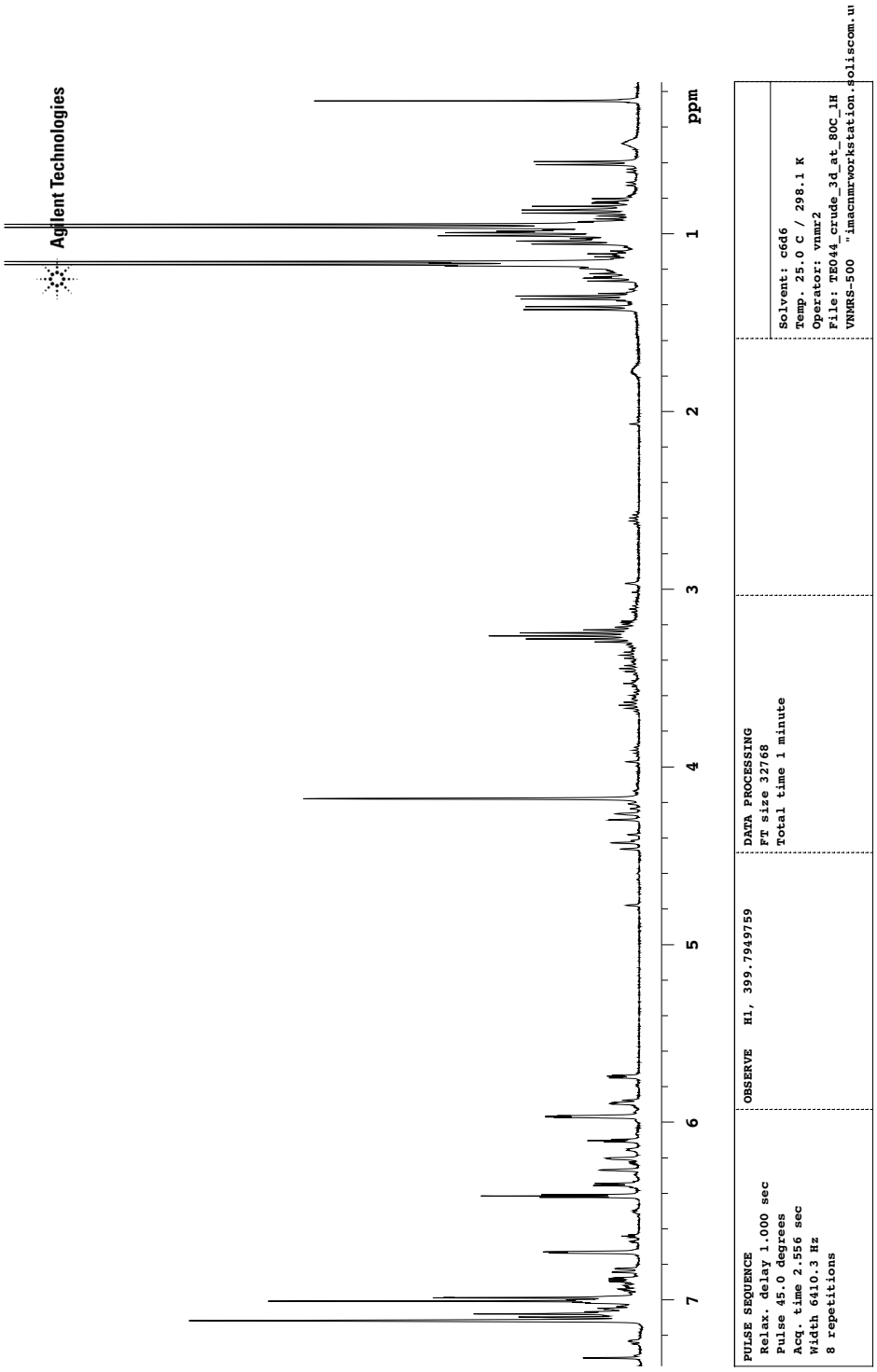

C.27. Section 10.5 to 10.7, final mixture, COSY

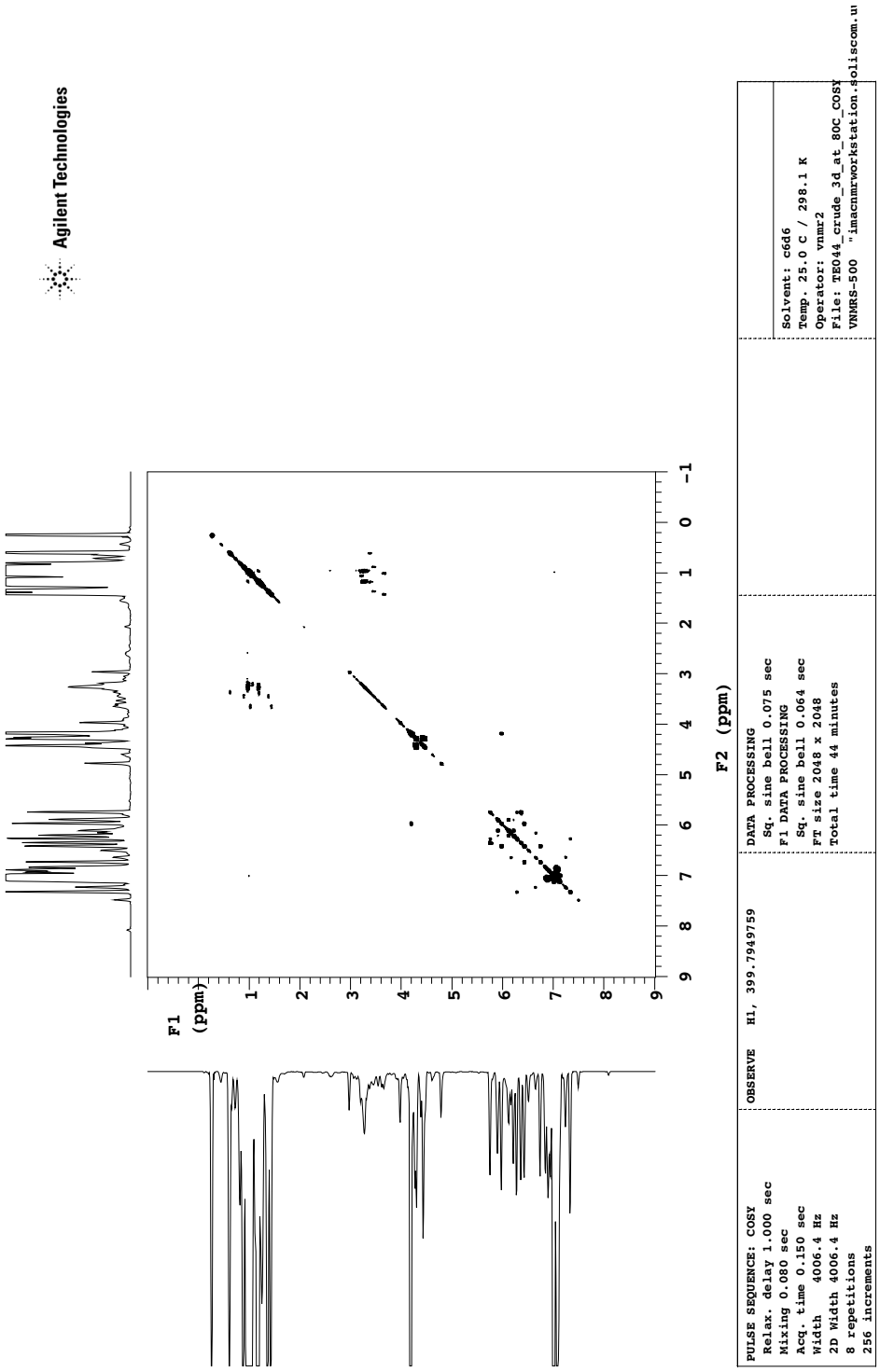

C.28. Section 10.5 to 10.7, final mixture, DEPT-135

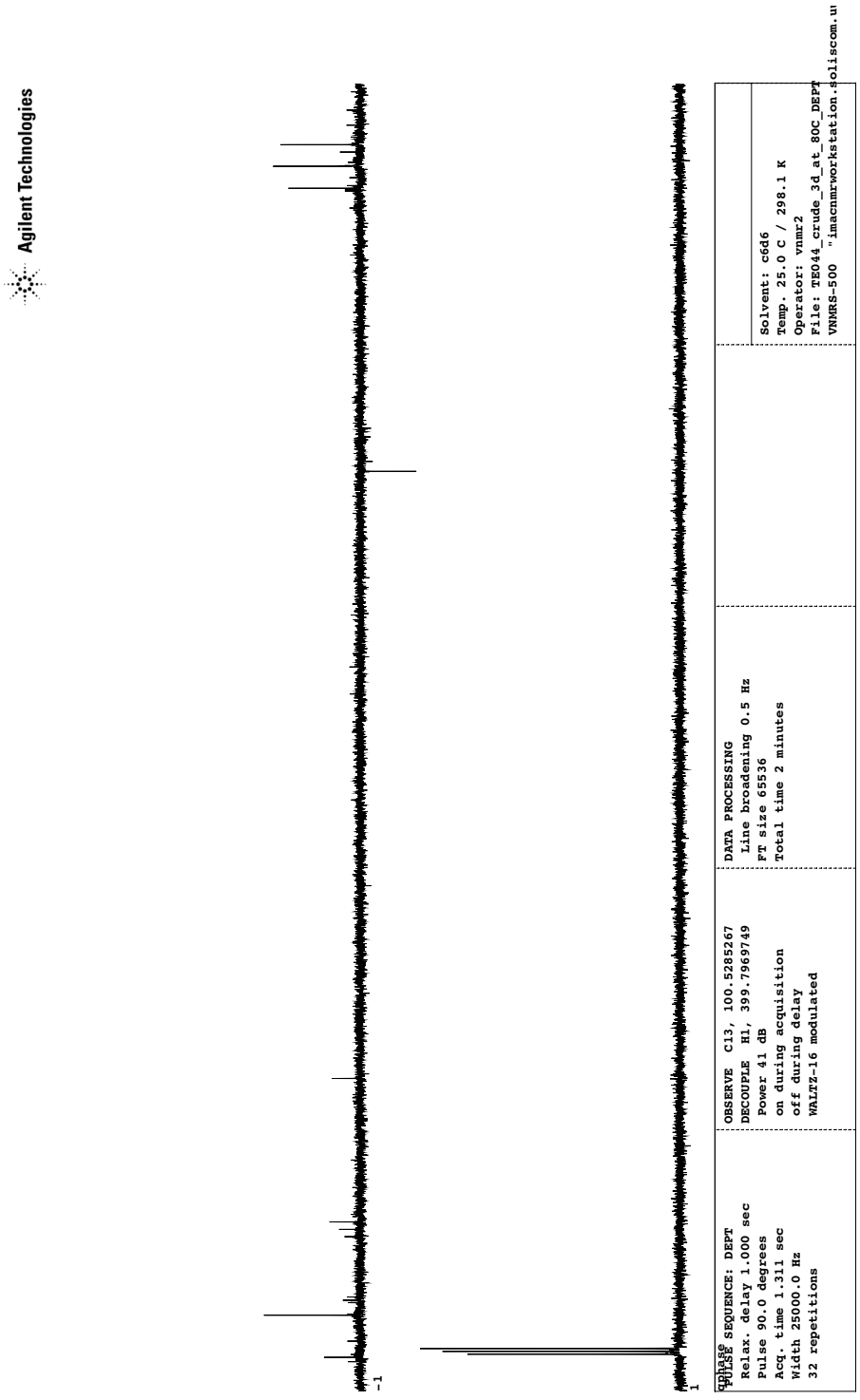

C.29. Section 10.5 to 10.7, final mixture, coupled ^{29}Si-NMR

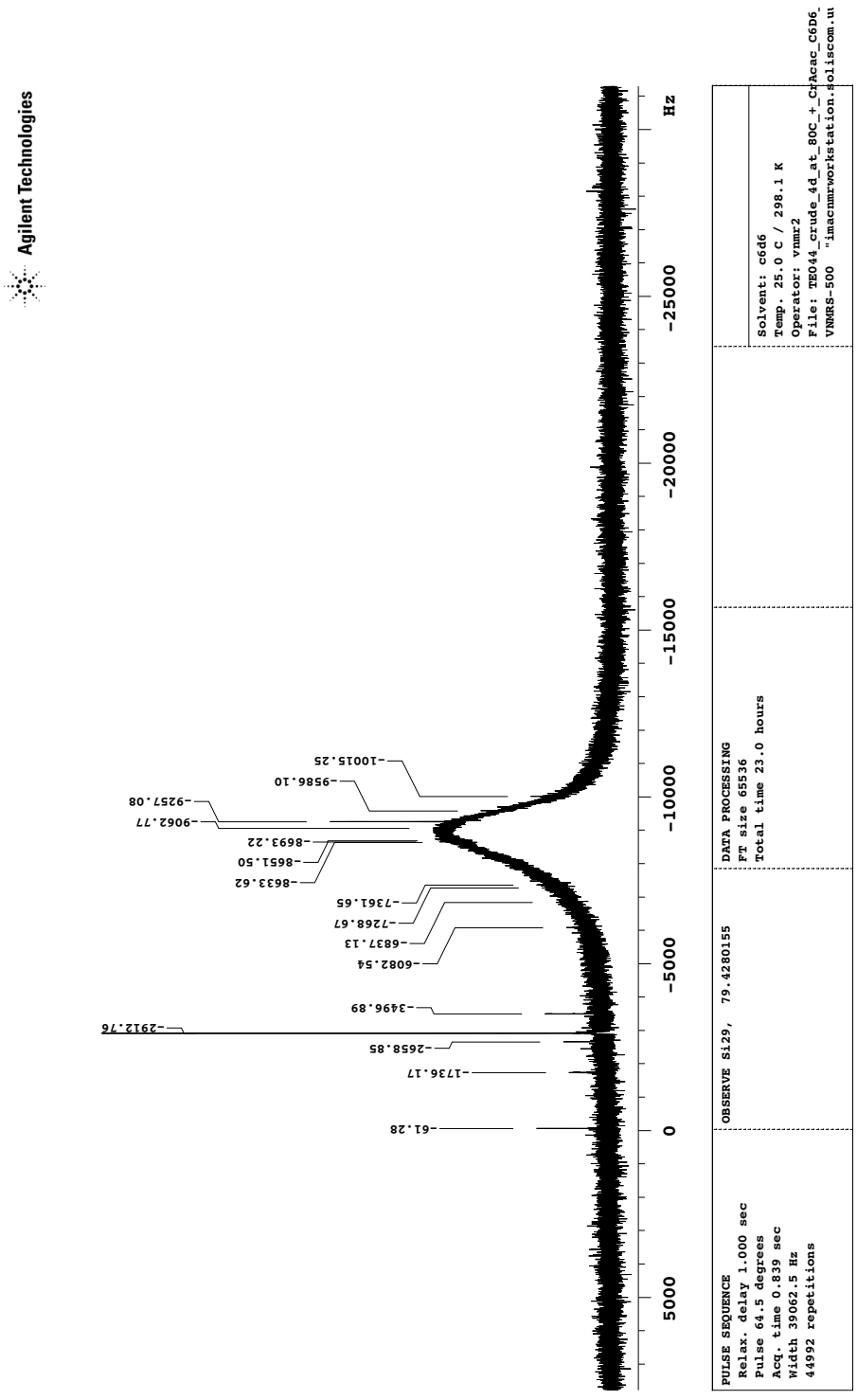

C.30. Compounds 20 and 18, resp. section 10.3 and 10.7, XRD

	20	**18**, unconstrained	**18**, constrained
Formula	$C_{22}h_{18}Cl_2N_4Si$	$C_{34}H_{42}ClN_4Si$	$C_{34}H_{43}ClN_4Si$
Formula weight	437.39	570.25	571.26
T [K]	150	150	150
λ [Å]	0.71073	0.71073	0.71073
Crystal system	Monoclinic	Monoclinic	Monoclinic
Space group	P2/n	C2/c	C2/c
a [Å]	11.4490(3)	20.2641(10)	20.2550(7)
b [Å]	7.31414(19)	9.9814(5)	9.9597(3)
c [Å]	13.0717(3)	15.6866(8)	15.6320(4)
α [°]	90	90	90
β [°]	112.241(1)	99.8426(8)	99.764(2)
γ [°]	90	90	90
V [$Å^3$]	1013.18(4)	3126.1(3)	3107.82(16)
Z	2	4	4
ρ_{calc} [g/cm^3]	1.4337(1)	1.212	1.221
μ[mm^{-1}]	0.397	0.190	0.191
F(000)	452.0	1220	1224
Crystal size [mm]	0.12 × 0.28 × 0.33	0.26 × 0.59 × 0.60	0.13 × 0.23 × 0.39
ϑ range [°]	2.0 - 30.0	2.3 - 27.5	2.0 - 33.8
Dataset	-16:16; -10:10; -18:18	-26:26; -12:12; -20:20	-31:31; -15:15; -24:24
Refl.: tot., uniq.	24319, 2959	23955, 3597	64810, 6268
R(int)	0.018	0.016	0.030
Obs. data [$I < 2\sigma(I)$]	2703	3376	5603
R	0.0265	0.0401	0.0410
wR_2	0.0737	0.1048	0.1094
S	1.06	1.05	1.02
Max., Av. Shift/Error	0.00, 0.00	0.01, 0.00	0.01, 0.00
Min,. Max. $\Delta\rho_{elect}$ [e $Å^{-3}$]	-0.25, 0.34	-0.33, 0.49	-0.65, 0.70

Table 14: *Crystal data and structure refinement data for **20** and **18**.*